The Role of Movement in Early Embryonic Joint Development

By

Devi Lakshmi Bridglal

Imperial College London

Imperial College London

Faculty of Engineering

Department of Bioengineering

This thesis is submitted in partial fulfilment of the requirements for the degree of Doctor of Philosophy

'The things that link bone with bone, cartilage, ligaments, membranes, are fashioned out of the same primordial tissue, and come into being pari passu, with the bones themselves. The entire fabric has its soft parts and its hard, its rigid and its flexible parts; but until we disrupt and dismember its bony, gristly and fibrous parts, one from another, it exists simply as a 'skeleton', as one integral and individual whole.'

D'Arcy Wentworth Thompson

1860–1948

Devi Lakshmi Bridglal

The Role of Movement in Early Embryonic Joint Development, © November 2019

Supervised by Dr. Niamh C. Nowlan

Imperial College London, United Kingdom

DECLARATION OF ORIGINALITY

I declare that this thesis, and the research presented within, is the product of my own work. Any ideas or quotations from the work of other people, published or otherwise, or from my own previous work are fully acknowledged in accordance with the standard referencing practices of the discipline.

This thesis was carried out between October 2015 and November 2019 under the supervision of Dr. Niamh C. Nowlan in the Department of Bioengineering at Imperial College London, UK.

DECLARATION OF COPYRIGHT

The copyright of this thesis rests with the author. Unless otherwise indicated, its contents are licensed under a Creative Commons Attribution-NonCommercial 4.0 International Licence (CC BY-NC).

Under this licence, you may copy and redistribute the material in any medium or format. You may also create and distribute modified versions of the work. This is on the condition that: you credit the author and do not use it, or any derivative works, for a commercial purpose.

When reusing or sharing this work, ensure you make the licence terms clear to others by naming the licence and linking to the licence text. Where a work has been adapted, you should indicate that the work has been changed and describe those changes.

Please seek permission from the copyright holder for uses of this work that are not included in this licence or permitted under UK Copyright Law.

ABSTRACT

Appendicular skeletogenesis involves the development of both synovial joints and long bones. Alterations or absences in fetal movement and the resulting changes in mechanical stimulation are strongly implicated in a number of musculoskeletal clinical conditions which arise *in utero*, by disruption of specific processes critical to normal skeletogenesis: morphogenesis, the process of shape formation, cavitation, the separation of joint surfaces, and mineralisation, the transition of prenatal cartilage to bone. This doctorate explored the relationship between the role of movement and skeletal development.

The embryonic chick was immobilised for varying time periods, and the effect on hip joint morphogenesis and cavitation investigated. A defined time period of movement was found to be critical for normal hip joint morphogenesis and cavitation (Chapter 4). Applied *in ovo* external movements were then used to 'rescue' the effects of immobility on hip joint morphology and cavitation failure. A single, timed application of movement was found to ameliorate the effects of immobility on hip morphogenesis and cavitation (Chapter 5). Finally, a culture system was adapted in which *in vitro* prenatal murine forelimb and hind limb rudiments were subjected to controlled magnitudes of movements, in order to (1) explore the effects of dynamic loading on elbow and knee morphology and mineralisation compared to statically-cultured limbs, and (2) promote more normal morphogenesis and mineralisation in a muscleless mouse model of immobility. Dynamic loading led to an increase in joint outgrowth and shape complexity, and some increase in rudiment mineralisation, and also promoted more normal morphogenesis and mineralisation in the muscleless mutant (Chapter 6).

This research provides new insights into the role of movement on fetal skeletal development, and has advanced our understanding of how the timing of movement can alter the progression of joint shape, cavitation, or mineralisation. Knowledge of skeletal development is critical to developing strategies for early screening, diagnosis, prevention, and treatment of musculoskeletal abnormalities.

ACKNOWLEDGEMENTS

Above all, I would like to whole-heartedly thank Dr. Niamh C. Nowlan for her supervision, support, and encouragement throughout this PhD. Her willingness to guide, her open-door policy, and breadth of knowledge have absolutely gotten me through this PhD in one (slightly battered) piece. I don't really have the words to express my gratitude to you. Thank you again.

I would like to thank all members of the Developmental Biomechanics group I had the pleasure of working with, past and present. Dr. Vikesh Chandaria, Dr. Stefaan Verbruggen, Dr. Aurélie Levillain, Dr. Saima Ahmed, Dr. Nidal Khatib, Dr. Cristian Parisi, Dr. Kaushik Mukherjee Dr. Rebecca Rolfe, Samantha Martin, Vivien Sotiriou, Yuming Huang, Josepha Godivier, and James Monsen. I thank you all for the many lunches, coffees, and pints throughout this PhD, the impassioned discussions, the laughs, the support, and for the happiest research years I could ever hope for. I will look back at my time at Imperial so fondly, not in small part to you all. Special thanks to Vikesh and Stefaan for nurturing me from an embryonic MRes student, to a live-and-kicking PhD candidate, and to Aurélie and Saima for your guidance in my post-natal PhD years. I am grateful to Dr. Colin Boyle for his assistance with Jupyter and statistical wizardry, and to technical staff in the Department of Bioengineering for friendly chats, and their hard work in maintaining shared facilities.

Thanks to my wonderful sister for her unwavering encouragement and faith (you are my favourite sister), to my mum for taking the time to understand, and to my dad for trying very hard to understand ("What is it that you do so I can tell people?"). I love you all. Special thanks to my children, Felix and Esme, for continual, loving indifference, except in the case of mealtimes. Thanks to all friends outside of Bioengineering for the enthusiastic nodding whenever I spoke of experiments and research, for uplifting me, and your sympathy/pity at my eternal student status. It is heartily welcomed.

Finally, thanks to Yean for your (now) life-long service to bike maintenance and reaching objects from tall shelves at my request. You proposed a wonderful hypothesis that I look forward to corroborating for many years to come.

This research was funded by the European Research Council under the European Union's Seventh Framework Programme (ERC Grant agreement no. [336306]).

PUBLICATIONS AND PRESENTATIONS RESULTING FROM THIS WORK

- Bridglal, D.L., Boyle, C.J., Rolfe, R.A., Nowlan, N.C., "Quantifying the tolerance of chick hip joint development to temporary paralysis and the potential for recovery", Accepted 5th August 2020, *Developmental Dynamics*
- Bridglal, D.L., Nowlan, N.C., "The effects of applied flexion and compressive loading on mineralisation and joint morphogenesis in the developing mouse limb", EMBO Workshop: Limb Development and Regeneration: New Tools for a Classic Model System, Barcelona, 2nd–5th July 2019, *flash talk and poster*
- Bridglal, D.L., Nowlan, N.C., "Timing of movement is essential for cavitation and morphogenesis of the developing chick hip joint", World Congress of Biomechanics, Ireland, 8th–12th July 2018, *oral presentation*
- Bridglal, D.L., Nowlan, N.C., "Identifying Critical Time Points for Early Chick Hip Development", 14th International Conference on Limb Development and Regeneration, MRC Institute of Genetics & Molecular Medicine, UK, 23rd–26th July 2017, *oral presentation*
- Bridglal, D.L., Nowlan, N.C., "Rescuing Hip Joint Shape after Immobility", Anatomical Society Summer Meeting, Ireland, 27th–29th June 2017, *poster*
- Bridglal, D.L., Nowlan, N.C., "Temporal effects of movement on early joint shape development in the chick", Understanding Anatomy through Embryology Symposium, Anatomical Society Winter Meeting, UK, 19th–21st December 2016, *oral presentation*

List of Acronyms

3D	Three-Dimensional
αMEM	alpha-Minimum Essential Medium
AMC	Arthrogryposis multiplex congenita
ANOVA	Analysis Of Variance
BABB	Benzyl Alcohol:Benzyl Benzoate
DDH	Developmental dysplasia of the hip
DMB	Decamethonium Bromide
e	Embryonic day
FADS	Fetal akinesia deformation sequence
KOH	Potassium Hydroxide
MSC	Mesenchymal Stem Cell
OCT	Optimum Cutting Temperature
OPT	Optical Projection Tomography
PB	Pancuronium Bromide
PBS	Phosphate Buffered Saline
PPI	Pore Per Inch

TABLE OF CONTENTS

Declaration of Originality 3

Declaration of Copyright 4

Abstract 5

Acknowledgements 6

Publications and Presentations Resulting From This Work 7

List of Acronyms 8

Table of Contents 9

List of Tables 13

List of Figures 14

Chapter 1 19

1. Introduction 19

1.1 Movement, and embryonic skeletal development 19

1.2 Objectives and hypothesis 21

1.3 Thesis structure 22

Chapter 2 23

2. Background 23

2.1 The skeleton, and synovial joints 23

2.2 Anatomy of a synovial joint 24

2.2.1 The hip 25

2.2.2 The knee 26

2.2.3 The elbow 27

2.3 Skeletal development 28

2.3.1 Chondrogenesis and mineralisation 28

2.3.2 Synovial joint formation 32

2.3.3 Cavitation 33

2.3.4 Morphogenesis 34

2.3.5 Link between cavitation, movement, and morphogenesis 35

2.4 Cartilage and bone mechanobiology 35

2.5 Clinical conditions of altered movement 36

2.6 Animal models of altered movement 39

2.6.1 Chick models 39
2.6.2 Mouse 43
2.6.3 Zebrafish 44
2.6.4 Joint forces in animal models of immobilisation 45
2.7 Summary 46
Chapter 3 47
3. Materials and Methods 47
3.1 Chick 47
3.1.1 Incubation 47
3.1.2 Immobilisation 48
3.1.3 Membrane dissection and manipulation 48
3.1.4 Harvesting 48
3.2 Mouse 49
3.2.1 Breeding 49
3.2.2 Harvesting 50
3.2.3 Dissection 50
3.3 Development of mammalian culture system 50
3.3.1 The bioreactor, and current culture set-up 50
3.3.2 Age of limb explants 52
3.3.3 Culture duration, and osteogenic media 54
3.3.4 Validation and calibration of mechanical stimulation 58
3.4 3D shape analysis 60
3.4.1 Staining 61
3.4.2 Embedding and trimming limbs 61
3.4.3 Imaging limbs with optical projection tomography 62
3.4.4 Joint shape and mineralisation ratio analysis 62
3.5 Histology 65
3.5.1 Embedding and sectioning 65
3.5.2 Staining 66
3.6 Licensing 66
Chapter 4 67
4. Early Chick Hip Development: A Critical Period of Movement 67
4.1 Introduction 67
4.2 Materials and Methods 68
4.2.1 Immobilisation regimes – windowing and paralysis 68
4.2.2 Controls 69

4.2.3 Specimen numbers 69
4.2.4 Joint shape and cavitational analysis 69
4.2.5 Statistical analysis 70
4.3 Results 71
4.3.1 Cumulative immobilisation 71
4.3.2 Single–day immobilisation 74
4.3.3 Two–day immobilisation 78
4.3.4 Three–day immobilisation 81
4.4 Discussion 85
Chapter 5 91
5. Early Chick Hip Development: The Effect of External Manipulation 91
5.1 Introduction 91
5.2 Materials and Methods 92
5.2.1 Chick treatment 92
5.2.2 Specimen numbers 92
5.2.3 Joint shape and cavitational analysis 93
5.2.4 Statistical analysis 93
5.3 Results 93
5.3.1 Shape outlines 93
5.3.2 Measurements 94
5.3.3 Cavitation 95
5.4 Discussion 97
Chapter 6 99
6. Early Mouse Limb Development: The Effects of Dynamic Loading 99
6.1 Introduction 99
6.2 Materials and Methods 101
6.2.1 Harvest, culture, and number of limbs 101
6.2.2 Joint shape and mineralisation ratio analysis 102
6.2.3 Statistical analysis 102
6.3 Results 103
6.3.1 Static growth of murine prenatal limbs *in vitro* 103
6.3.2 Effect of mechanical stimulation on cartilage and mineralisation *in vitro* 110
6.3.3 Recovery of skeletal development in mechanically-stimulated rudiments 112
6.4 Discussion 119
Chapter 7 127

7. Conclusions 127
7.1 Summary of Key Outcomes 127
7.2 Clinical applications 128
7.3 Limitations and future work 129
7.4 Conclusions 130
References 133
Appendix I – Copyright Permissions 146
Appendix II – Timed Immobilisation Control Groups 149

LIST OF TABLES

Table 4.1: Number of chick hind limbs analysed for shape changes and histologically at e9 69
Table 5.1: Total number of paired chick hind limbs assessed for cavitation and morphology 92
Table 6.1: Number of control murine forelimbs and hind limbs analysed for elbow and knee joint morphology and mineralisation ratio 101
Table 6.2: Number of control and Pax3$^{Sp\text{-}d/Sp\text{-}d}$ murine forelimbs and hind limbs analysed for elbow and knee joint morphology and mineralisation ratio 102

LIST OF FIGURES

Figure 2.1: Common structural features of synovial joints 24
Figure 2.2: (a) Frontal section through the right hip joint; (b) Anterior and posterior views of the bony anatomy of the hip joint 26
Figure 2.3: Anterior and posterior views of the bony anatomy of the knee joint 27
Figure 2.4: Anterior and posterior views of the bony anatomy of the elbow joint 28
Figure 2.5: The first appearance of key events during early human, mouse and chick long bone development 29
Figure 2.6: Early endochondral ossification 30
Figure 2.7: A summary of regionalised gene expression in the developing growth plate 31
Figure 2.8: The first appearance of key events during early human, mouse and chick joint development 33
Figure 2.9: Images of chick e10 control elbow showing the humerus, radius, and ulna 33
Figure 2.10: Early joint development: joint specification, interzone formation, cavitation, and morphogenesis 35
Figure 2.11: Congenital dislocation of the left hip 38
Figure 2.12: Histological sections of the right hip joint through the anterior-posterior plane of the femur for each timepoint 40
Figure 2.13: Outlines of cartilage shape in distal femora of control and immobilised chick embryos 42
Figure 2.14: Chick knee explants were cultured under a range of mechanical stimulation 42
Figure 2.15: Control, reduced muscle, and muscleless murine forelimb rudiments 44
Figure 2.16: Representative outlines of the 5dpf zebrafish jaw joint for each condition (n=4) ... 45
Figure 3.1: Membrane dissection and manipulation of the chick hind limb 49
Figure 3.2: (a) Ebers TC-3 bioreactor system and (b) compression culture chambers with foam support and culture media. 51
Figure 3.3: Current bioreactor set up 52
Figure 3.4: Limb explants harvested at different ages after 3 days of static culture 53
Figure 3.5: Limb explants after 3 and 6 days of static culture, stained with 0.015% Alcian blue and 0.01% Alizarin red for cartilage and mineralisation 54
Figure 3.6: Dot plots of measurements of the murine elbow joints 56
Figure 3.7: Dot plots of measurements of the murine knee joints 57
Figure 3.8: Dot plots of mineralisation ratio of the murine forelimb and hind limb rudiments ... 58
Figure 3.9: Increasing compression of the foam support resulting in a bending action at the elbow and knee joint at e14.5, as shown by the decrease in internal joint flexion angle. 59

Figure 3.10: Flexion angle increased linearly with compressive magnitude 60
Figure 3.11: Representative image of hip measurements based on anatomical landmarks 63
Figure 3.12: Representative image of elbow measurements based on anatomical landmarks 63
Figure 3.13: Representative image of knee measurements based on anatomical landmarks 64
Figure 4.1: Four different immobilisation regimes were used: (a) cumulative, (b) single, (c) two–day, and (d) three–day..... 68
Figure 4.2: Shape profile outlines of the acetabulum and femoral head of the hip joint in embryonic chicks immobilised under the 'cumulative' immobilisation regime 72
Figure 4.3: Dot plot graphs of measurements of the femoral head (a–d) and acetabulum (e–g) of the hip joint in embryonic chicks immobilised under the 'cumulative' immobilisation regime... 73
Figure 4.4: Histological sections of the femoral head and acetabulum of the hip joint in embryonic chicks immobilised under the 'cumulative' immobilisation regime..... 74
Figure 4.5: Shape profile outlines of the frontal femoral head and acetabulum of the hip joint in embryonic chicks immobilised for a single 24–hour period 75
Figure 4.6: Dot plot graphs of measurements of the femoral head (a–d) and acetabulum (e–g) of the hip joint in embryonic chicks immobilised for a single 24–hour period 76
Figure 4.7: Histological sections of the femoral head and acetabulum of the hip joint in embryonic chicks immobilised for a single 24–hour period 77
Figure 4.8: Shape profile outlines of the frontal femoral head and acetabulum of the hip joint in embryonic chicks immobilised for a single 48–hour period 78
Figure 4.9: Dot plot graphs of measurements of the femoral head (a–d) and acetabulum (e–g) of the hip joint in embryonic chicks immobilised for a single 48–hour period 79
Figure 4.10: Histological sections of the femoral head and acetabulum of the hip joint in embryonic chicks immobilised for a single 48–hour period 81
Figure 4.11: Shape profile outlines of the frontal femoral head and acetabulum of the hip joint in embryonic chicks immobilised for a single 72–hour period 82
Figure 4.12: Dot plot graphs of measurements of the femoral head (a–d) and acetabulum (e–g) of the hip joint in embryonic chicks immobilised for a single 72–hour period 83
Figure 4.13: Histological sections of the femoral head and acetabulum of the hip joint in embryonic chicks immobilised for a single 72–hour period 84
Figure 5.1: Shape profiles of the femoral head and acetabulum comparing unmanipulated and externally manipulated hip joints..... 94
Figure 5.2: Dot plot graphs of the femoral head and acetabulum comparing unmanipulated and externally manipulated hip joints..... 95
Figure 5.3: Histological sections of externally manipulated and unmanipulated paired hip joints 96

Figure 6.1: e15.5 hind limb dynamically cultured for 6 days 102
Figure 6.2: Shape profile outlines of the rudiments of the wild-type embryonic murine elbow joint 104
Figure 6.3: Dot plot graphs of measurements of the wild-type embryonic murine elbow joint 105
Figure 6.4: Shape profile outlines of the rudiments of the wild-type embryonic murine knee joint 107
Figure 6.5: Dot plot graphs of measurements of the wild-type embryonic murine knee joint .. 108
Figure 6.6: Dot plot graphs of mineralisation ratio of the wild-type embryonic murine forelimb and hind limb rudiments 109
Figure 6.7: Shape profile outlines of the rudiments of the wild-type and Pax3$^{Sp\text{-}d/Sp\text{-}d}$ mutant embryonic murine elbow joint 114
Figure 6.8: Dot plot graphs of measurements of the wild-type and Pax3$^{Sp\text{-}d/Sp\text{-}d}$ mutant embryonic murine elbow joint 115
Figure 6.9: Shape profile outlines of the rudiments of the wild-type and Pax3$^{Sp\text{-}d/Sp\text{-}d}$ mutant embryonic murine knee joint 116
Figure 6.10: Dot plot graphs of measurements of the wild-type and Pax3$^{Sp\text{-}d/Sp\text{-}d}$ mutant embryonic murine knee joint 118
Figure 6.11: Dot plot graphs of mineralisation ratio of the wild-type and Pax3$^{Sp\text{-}d/Sp\text{-}d}$ mutant embryonic murine forelimb and hind limb rudiments 119
Figure 6.12: Summary of effects seen in murine forelimbs and hind limbs culture systems 121

Chapter 1

1. Introduction

1.1 Movement, and embryonic skeletal development

A normal pregnancy can range from 36 to 42 gestational weeks (Jukic, Baird et al. 2013). In human embryogenesis, the cartilaginous template of the appendicular skeleton is formed as early as 7 fetal weeks (Senior 1919). The cartilaginous template of the upper and lower limbs follows two main paths. One path leads to the formation of synovial joints, whereby the parallel processes of (1) cavitation, the separation of skeletal rudiments, and (2) morphogenesis, the shaping of joint surfaces into reciprocal, interlocking structures, must occur correctly for the correct function of the skeleton. The second path leads to the formation of mineralised bone, which first occurs in the mid-shaft of the long bones. The mechanical environment plays an important role not just in the physiological function of cartilage (reviewed in Chen, Tambe et al. 2013) and bony remodelling and repair in adult life (reviewed in Robling and Turner 2009), but also during fetal development.

Prenatal movements in the womb are critical for normal skeletal development, evidenced by the number of musculoskeletal clinical conditions and syndromes where absent or abnormal mechanical stimulation of the unborn infant are implicated as a risk factor (Rodriguez, Palacios et al. 1988). The most commonly occurring joint condition, developmental dysplasia of the hip (DDH), has an incidence of 1.3 per 1000 live births, and is characterised by hip joint instability or malformation (Leck 2000). Arthrogryposis multiplex congenita (AMC) is a term used to describe multiple joint contractures, and has an incidence of 1 per 3000 to 5000 live births (Lowry, Sibbald et al. 2010). Fetal akinesia deformation sequence (FADS) is a description of recognised abnormalities, of which the main symptoms are multiple joint contractures, skeletal fractures, slender hypomineralised bones, and clubfoot, with an incidence of 1 in 15000 (Bayat, Petersen et al. 2009). Absent or reduced fetal movement is comorbid to these select musculoskeletal

conditions, and, if the fetus is not terminated (often the case in FADS due to the very low chance of survival), patients often undergo lengthy or invasive treatments, such as physical therapy, casting, splinting, or multiple surgeries. Abnormal joint shapes which arise *in utero* can severely impact patients' quality of life, limiting the range of motion and increasing the risk of developing degenerative joint disease, such as osteoarthritis (Sandell 2012). Hence, further understanding of prenatal skeletal formation is clinically relevant to developing screening and diagnostic tools, and enhancing current treatments.

An absence of fetal movement and mechanical stimulation is strongly implicated in disrupting a number of processes critical to normal skeletogenesis: joint morphogenesis, the formation of complex, reciprocal joint shapes, is disrupted in DDH patients with malformed hips. Cavitation, the physical separation of opposing joint rudiments, fails to progress normally in patients with multiple joint contractures. Mineralisation, whereby cartilaginous templates begin the transition to ossified bone, is disrupted in patients with FADS. Varied animal models of reduced or absent movement have consistently presented with detrimental effects on aspects of skeletal development, including morphogenesis, synovial joint cavitation, and cartilaginous ossification (reviewed in Nowlan, Sharpe et al. 2010). The majority of studies performed to date have focused on long-term removal of movement and mechanical stimulation. Although the effects of absent movement and altered mechanical stimulation is well-documented, it remains unclear how variations in the timing of movement and mechanical stimulation affect aspects of skeletal development, such as cavitation, morphogenesis, or mineralisation.

This doctorate targeted two gaps in scientific knowledge: (1) The relationship between timing of fetal movement, cavitation, and morphogenesis is not yet understood, and it is unknown whether there is a defined, critical time period where movement must occur for the progression of normal joint development. (2) Prenatal interventions aiming to promote skeletal recovery in the immobilised embryo remain under-researched, and it is unknown how applied loading affects cavitation, morphogenesis, and mineralisation in models of reduced or absent movement. Knowledge on the relationship between timing of movement, cavitation, morphogenesis and mineralisation is valuable. Identifying a critical time period for movement for normal fetal skeletal development potentially enables targeted *in utero* screening for at-risk infants. Charactering the effects of applied loading on skeletal development may determine whether a prenatal intervention may make a substantial difference in patients' adult lives.

1.2 Objectives and hypothesis

The aim of this doctorate was to experimentally explore the role of timed mechanical stimulation on the development of selected skeletal rudiments. In order to achieve this aim, the following objectives were determined:

Objective 1: Identify the critical time period for movement for normal chick hip cavitation and morphogenesis

Objective 2: Externally induce cavitation in the immobilised joint and characterise the effects on *in ovo* chick hip joint morphogenesis

Objective 3: Adapt and optimise an existing chick bioreactor culture system for prenatal murine culture

Objective 4: Characterise murine joint morphogenesis and mineralisation over six days of *in vitro* culture

Objective 5: Explore the role of *in vitro* mechanical stimulation on murine morphogenesis and mineralisation

Objective 6: Promote more normal *in vitro* morphology and mineralisation in a muscleless mouse model of immobility using mechanical stimulation

The immobilised chick embryo was used to test the following hypotheses:

Hypothesis 1: There is a time period of defined length and duration critical for normal cavitation and morphogenesis

Hypothesis 2: External manipulation of the immobilised chick embryo hind limb, just prior to the point of cavitation, allows for morphogenesis and cavitation of the hip joint to proceed more normally, even under continued immobilisation

Using a mammalian bioreactor culture system, culture of prenatal murine limbs was used to test the following hypotheses:

Hypothesis 3: *In vitro* culture of murine prenatal limbs leads to greater outgrowth and mineralisation of the murine limbs, compared to uncultured limbs

Hypothesis 4: *In vitro* dynamic mechanical stimulation leads to a more developed joint shape and increased mineralisation, compared to statically-cultured murine limbs

Hypothesis 5: *In vitro* mechanostimulation from dynamic loading promotes more normal morphogenesis and mineralisation in $Pax3^{Sp\text{-}d/Sp\text{-}d}$ muscleless mutant murine prenatal limbs, compared to unloaded muscleless mutant limbs

1.3 Thesis structure

Chapter 2: A review of the current literature on synovial joint formation and the role of mechanical stimulation during skeletal development is included here. Animal models and clinical conditions are discussed, and place the work in this thesis in the appropriate context.

The hypotheses set out in section 1.2 are addressed Chapters 3 to 6.

Chapter 3: Methods used to acquire and process chick and mouse embryos for imaging, and joint and mineralisation analysis are included here. The development of a mammalian whole limb bioreactor culture set-up is also described.

Chapter 4: Work in this chapter explored the relationship between movement, cavitation, and morphogenesis during embryonic chick hip joint development. Experiments in this chapter were conducted to test Hypothesis 1. Results from this chapter are put into the context of current scientific knowledge.

Chapter 5: Work in this chapter characterised the effect of external mechanical stimulation in the immobilised embryonic chick hip joint. Experiments in this chapter were conducted to test Hypothesis 2. Results from this chapter are put into the context of current scientific knowledge.

Chapter 6: Here, the mammalian bioreactor culture system described in Chapter 3 was used. Murine prenatal limbs were cultured to explore the effects of static culture on the growth of murine prenatal limbs, and the effect of dynamic mechanical stimulation on *in vitro* cartilage growth and mineralisation. Muscleless mutants were then dynamically cultured, to investigate whether mechanical stimulation could bring about more normal shape and mineralisation *in vitro*. Experiments in this chapter were conducted to test Hypotheses 3, 4, and 5. Results from this chapter are put into the context of current scientific knowledge.

Chapter 7: A summary of the main findings of this thesis is contained here. Avenues of future research are also proposed.

Chapter 2

2. Background

2.1 The skeleton, and synovial joints

The skeleton is defined as *"the bony or more or less cartilaginous framework supporting the soft tissues and protecting the internal organs of a vertebrate"* (Merriam Webster Dictionary). In adult humans, the 126 bones of the appendicular skeleton function to support the appendages of the upper and lower limbs (Gray 2004). The appendicular skeleton includes the pelvic and shoulder girdles, which are in turn attached to the 80 bones of the axial skeleton, comprised of the skull and vertebral column (Gray 2004). The skeleton has three major mechanical functions: to support the body and maintain shape, to protect vital internal organs, and to allow for movement, the area of focus for this thesis (Clarke 2008).

Synovial joints are located between limb bony surfaces in all vertebrates with well-developed movement between two bones. Synovial joints are composed of specific, reciprocally shaped bony surfaces, each capped by a thin layer of articular cartilage (reviewed in Fox, Bedi et al. 2009). Cartilage is a firm and flexible connective tissue. The composition and structural integrity of the cartilage matrix give cartilage low-friction and load-bearing properties (Buckwalter and Mankin 1998). This extracellular matrix consists of collagen, proteoglycans and water, which is secreted by embedded chondrocytes (reviewed in Buckwalter and Mankin 1998). There are three types of cartilage: fibrocartilage is predominantly found in the intervertebral discs, elastic cartilage is found in the outer ear, and hyaline, articular cartilage is found in the larynx and trachea, nose, and, most relevant to this thesis, is transiently produced during endochondral ossification (reviewed in Fox, Bedi et al. 2009). The sliding surfaces of articular cartilage are viscoelastic, avascular and aneural, with limited regenerative capacity. These surfaces are bathed by synovial fluid, which functions to absorb shock, to reduce friction, and to act as a nutrient and waste transport medium for chondrocytes embedded within the articular cartilage (reviewed in Fox,

Bedi et al. 2009). Synovial fluid and joint surfaces are surrounded by a fibrous joint capsule, whilst ligaments work to augment mechanical stability of the joint, to guide joint motion, and to prevent excessive motion (Clarke 2008) (Figure 2.1).

Bones have attachment points for tendons, which allow for transmission of tensile loads from muscle to bone, thereby producing joint motion, or maintaining body posture. Long bones typically contain two distinct morphological types of bone: cancellous, or spongy bone, is located at bone epiphyses with an open, honeycomb-like structure, and cortical bone, which forms a dense cylinder surrounding the central marrow cavity down the long shaft of the bone. Bone consists mainly of collagen fibres and hydroxyapatite, along with additional minerals such as silicon, carbonate, and zinc (Clarke 2008).

2.2 Anatomy of a synovial joint

There are three main types of joint: fibrous, which are immobile joints only held together by ligaments, cartilaginous, where the connection between articulating bones is formed of cartilage, and synovial joints, which allow for movement (Betts, Young et al. 2013a). Synovial joints are the joints most relevant to this thesis. Synovial joint shapes allow for a wide range of movement: abduction, movement away from the mid-line of the body; adduction: movement toward the mid-line of the body; extension: straightening limbs at a joint; flexion: bending the limbs at a joint; and rotation: a circular movement around a fixed point (Betts, Young et al. 2013b).

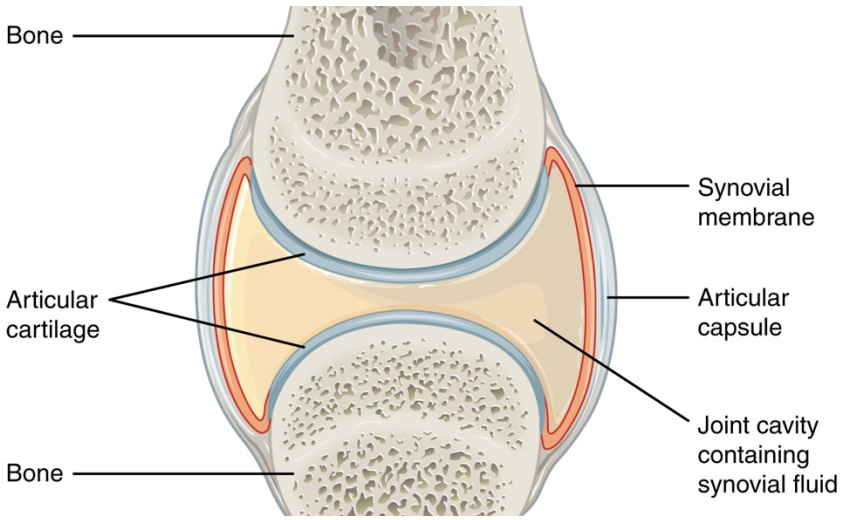


Figure 2.1: Common structural features of synovial joints. A key feature of synovial joints is the presence of a synovial fluid-filled joint cavity, inside of which reciprocal ends of the articulating joint meet. The bony joint interface is surfaced with hyaline cartilage, and lubricating synovial fluid allows for smooth, virtually frictionless movement between adjacent bone. The articular capsule forms the wall of the joint cavity, containing the joint ends and synovial fluid. Adapted from Synovial Joints, OpenStax (Betts, Young et al. 2013b).

2.2.1 The hip

In this thesis, development of the hip joint under varying mechanical stimuli was selected for investigation in chick embryos. The hip, or acetabulofemoral joint, is a ball-and-socket articulation between the femoral head on the proximal femur, and the acetabulum in the pelvis (Betts, Young et al. 2013a) (Figure 2.2). The pelvic girdle consists of the two hip bones, termed the os coxae. These hip bones connect anteriorly at the pubic symphysis joint, and connect posteriorly with the sacrum at the sacroiliac joints. The hip bones, sacrum, coccyx, and pubic symphysis form a deep, closed ring, termed the bony pelvis. Functionally, this ring provides strength and stability for the vertebral column and organs of the pelvis and lower abdomen. The pelvic girdle also serves as the point where the appendicular skeleton of the lower limbs unites with the axial skeleton. In human infants, each hip bone consists of three bones which are separated by cartilage: the superior ilium, the inferior and posterior ischium, and the inferior and anterior pubis. By early adulthood, these three bones fuse together. The acetabulum is a deep socket formed at the intersection between the ilium, ischium, and pubis, wherein the proximal femoral head articulates to form the hip joint (Betts, Young et al. 2013c).

The femur, found in the thigh, is the longest, and heaviest long bone in the human body (Betts, Young et al. 2013d). The proximal femur consists of a round head, which contains a central, ovoid indentation, termed the fovea capitis (Betts, Young et al. 2013b). The foveal ligament connects the fovea capitis with the acetabulum. The femoral neck is a contracted region distal to the head, and connects the femoral head with the femoral shaft. Projecting just laterally from the femoral neck, the greater trochanter is a large, quadrilateral, bony eminence. The lesser trochanter is conical in shape, projecting inferiorly and medially to the greater trochanter (refer to Figure 2.2). Together, these form the sites of insertion for several gluteal muscles and thigh muscles. In humans, the hip transfers the weight of the upper body into the lower limbs during standing and walking, allowing for movement of the upper leg. The hip joint has a range of movements: flexion, extension, abduction, adduction, lateral rotation, medial rotation, and circumduction of the thigh (Betts, Young et al. 2013c). The hip joint is extremely stable, due to the very strong and dense articular capsule and associated ligaments, the deep insertion of the femoral head into the acetabulum, and the muscles surrounding the joint (Betts, Young et al. 2013a).

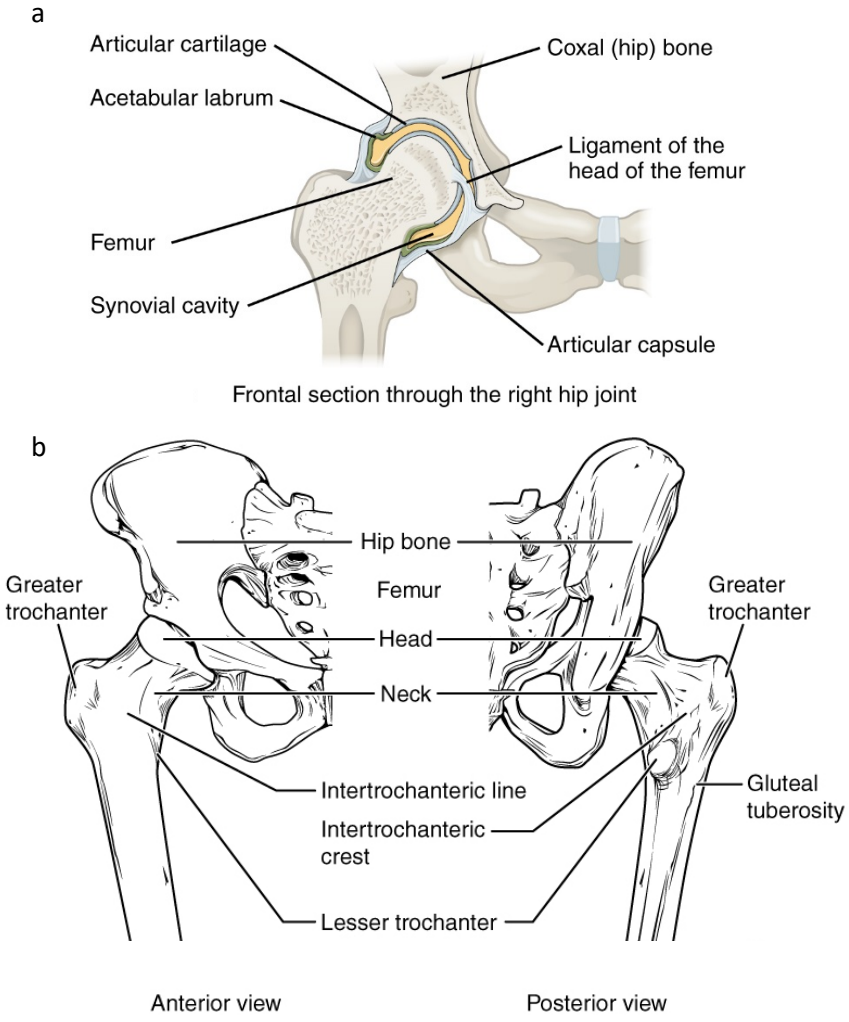


Figure 2.2: (a) Frontal section through the right hip joint; (b) Anterior and posterior views of the bony anatomy of the hip joint. Adapted from Anatomy of Selected Synovial Joints and Bones of the Lower Limb, OpenStax (Betts, Young et al. 2013a, Betts, Young et al. 2013d).

2.2.2 The knee

Further in this thesis, I decided to explore the effects of a cyclic loading regime in murine hindlimbs and forelimbs. The knee, or tibiofemoral, joint is a modified hinge joint, and is the largest and most complex synovial joint in the human body. Formed by the distal femur, patella, and proximal tibia, the knee consists of three joints within a single synovial capsule: the lateral tibiofemoral joint between the lateral femoral condyle, lateral meniscus, and lateral tibial condyle, the medial tibiofemoral joint between the medial femoral condyle, medial meniscus, and medial tibial condyle, and the intermediate patellofemoral joint between the patellar surface of the femur and the patella (Betts, Young et al. 2013d) (Figure 2.3). The distal end of the femur is somewhat cuboid in form, and is wider mediolaterally than anteroposteriorly. The distal end consists of the medial and lateral condyles, and superior to these are the medial and lateral

epicondyles, onto which the ligaments of the knee attach. The intercondylar fossa is located between the posterior medial and lateral condyles, whilst the patellar surface is located anteriorly (Betts, Young et al. 2013d). The patella articulates with the lateral and medial femoral condyles, forming the patellofemoral joint. Assessment of the patella or the patellofemoral joint was not included in this thesis.

The tibia is the weight-bearing bone of the leg, located on the medial side, next to the fibula. The proximal end of the tibia enlarges into the medial and lateral condyles, which are separated anteriorly and posteriorly by the intercondylar area. The medial and lateral menisci, two fibrocartilaginous semilunar-shaped structures, lie between the femoral and tibial condyles. These work to distribute the load of the upper body to the lower, and to stabilise the knee during movement. The inferior surface of the lateral condyle articulates with the fibula, which does not articulate with the femur. The knee joint permits flexion, extension, slight medial rotation, and lateral rotation of the leg when flexed (Betts, Young et al. 2013d).

2.2.3 The elbow

As stated in Chapter 1, the effects of a cyclic loading regime in murine hindlimbs and forelimbs is explored further in this thesis. The elbow was chosen, alongside the knee. The elbow is a hinge joint, formed between the distal humerus in the upper arm, and proximal ends of the ulna and radius in the lower arm (Betts, Young et al. 2013e) (Figure 2.4). The distal humerus is a flattened and broad structure, with several eminences. Laterally, the rounded, protruding capitulum articulates with the radial head. Superior to the capitulum is an anterior indentation, the radial fossa, which articulates with the radial head under flexion. Medially, the spool-shaped trochlea,

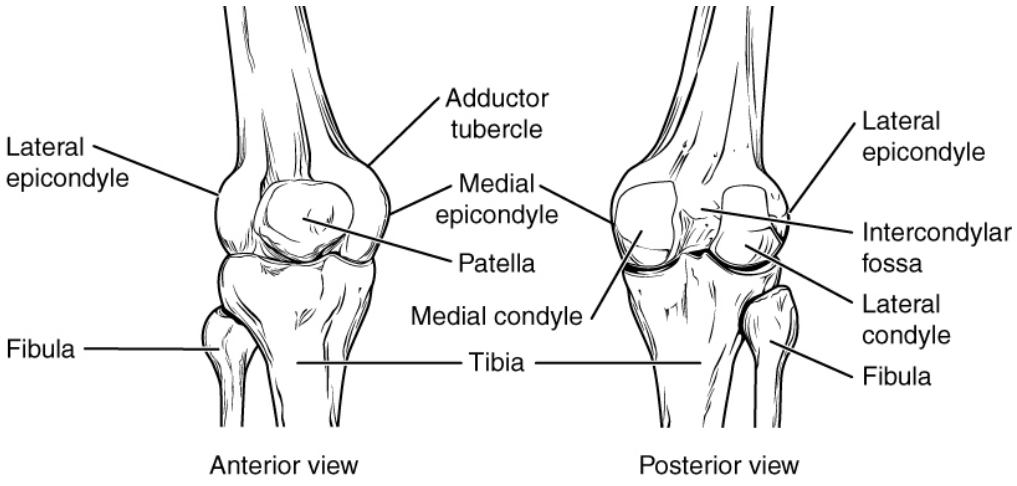


Figure 2.3: Anterior and posterior views of the bony anatomy of the knee joint. Adapted from Bones of the Lower Limb, OpenStax (Betts, Young et al. 2013d).

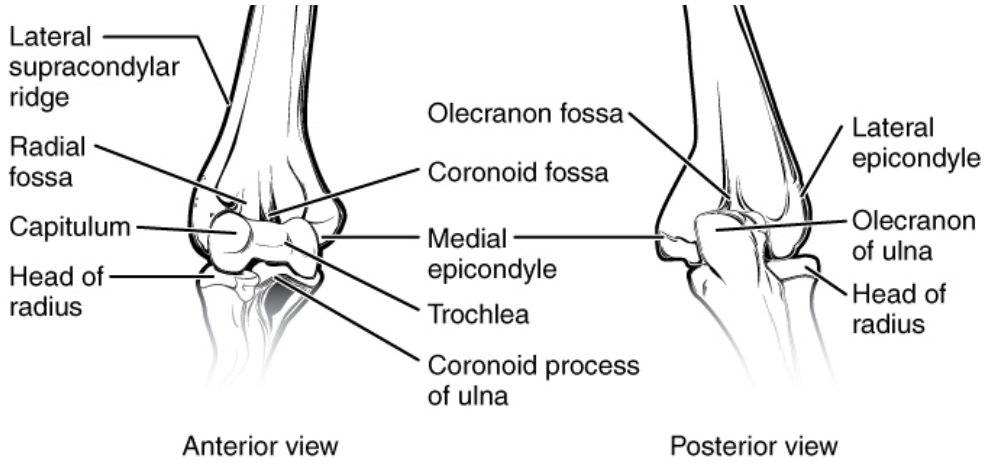


Figure 2.4: Anterior and posterior views of the bony anatomy of the elbow joint. Adapted from Bones of the Upper Limb, OpenStax (Betts, Young et al. 2013e).

articulates with the trochlear notch of the ulna. An anterior indentation, the coronoid fossa, receives the coronoid process of the ulna under flexion. A posterior indentation, the olecranon fossa, receives the olecranon of the ulna under extension. The medial and lateral epicondyles project mediolaterally, onto which most muscles of the forearm attach (Betts, Young et al. 2013e).

Located medially, the ulna is the longer of the two bones of the lower arm (Betts, Young et al. 2013). At its proximal end, the olecranon forms the most pointed end of the elbow. The coronoid process is a triangular eminence from the anterior proximal ulna, inferior to the olecranon. Between the olecranon and coronoid process is the curved trochlear notch. All three articulate with the humeral trochlea. Inferior and lateral to the trochlear notch is the radial notch, into which the head of the radius articulates. Located laterally, the proximal radial head articulates with the radial notch on the ulna and the capitulum of the humerus (Betts, Young et al. 2013e). The elbow allows for flexion and extension of the forearm (Betts, Young et al. 2013e).

2.3 Skeletal development

2.3.1 Chondrogenesis and mineralisation

Skeletal identity is conferred early in the developing limb bud (Yang 2013). Cells from the lateral plate mesoderm migrate to the limb bud site, and proliferate as mesenchymal stem cells (MSCs) (Lefebvre and Bhattaram 2010). The emergence of patterning and limb formation occurs in a proximal-to-distal, anterior-to-posterior fashion, with more distal and more posterior elements being developmentally 'younger' than more proximal and anterior elements (Yang 2013). It is important to acknowledge the contribution of the embryonic chick has provided on understanding the basic biology and genetics of limb development (reviewed in Davey, Towers et al. 2018).

There are two routes for bone formation, both of which begin with the condensation of MSCs. The first, intramembranous ossification, occurs in the craniofacial and medial clavicular bones. MSCs cluster together and differentiate directly into osteoprogenitor cells, then osteoblasts, secreting bone matrix (Gilbert 2000). The second route, followed by long bones and the vertebrate skeleton, is known as endochondral ossification (Hall 1987). Both mammalian and avian long bone development begin with MSC condensation, differentiation into hypertrophic cartilage, and formation of the perichondrium. The formation of a Y-shaped mesenchymal condensation is one of the earliest events in endochondral ossification and appendicular skeletal development (Fell 1925). MSCs actively aggregate, densely pack, and upregulate expression of cell adhesion molecules (Hall and Miyake 1992, Lefebvre and Bhattaram 2010). Expression of *SOX9* occurs very early in the committed mesenchymal chondroprogenitors, and is the major driving force for expression of chondrogenic lineage genes (reviewed in Hata, Takahata et al. 2017). MSCs then differentiate into chondrocytes, and start to produce cartilage extracellular matrix (Lefebvre and Bhattaram 2010). Chondrocytes then undergo rapid proliferation, drive linear growth of the cartilage anlagen and form the template for bone. Eventually, chondrocytes in the mid-section of the rudiment cease proliferation and become hypertrophic, acquiring a more rounded morphology (Gilbert 2000). More peripheral cells form the perichondrium and retain a more fibroblastic morphology (Caplan and Pechak 1987, Rooney and Archer 1992). Core events for skeletal development occur in the human, mouse, and chick, albeit with very different timings. Major events in limb development occur over roughly a two month period in the human, a two week period in the mouse, and a one week period in the chick (Figure 2.5).

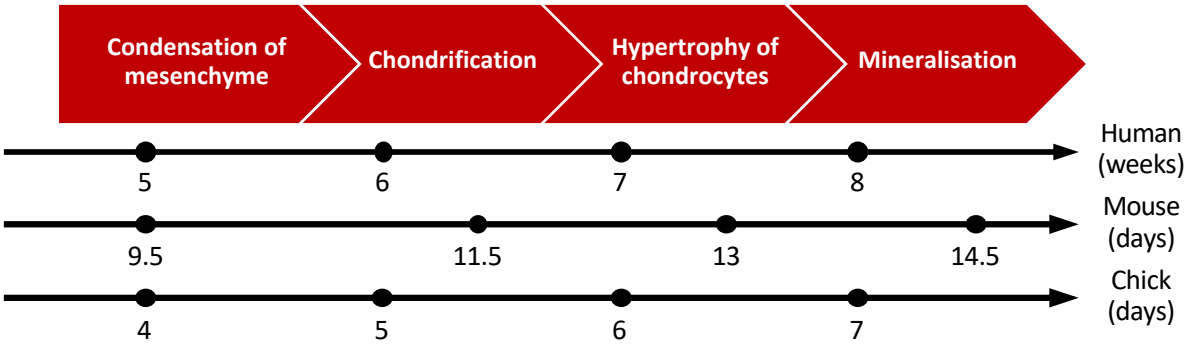


Figure 2.5: The first appearance of key events during early human, mouse and chick long bone development (Fell 1925, Fell and Canti 1934, Gardner, Gray et al. 1959, Gardner and O'Rahilly 1968, O'Rahilly and Gardner 1972, Hall 1987, Hall and Miyake 1992)

It is here that long bone development diverges between mammalian and avian species. In the mammal, the surrounding perichondrium becomes invaded by capillaries, and then the hypertrophic chondrocytes begin secretion of fibronectin and collagen X, enabling mineralisation by calcium carbonate and the formation of the periosteal bone collar (Gilbert 2000). As the matrix calcifies, nutrients can no longer reach the chondrocytes. Core chondrocytes thus undergo apoptosis, allowing for blood vessels to invade, carrying osteogenic cells. The first area of ossification, termed the primary ossification centre, forms prenatally in the mid-diaphysis (shaft) of the long bones, followed by secondary ossification centres post-natally in the distal epiphyses (Figure 2.6).

In the chick, chondrocytes also undergo hypertrophy, and the perichondrium differentiates into two layers, the innermost of which is fated to produce osteoblasts. These osteoblasts deposit osteoid between the cartilage and perichondrium, transforming the perichondrium into periosteum (Hall 1987). Mineralisation of osteoid occurs shortly after, forming the periosteal bone collar. In the bird, periosteal ossification occurs prior to vascular invasion below the layer of periosteum (Hall 1987). The outer bone collar increases in both length and thickness, whilst the cartilaginous core erodes to form the marrow cavity. Avian long bones lack the primary ossification centre, and vascular invasion of hypertrophic cartilage occurs after mineralisation, post-embryonic life (Fell 1925, Hall 1987). Hypertrophic cartilage is also resorbed to form hollow bones, essential for flight (Dumont 2010).

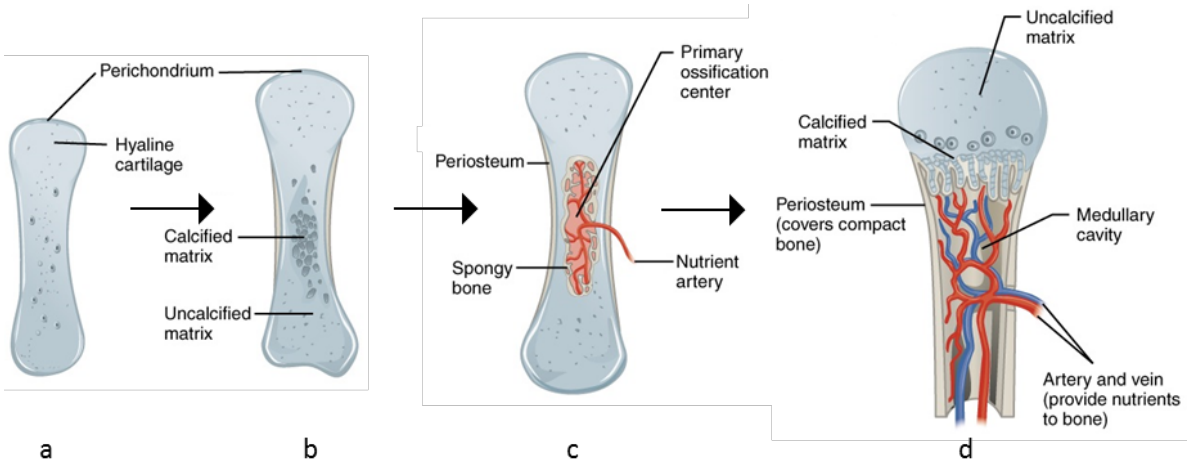


Figure 2.6: Early endochondral ossification. (a) Mesenchymal cells differentiate into chondrocytes. (b) The cartilage template of the future ossified skeleton and the perichondrium form. (c) Capillaries invade cartilage, and the perichondrium differentiates into periosteum. The bone collar develops. Primary ossification centre develops. (d) Cartilage and chondrocytes continue to grow at ends of the bone. Secondary ossification centres develop later. Adapted from Bone Formation and Development, OpenStax (Betts, Young et al. 2013).

It is pertinent to mention normal molecular signalling during skeletal development. During endochondral bone formation, patterns of molecular signalling change over time (Figure 2.7). Immature chondrocytes within the growth plate initially express the transcription factors Sox5, Sox6 and Sox9, Type II α1 collagen and aggrecan (Lefebvre, Li et al. 1998, Inada, Yasui et al. 1999, de Frutos, Vega et al. 2007). Maturation into pre-hypertrophic chondrocytes is indicated by the loss of expression of Sox5, Sox6, Sox9, Type II α1 collagen and aggrecan, and expression of parathyroid hormone 1 receptor and Indian hedgehog, and later expression of Type X α1 collagen (Vortkamp, Lee et al. 1996, St-Jacques, Hammerschmidt et al. 1999, de Frutos, Vega et al. 2007). The progression of pre-hypertrophic to late hypertrophic chondrocytes is indicated by the loss of Type X α1 collagen expression, and the expression of vascular endothelial growth factor A and matrix metalloproteinase 13, both preluding growth plate invasion by endothelial cells, osteoclasts, and osteoblasts (Gerber, Vu et al. 1999, Carlevaro, Cermelli et al. 2000, Zelzer, McLean et al. 2002, Zelzer, Mamluk et al. 2004).

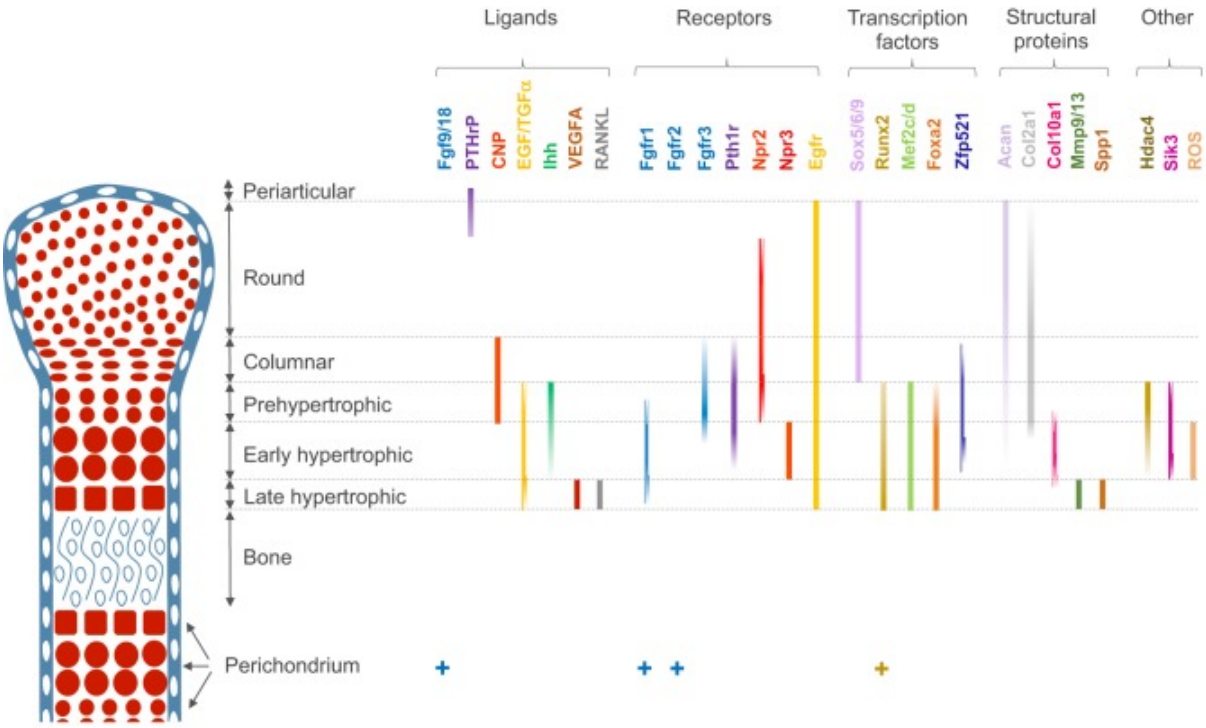


Figure 2.7: A summary of regionalised gene expression in the developing growth plate. The expression of classes of genes and/or proteins are displayed (Kozhemyakina, Lassar et al. 2015).

2.3.2 Synovial joint formation

Mature synovial joints comprise of several tissue types, such as the joint capsule, associate ligaments, and articular cartilage. The first distinct histological indication of joint development is termed the interzone, the sight of future joint cavitation. These presumptive joint sites interrupt the Y-shaped condensation of the limb buds and follow a different developmental path. The interzone consists of closely-bounded mesenchymal cells, and soon acquires a trilaminar arrangement, with two compacted cell layers bound to the epiphyseal ends of the future joint, and a more diffuse inner layer in between (Mitrovic 1977, Mitrovic 1978). Mesenchymal cells at the interzone become flattened, and begin expression of *WNT4*, *WNT9a*, and *GDF5* (Mitrovic 1977, Storm and Kingsley 1996, Storm and Kingsley 1999, Hartmann and Tabin 2001, Koyama, Shibukawa et al. 2008). Similarly to long bone development, major events in synovial joint development occur over different timescales in the human, mouse, and chick (Figure 2.8). The interzone cells are crucial for the development of synovial joints. Excision of the elbow interzone from e4.5 chick embryos leads to an uninterrupted, continuous forelimb bone, and failure of cavitation in the humerus, radius and ulna (Holder 1977). Additionally, mechanical disturbance of the joint interzone in chicks at e4.5 deranges joint formation at e10 by delaying separation of opposing joint rudiments, with weak definition of epiphyseal ends (Figure 2.9) (Rux, Decker et al. 2019).

Koyama *et al*. previously proposed that interzone cells serve wholly as joint progenitors, known as the interzone progenitor model (Koyama, Ochiai et al. 2007, Koyama, Shibukawa et al. 2008). This model states that once the interzone has formed, all cells of the interzone are specified as joint progenitors for tissues as diverse as articular cartilage, intra-joint ligaments, menisci, and the lining of the synovium, designated by *GDF5* expression (Koyama, Ochiai et al. 2007, Koyama, Shibukawa et al. 2008). However, a recent study proposed the influx model of joint development, based on experiments indicating that cells outside of the interzone are integrated by continuous flux into the developing joint, and that joint-forming cells are not specified in one single early event (Shwartz, Viukov et al. 2016). *SOX9*-positive, *GDF5*-negative cells from the joint vicinity migrate into the developing joint, activate *GDF5* expression, and temporally contribute to different regions of the developing joint (Shwartz, Viukov et al. 2016).

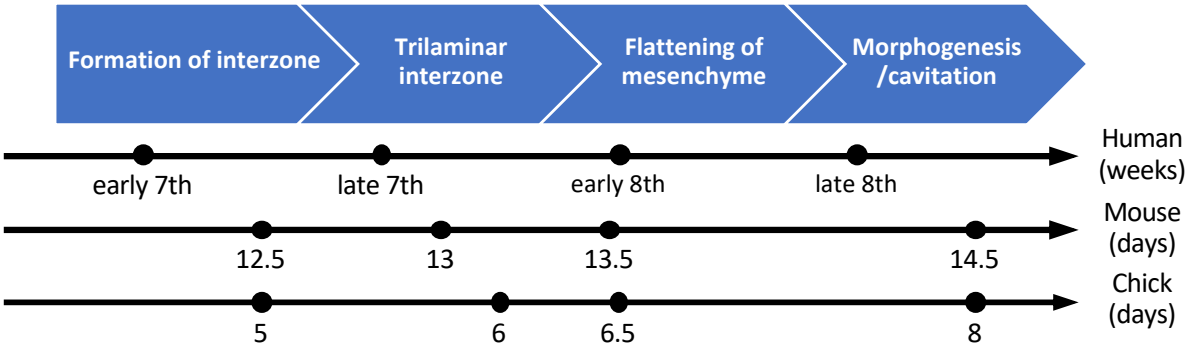


Figure 2.8: The first appearance of key events during early human, mouse and chick joint development (Fell 1925, Fell and Canti 1934, Gardner, Gray et al. 1959, Gardner and O'Rahilly 1968, O'Rahilly and Gardner 1972, Hall 1987, Hall and Miyake 1992, Kahn, Shwartz et al. 2009, Nowlan, Bourdon et al. 2010)

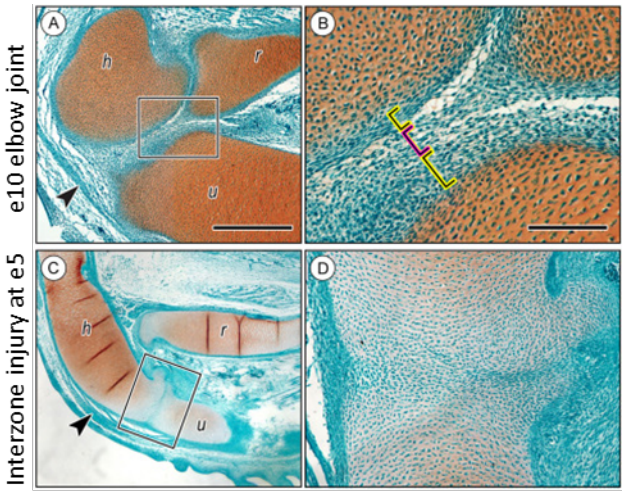


Figure 2.9: Images of chick e10 control elbow showing the humerus (h), radius (r), and ulna (u). (B) Magnified image of boxed area in (A) showing well-separated rudiments. (C and D) Images of e10 elbow wherein the interzone was mechanically damaged at e5. Joint development was substantially delayed, as noted by minimal separation of the opposing elements and by defective definition of the epiphyses compared to controls. Scale bar for A and C, 250um; for B and D; 100um. Adapted from Rux and Decker (Rux, Decker et al. 2019).

2.3.3 Cavitation

Cavitation is critical to the progression of joint formation, and failure leads to abnormal joint form and function. Cavitation is the physical separation of opposing joint rudiments along the inner layer of the trilaminar interzone, which permits the continuation of early rudiment morphogenesis into interlocking structures (Haines 1947). It is suggested that cavitation is induced by mechanical forces along the interzone, collagen fibril rearrangement, and synthesis of the fluidic extracellular matrix, in particular hyaluronan, within the joint space (Dowthwaite, Flannery et al. 2003, Pacifici, Koyama et al. 2005, Pacifici, Koyama et al. 2006). A large number of

animal models of reduced or absent movement result in a complete or partial failure of joint cavitation initiation or maintenance, indicating that fetal movement is essential for joint cavitation (reviewed in section 2.6). Additionally, production and accumulation of hyaluronan contribute to the loss of the innermost interzone tissue integrity, contributing to formation of a fluid-filled cavity and joint separation (Pitsillides, Archer et al. 1995, Dowthwaite, Edwards et al. 1998, Dowthwaite, Flannery et al. 2003, Pacifici, Koyama et al. 2005, Matsumoto, Li et al. 2009, Dy, Smits et al. 2010). The interzone is highly cellular and low in secreted matrix (Archer, Morrison et al. 1994), which causes a weakening of tissue integrity. The stiffness of the interzone is less than neighbouring cartilage, and it has been suggested that movement physically disrupts the tissue of the interzone (Ito and Kida 2000, Khan, Redman et al. 2007, Roddy, Prendergast et al. 2011).

2.3.4 Morphogenesis

Morphogenesis is the complex process by which opposing joint ends mould around each other to form complex, reciprocal, interlocking structures. Morphogenesis is considered to be the least understood aspect of joint formation, but it is known that key anatomical structures emerge prior to cavitation, with evidence suggesting that morphogenesis is a more continuous process than previously proposed (Figure 2.10) (Pacifici, Koyama et al. 2005, Roddy, Prendergast et al. 2011, Nowlan and Sharpe 2014). The mechanisms which govern morphogenesis remain unclear; however both genetic and mechanical factors have been implicated. Dynamic mechanical forces are proposed to regulate joint morphogenesis by influencing local cell proliferation, orientation, migration and differentiation, and may be responsible for joint shape changes (Roddy, Kelly et al. 2011, Brunt, Norton et al. 2015, Brunt, Skinner et al. 2016). There is a growing body of evidence that mechanical stimulation promotes cell activity and morphogenesis (reviewed in section 2.6). Recent efforts have identified putative mechanosensitive genes and multiple signalling pathways which may link mechanical forces to downstream morphological outputs (Nowlan, Prendergast et al. 2008, Roddy, Kelly et al. 2011, Rolfe, Nowlan et al. 2014). Components of the *Wnt* signalling pathways were most strongly disturbed in the Splotch-delayed immobile muscleless mouse mutant, with down-regulated genes including *Cd44*, *Dll1*, and *Fgf4*, and up-regulated including *Sfrp2*, *Dkk2*, *Rspo2* and *Rspo3* (Rolfe, Nowlan et al. 2014). This thesis contributed to the wider literature by focusing on the morphological and cavitational downstream effects of a short period of immobility, aiming to identify specific windows of time where fetal movement is particularly important for skeletal development, and testing if applied movement could partially ameliorate the effects of abnormal movements. Work in this thesis additionally describes the development a mammalian bioreactor system capable of culturing and loading embryonic limbs.

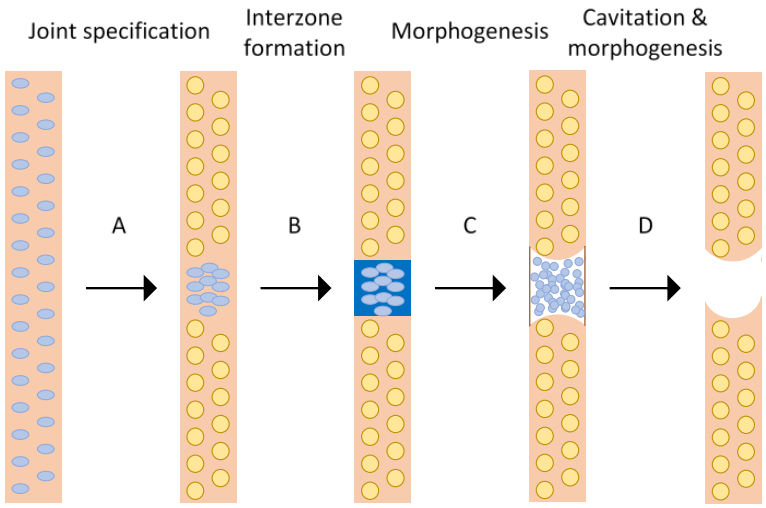


Figure 2.10: Early joint development has four stages: joint specification, interzone formation, cavitation, and morphogenesis. (a) MSCs condense within the cartilage anlagen at the site of the future joint, forming a compacted layer. (b) MSCs form a dense interzone and differentiate into joint progenitor cells. (c) Reciprocal ends of the joint begin to morph into specific joint shapes. (d) The joint ends physically separate, allowing for further morphogenesis and joint maturation.

2.3.5 Link between cavitation, movement, and morphogenesis

Cavitation is thought to be induced by muscle movements tearing weakened interzonal tissue in the future joint space (Ito and Kida 2000). It is known that movement is needed for joint cavitation and joint morphogenesis, and that there are indications that aberrant cavitation is linked to abnormal joint morphogenesis (Nowlan and Sharpe 2014). Previous experiments carried out on the chick generally focused on immobilising for relatively long periods of time (reviewed in section 2.6). Immobilisation from e4–9, for example, covers all the major steps of joint development, from the nascent limb bud, to joint cavitation and maturation of joint shape (Nowlan and Sharpe 2014). From these studies, it is known that the effects of a period of immobility vary depending on precisely when immobilisation occurs. Additionally, embryos have been harvested at varying timepoints after the critical step of cavitation. It is currently unknown whether there is a critical time period for movement leading to cavitation, and whether cavitation is sufficient for early joint morphogenesis. Is there a critical mechanosensitive event during early joint development that is suppressed during immobilisation that leads to characteristic morphological changes?

2.4 Cartilage and bone mechanobiology

Cartilage and bone are mechanosensitive tissues in adulthood, as well as during development, and there is significant evidence that normal development of cartilage and bone respond to mechanical stimulation (Nowlan, Murphy et al. 2007, Kelly and Jacobs 2010, O'Conor, Case et al. 2013, Steward and Kelly 2015). Numerous cell culture studies demonstrate that chondrocytes

and osteocytes respond favourably to mechanical stimulation, embarking on normal developmental paths. For example, at the cell level, sinusoidal tensile mechanical stimulation improved chondrocyte proliferation and cartilage phenotype (Ouyang, Xie et al. 2019), and osteoblast differentiation (Chen, Guo et al. 2017), compared to statically-cultured cells.

At the tissue level, animal models of reduced or absent movement are known to have absent cavitation, altered cartilage morphology, and reduced mineralisation (Nowlan, Bourdon et al. 2010). The question arises: can externally applied mechanical stimulation recapitulate mechanosensitive pathways, and contribute to more normal skeletal development? Few studies have explored skeletal recovery due to the effects of immobility (reviewed in section 2.6). However, no study has looked at the role of externally applied mechanical stimulation for skeletal recovery in the whole chick embryo. Additionally, no study has explored the role of applied mechanical stimulation in skeletal recovery in a mammalian model.

2.5 Clinical conditions of altered movement

Normal skeletal development is not simply driven genetically, but also mechanically. Reduced or absent muscle forces can be due to the influence of the physical environment on the fetus, or neuromuscular, where the fetus itself cannot generate movement (Nowlan 2015). Many clinical conditions, described below, are linked to a lack of fetal movement *in utero*.

Developmental dysplasia of the hip (DDH) describes abnormalities in the hip joint and denotes a spectrum of disorders affecting the hip joint, from dysplasia, to subluxation, to dislocation (Aronsson, Goldberg et al. 1994). Dyplasia refers to morphological abnormalities of the femoral head, acetabulum, or both. The typically cup-shaped acetabulum is shallower than normal, leading to a loss of the tight fit between the femoral head and pelvis. The hip may be subluxated, with the femoral head partially out of the acetabulum, or completely dislocated, with the femoral head completely out of the acetabulum (Figure 2.11). DDH typically arises *in utero* or shortly after birth. DDH is observed in 1.3 per 1000 live births (Leck 2000), and if persistent DDH is diagnosed too late, it can lead to early-onset osteoarthritis (Wedge and Wasylenko 1979). Incidence of late diagnosis of DDH is 1.28 per 1000 live births between one to eight years (Broadhurst, Rhodes et al. 2019). DDH preferentially affects the left side in 64% of patients, thought to be so as the left side is commonly adducted against the mother's spine (Aronsson, Goldberg et al. 1994). Treatment involves splinting, and in severe cases, surgery (Aronsson, Goldberg et al. 1994). Prior to birth, a reduction in or restriction of fetal movement are recognised risk factors for DDH. First-born children may be twice as likely as successive siblings to be diagnosed with DDH (Woodacre, Ball et al. 2016). This is theorised to be, in part, due to reduced elasticity of the uterus, resulting in a more restrictive uterine environment and increased compressive forces on first-born fetuses

(Ortiz-Neira, Paolucci et al. 2012). One study demonstrated a decreasing risk of DDH with increasing parity (Chan, McCaul et al. 1997). Reduced amniotic fluid, or oligohydramnios, is considered an independent risk factor for DDH, likely due to a constrictive uterine environment (Manoukian and Rehm 2019). The displacement of the uterine wall in cases of oligohydramnios is shown to be significantly less than those of normal pregnancies, with significantly decreased kick forces, decreased change in joint angle, and some decreased muscle forces (Verbruggen, Kainz et al. 2018). Breech position, where the movement of the hips is limited, is also a risk factor for DDH (Muller and Seddon 1953). Displacement of uterine wall is significantly lower in breech babies compared to cephalic babies, as was kick reaction force (Verbruggen, Kainz et al. 2018). Breech presentation predisposed the hip to decreased stability which is present prior to birth, and not a result of delivery forces (Andersson and Oden 2001). Other conditions that lead to a restriction of movement within the intrauterine environment, such as a small uterus, or large fetus, are environmental risk factors for DDH. Interestingly, twins do not have any increased risk of DDH, despite their obvious restriction of space *in utero* (De Pellegrin and Moharamzadeh 2010). In one recent computational study, no significant difference was found between twins and single babies in kick force or uterine wall displacement (Verbruggen, Kainz et al. 2018). One theory posits that the movement and interactions between twins increase the biomechanical stimulation at the developing hip (Verbruggen, Kainz et al. 2018).

Arthrogryposis multiplex congenita (AMC) describes multiple congenital contractures present at birth. AMC is present in 1 in 3000 to 5000 live births, with genders equally affected (Lowry, Sibbald et al. 2010). The etiology of AMC is unclear, but any factor which decreases fetal movement may result in joint contractures. The most common reasons for a reduction in fetal movement are abnormal muscle and/or neural development (Bamshad, Van Heest et al. 2009). There are two types of AMC, based upon a normal or abnormal neurological examination. If abnormal neurological function presents, it is indicative of abnormalities in the central nervous system or neuromuscular system due to dysgenesis, degeneration, or both. If normal neurological function present, it is indicative of connective tissue disorders, amyoplasia, or decrease in uterine space (Hall (Hall, Reed et al. 1983, Bamshad, Van Heest et al. 2009). This lack of joint movement is linked to the development of extra connective tissues around affected joints, which in turn leads to contractures and fibrosis, and accounts for one third of all cases of AMC. All forms of AMC are associated with reduction of fetal movement. Treatment involves casting and splinting, physical therapy, surgical reductions and soft tissue release.

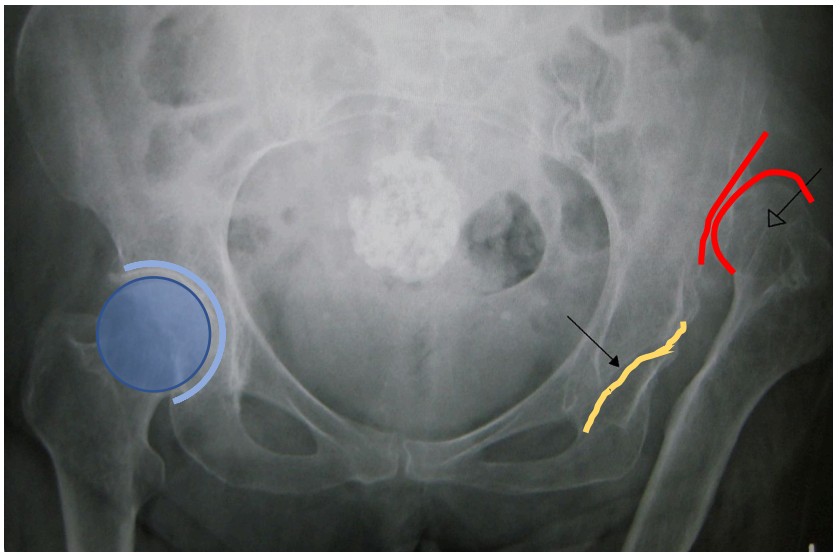


Figure 2.11: Congenital dislocation of the left hip. Closed arrow and yellow line indicate the original acetabulum, which has resorbed. Red line indicated formation of a false acetabulum from the dislocated femoral head. Red curve indicated flattening of femoral head. Adapted from Heilman (Heilman 2010).

Fetal akinesia deformation sequence (FADS) is a condition characterised by decreased fetal movement, with the incidence estimated as 1 in 15000 (Bayat, Petersen et al. 2009). FADS is a description of a recognised sequence of abnormalities resulting from absent or decreased fetal movement (Kirkinen, Herva et al. 1987, Nemec, Nemec et al. 2011). The main symptoms of FADS include multiple joint contractures (AMC), facial abnormalities, increased amniotic fluid due to absence of fetal swallowing, intrauterine growth restriction, and pulmonary hypoplasia (Hall 2009). Genetic, environmental and maternal factors have been recognised as underlying causes for fetal akinesia, including neurological abnormalities, muscles dystrophies and dysplasias, and connective tissue disorders (Hall 2009). Common skeletal symptoms include thin, fracture-prone bones, thick or absent clavicles, adducted thumbs, congenital kyphosis scoliosis, lumbar lordosis, dislocations, and clubfoot (Hall 2009). Affected fetuses almost always die *in utero* or very shortly after birth, due to pulmonary hypoplasia (Hall 2009).

Metabolic bone disease of prematurity is a consequence of pre-term birth which leads to skeletal demineralisation, bone softening, and bone fractures. The condition can range from altered biochemistry, to overt rickets and pathological fractures (Sharp 2007). The incidence is in 30% of pre-term infants (Sharp 2007). Pre-term infants miss important developmental steps in the third trimester. The third trimester not only accounts for 80% of fetal bone mineralisation acquisition (Greer 1994), but also the mechanical loads exerted on preterm bones is lower than *in utero* loads (Sharp 2007). Movement of the embryo in the third trimester has been compared to 'resistance training', where decreased uterine space and fetal movement leads to high stress

and strain in the skeleton. (Sharp 2007). In premature infants, physical activity combined with massage was shown to improve bone mineralisation (Aly, Moustafa et al. 2004), with spontaneous activity also affecting bone strength (Eliakim, Nemet et al. 2002). The impact of metabolic bone disease of prematurity has not been fully established, due in difficulty controlling inter-related factors such as birth weight, comorbidities, nutrition, and later diet (Chinoy, Mughal et al. 2019).

2.6 Animal models of altered movement

Researchers have long used animal models of abnormal fetal movement to observe the impact of fetal movement on joint cavitation, yet fewer on joint morphogenesis. Studies in the chick embryo demonstrate that movement is needed for cavitation in almost every major synovial joint, through avascular and aneural hind limb transplantation (Fell and Canti 1934, Hamburger and Waugh 1940), pharmacological immobilisation with decamethonium bromide (DMB) (Drachman and Coulombre 1962, Drachman and Sokoloff 1966, Murray and Drachman 1969, Mitrovic 1982, Osborne, Lamb et al. 2002, Nowlan, Chandaria et al. 2014), spinal cord extirpation (Drachman (Drachman and Sokoloff 1966, Murray and Drachman 1969), and through explant culture in vitro (Fell and Canti 1934, Lelkes 1958, Mitrovic 1982, Chandaria, McGinty et al. 2016). The chick provided some of the earliest insights into joint development and cavitation. Experiments initially focused on observation of cavitation, but more current studies have been using 3D shape analysis. Mammalian models of reduced movement provide insight into *in utero* environmental conditions needed for joint development, but also use mutant models of impeded muscle development and mechanical stimulation to the developing embryo. Other organisms, such as the zebrafish, are notable for the ability to image all joint musculoskeletal tissues at high resolution to explore the jaw joint.

2.6.1 Chick models

Several studies have used the immobilised *in ovo* chick embryo to explore the role of movement on joint cavitation, thus keeping the developing joint in its native environment. Decamethonium bromide (DMB) has commonly been used to induce rigid immobilisation in chick embryos, causing all muscles to enter a state of tetanus. *In ovo* transplantation of nerveless limbs to a ventral or coelomic location leads to smooth, undetailed articulating surfaces and frequent primary or secondary fusion of joints (Hamburger and Waugh 1940). *In ovo* immobilisation with DMB, botulinum toxin or spinal cord extirpation leads to joint fusion and the absence of nearly all articular cavities in the head and neck of the chick by embryonic (e) day 19 (Murray and Drachman 1969). Correspondingly, *in ovo* immobilisation of chick embryos from e7–9 inhibits cavity formation in the knee, ankle and toe joints, and immobilisation from e8–11 results in absent or minimal cavitation in the knee, ankle and toe joints. Immobilisation from e4–9 resulted

in loss of cavitation of the hip joint (Nowlan, Chandaria et al. 2014) (Figure 2.12). Immobilisation in chicks from e6–8 and e7–8 show normal joint development at e8 in the knee, ankle and toe joints, prior to cavitation. Immobilisation of chicks with DMB from e7–10 irreversibly inhibits cavitation of the metatarsophalangeal joints at e21, whilst immobilisation in older embryos at e15–20 causes rapid regression of the previously fully-differentiated joint cavity by e21, replaced by fibrovascular or fibrocartilaginous tissue in all metatarsophalangeal joints. Movement is thus required for the full development and maintenance of the cavity (Drachman and Sokoloff 1966).

Rigid immobilisation with DMB and flaccid immobilisation with pancuronium bromide (PB) show a differential effect on the maintenance of the joint cavity in the chick embryo (Osborne, Lamb et al. 2002). Chicks were immobilised with either DMB or PB from e10–13 (prior to knee, ankle and metatarsophalangeal joint cavitation) or e13–15 (after knee, ankle and metatarsophalangeal joint cavitation). In the knee, ankle and metatarsophalangeal joints of chicks treated with either DMB or PB from e10–13, cavitation is completely absent at e13. In chicks treated with PB at e13–15, cavities disappear. Hence, short-term induction of immobilisation results in absent cavity formation, which leads to loss of overt joint spaces and cartilaginous fusion of articular cartilage in the chick knee, ankle and metatarsophalangeal joints. However, in chicks treated with DMB at e13–15, partial retention of the cavity is apparent (Osborne, Lamb et al. 2002). These data suggest that a joint cavity may be maintained under influence of static loading, whereas complete loss of both static and dynamic muscle activity results in the deterioration of cavity space.

Of the few studies that explore the role of movement upon joint shape, the immobilised, embryonic, post-cavitational chick has provided much of the information known, with a general

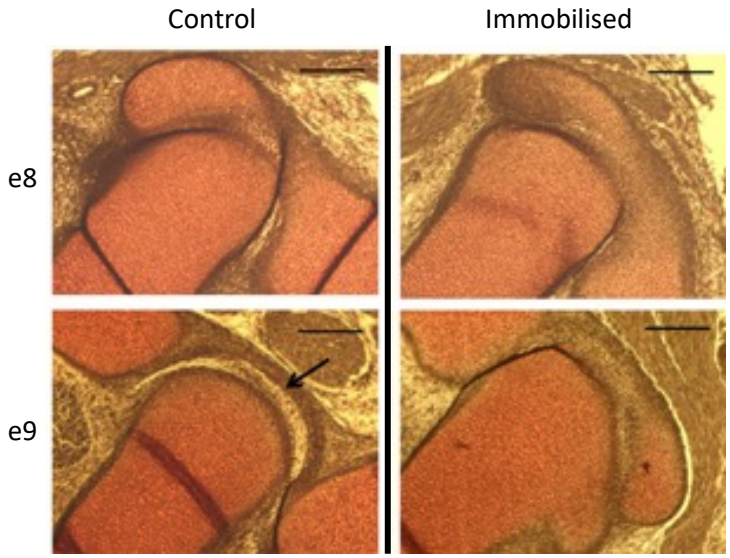


Figure 2.12: Histological sections of the right hip joint through the anterior-posterior plane of the femur for each timepoint. Cavitation of the hip joint has occurred by e9 in the controls but not in the immobilized specimens. Adapted from Nowlan (Nowlan, Chandaria et al. 2014).

'simplification' of shape seen. When immobilised with DMB from e8–11, e11 chick embryos develop flattened condyles as seen in histological sections (Drachman and Sokoloff 1966) whilst light microscopy reveals flattened knee, ankle and metatarsophalangeal joint epiphyses when immobilised with DMB or PB from e10–13 (Osborne, Lamb et al. 2002). 3D imaging using Optical Projection Tomography (OPT) has allowed for complex 3D joint shape analysis (Sharpe, Ahlgren et al. 2002). Immobilisation from e4.5–9 and e4.5–10 has a significant effect on the chick knee joint, causing a significant reduction in the width of the proximal epiphysis of the tibiotarsus and fibula. The condyles of the distal femur also flatten abnormally in the dorsoventral and lateral planes, as do the ventral outgrowths of the condyles (Figure 2.13) (Roddy, Prendergast et al. 2011). The immobilised chick hip from e4–9 also simplifies in morphology, with abnormal protrusion, flattening, and acetabular coverage of the femoral head, and abnormal orientation of pelvis relative to femur (Nowlan, Chandaria et al. 2014). Recently, the link between cavitation and shape has been explored in the chick. It is now known that morphogenesis precedes cavitation, with major anatomical features in the hip observable prior to cavitation (Nowlan, Chandaria et al. 2014). Embryonic chick hip joint cavitation initiates at embryonic day (e) 8.5, and is completed at e9. Chick hips immobilised continuously from e4 which were examined pre-cavitationally (e7 and e8) are morphologically indistinct from control hips (Nowlan, Chandaria et al. 2014). However, post-cavitationally, almost all aspects of the immobilised hip are affected. If cavitation fails to occur due to immobilisation, joint shape maturation also halts past e8.5 (Nowlan, Chandaria et al. 2014).

Early *in vitro* studies involved statically culturing limb explants or fragments of developing tissues. In cultivated *in vitro* chick knee explants, joint differentiation ceases and actual fusion of joint rudiments takes place, with absent knee joint cavitation by e6. Although earlier stages of joint formation can proceed in the complete absence of muscular action, nerve, and blood supply, joints cannot persist under static conditions (Fell and Canti 1934). This conclusion was corroborated with added manual manipulation of statically-cultured e6 chick knee joints. Movement of *in vitro* knee explants five times daily leads to development of an articular cavity and well-formed articular surfaces in the femorotibial joint, whilst unmoved knee joints experience complete cartilaginous fusion (Lelkes 1958). Complementing these studies, *in vitro* dynamic mechanical stimulation of e7 chick hind limbs cultured for 7 days within a bioreactor is shown to be dose-dependent, promoting characteristics of normal knee development, restoring condyle outgrowth that is otherwise lost in static cultures (Chandaria, McGinty et al. 2016). A physiological magnitude of movement promotes the most normal knee joint development, with under- or over-stimulation leading to detrimental effects on the joint (Figure 2.14).

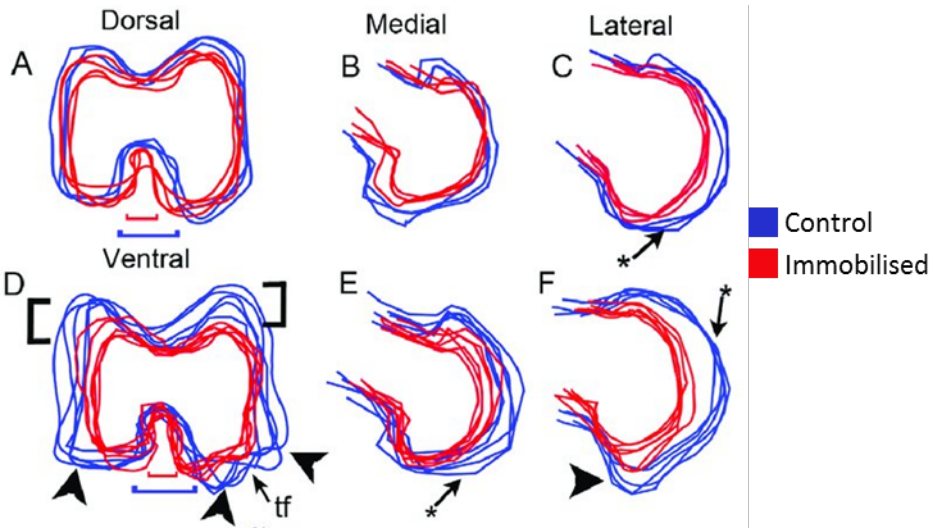


*Figure 2.13: Outlines of cartilage shape in distal femora of control (blue) and immobilised (red) chick embryos. Arrow heads indicate region of reduced outgrowth in the immobilised chick. *indicates flattening of rudiment surfaces. Black brackets show extent of growth reductions in the dorsal aspect of the condyles. Coloured brackets compare width of the intercondylar fossa of control and immobilised embryos (A, D). Adapted from Roddy (Roddy, Prendergast et al. 2011).*

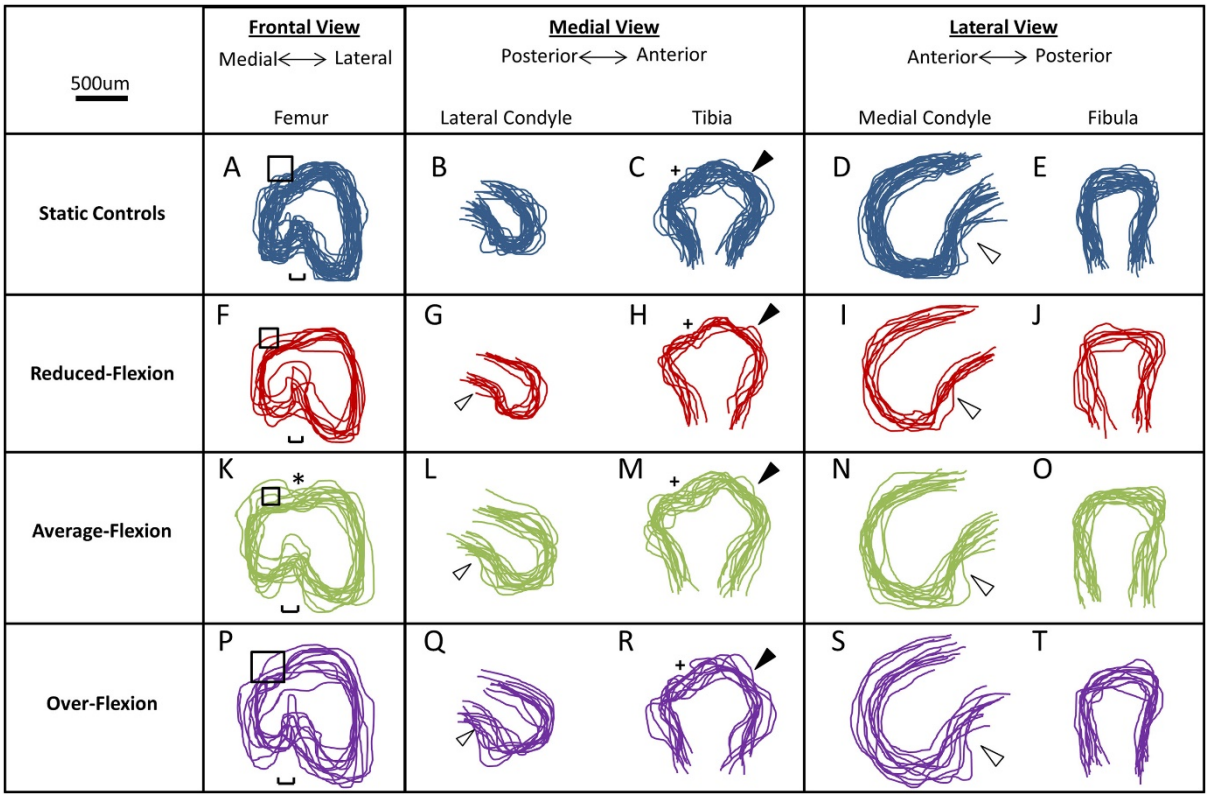


*Figure 2.14: Chick knee explants were cultured under a range of mechanical stimulation. The average-flexion movement regime led to more normal progression of morphogenesis than other movement regimes or static culture. Squares: dominance of the lateral condyle over the medial condyle; hollow arrows: posterior curl of condyles seen in moved explants; * dorsal groove between the two femoral condyles; single edged bars: intercondylar fossa; + concave curve of the tibial plateau; filled arrows: anterior tibial crest (Chandaria, McGinty et al. 2016).*

2.6.2 Mouse

Mammalian models also illustrate the critical role of fetal movement in joint cavitation. Rat embryos immobilised with injections of D-Tubocurarine (Rodriguez, Palacios et al. 1992), and simulation of oligohydramnios by daily extraction of amniotic fluid (Palacios, Rodriguez et al. 1992) presented asymmetrical joint contractures in the upper and lower limbs. Several muscleless mouse mutants have demonstrated that a reduction or complete absence of muscular contractions has a range of effects on joint cavitation. At e16.5, no hip joint cavities are present in the *mdg*$^{-/-}$ homozygous mutant (Pai 1965). At e18.5, *Splotch* mutants have craniofacial and vertebral fusions, and fusion of the shoulder and hip (Tremblay, Dietrich et al. 1998). Additionally, in mutant mouse models where limb muscles fail to develop (*splotch-delayed Sp-d*, *Six1*$^{-/-}$*Six4*$^{-/-}$ and *Myf5*$^{-/-}$*MyoD*$^{-/-}$ mice), the shoulder, elbow, some carpals, hip, and ankle joints fail to cavitate (Kahn, Shwartz et al. 2009).

Joint morphogenesis is also altered when spontaneous fetal movements *in utero* are missing. However, whereas almost all examined bones and joints of the immobilised chick are similarly affected by immobility, murine models of absent muscle have shown that the forelimb rudiments are more severely affected than the hind limb (Kahn, Shwartz et al. 2009, Nowlan, Sharpe et al. 2010, Sotiriou, Rolfe et al. 2019). The concave-convex morphology at the humeroradial joint is lost in *splotch-delayed*, *Six1*$^{-/-}$*Six4*$^{-/-}$ and *Myf5*$^{-/-}$*MyoD*$^{-/-}$ mice at e18.5, whereas the knee joint was intact (Kahn, Shwartz et al. 2009). Myogenin-mutant (*myg*^{m1}/*myg*^{m1}) mice have abnormal curvature of the vertebral column, and deformation of ribcage with abnormal alignment of ribs to vertebral bodies. The mutant sternum is 55% of the length of the control sternum, excessively ossified, with the intersternebral cartilage reduced or absent. The myogenin-mutant skeleton is overall more fragile (Hasty, Bradley et al. 1993). *The Myf5*$^{-/-}$*Myod*$^{-/-}$ double knockout has a shorter mandible, scapula, clavicle, femur, and tibia, an abnormal sternum, and an absent humeral deltoid tuberosity in e18.5 mice. There is reduced separation between the radius and ulna, and tibia and fibula. However, the shape and size of the knee joint are identical between wild-type and *Myf5*$^{-/-}$*Myod*$^{-/-}$ double knock-outs (Rot-Nikcevic, Reddy et al. 2006, Rot-Nikcevic, Downing et al. 2007). At e14.5, the muscleless mouse mutants *Myf5*$^{nlacZ/nlacZ}$*MyoD*$^{-/-}$ and *Splotch* have significant decreases in bone formation in the scapula, ulna, humerus, and femur. The elbow joint has a reduced joint line in both mutants, and a smaller humeral deltoid tuberosity in *Myf5*$^{nlacZ/nlacZ}$*MyoD*$^{-/-}$, and change in deltoid tuberosity shape but not size in *Splotch* mutants. However, in both mutants, the knee had few obvious shape abnormalities compared to the elbow (Nowlan, Bourdon et al. 2010, Nowlan, Sharpe et al. 2010). A detailed study on the reduced muscle *Myf5*$^{nlacZ/+}$*Myod*$^{-/-}$ and *Myf5*$^{nlacZ/nlacZ}$*Myod*$^{-/-}$ muscleless mutants revealed that the muscleless shoulder joint has a reduced glenoid cavity depth with flatter humeral heads, and an absent

greater tubercle. The humeral head height and axial width significantly increases in reduced muscle compared to muscleless. Reduced muscle mice also have wider distal humeral condyles in the elbow, with altered intercondylar region (Figure 2.15). Again, the knee was less affected compared to the elbow joint (Sotiriou, Rolfe et al. 2019).

2.6.3 Zebrafish

Pharmacological immobilisation of pre-cavitational zebrafish embryos demonstrate altered jaw morphology, and differential mechanosensitivity of the Meckel's cartilage and palatoquadrate, with Meckel's cartilage more affected by immobilisation and abnormally overlapping the palatoquadrate, leading to altered joint function (Figure 2.16). Temporally immobilising zebrafish shows that later muscle activity is required for normal joint shape. This study also concludes that muscle activity and not presence of muscle is required for joint integrity (Brunt, Norton et al. 2015). Flaccid immobilisation, rigid immobilisation, and hypermobility of the zebrafish jaw joint also affects the cartilage elements and jaw joint shape, by failed alignment of the Meckel's cartilage and palatoquadrate, an overlapping of the medial surface of the joint, and an enlarged lateral edge gap (Brunt, Skinner et al. 2016).

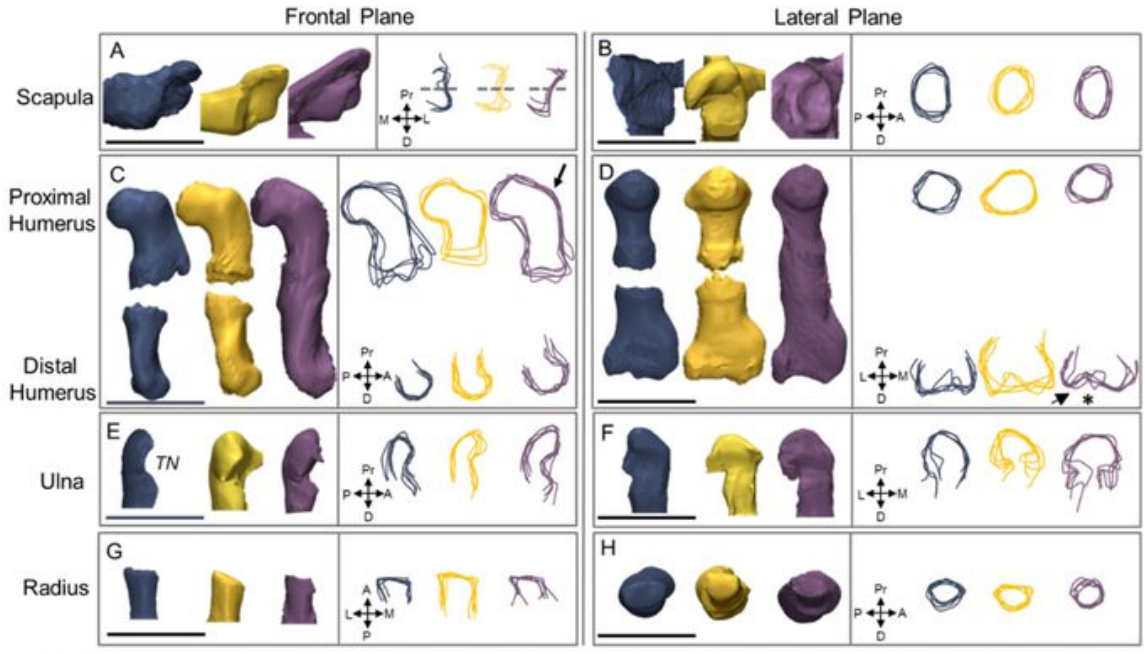


Figure 2.15: Control (blue), reduced muscle (yellow), and muscleless (purple) murine forelimb rudiments. Key features of shape changes in the joints include: abnormal angle and increased height of the glenoid cavity in the muscleless group (A, B, purple outlines), abnormal prominence of the lateral condyle in the distal muscleless humerus (D, arrowhead) and greater variation in the shape of the proximal ulna in the reduced and muscleless groups (F, yellow and purple outlines). Adapted from Sotiriou (Sotiriou, Rolfe et al. 2019).

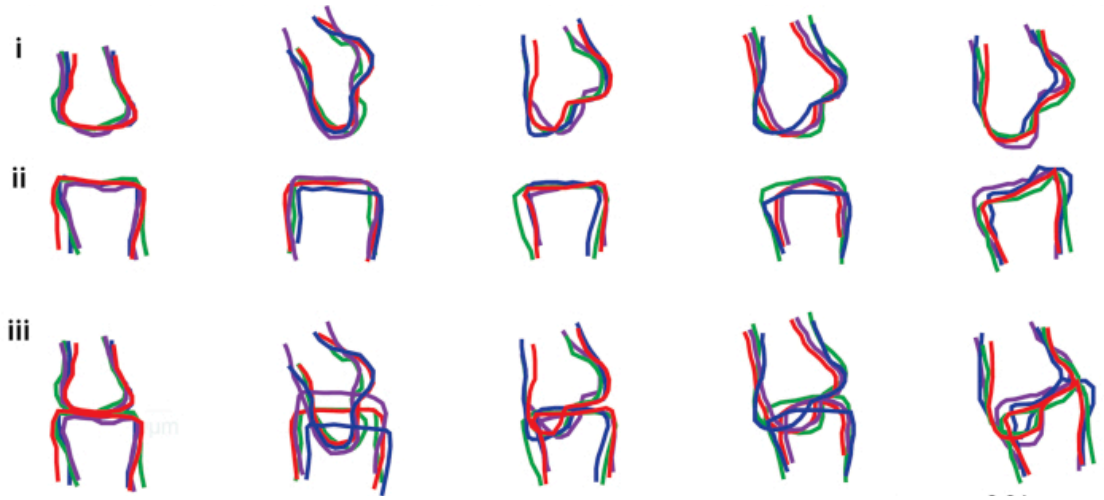


Figure 2.16: Representative outlines of the 5dpf zebrafish jaw joint for each condition (n=4). Meckel's cartilage jaw joint element (i), palatoquadrate jaw joint element (ii) and both elements to show the interaction between the Meckel's cartilage and palatoquadrate at the jaw joint (iii). Adapted from Brunt (Brunt, Norton et al. 2015) .

2.6.4 Joint forces in animal models of immobilisation

It is well known that joint movements are the result of muscle contractions producing force, which result in skeletal stimulation in the form of stress and strain. The physiological force generated within a joint in response to forces acting upon the joint is known as the joint reaction force (Martin, Burr et al. 1998). Isotonic contraction generates force by changing the length of the muscle, and can be concentric, causing the muscle to shorten, or eccentric, causing muscle to elongate in response to a greater opposing force (Betts, Young et al. 2013f). Isometric contraction, on the other hand, generates force without a change in muscle length (Betts, Young et al. 2013f). Various models of immobility affect the normal forces and muscle contraction exerted in the developing joint. DMB acts as a depolarising neuromuscular blocking agent, binding to the acetylcholine receptors of the motor end plate and generating an action potential. DMB is resistant to breakdown and leads to continued depolarisation of all skeletal muscle fibres (Macharia, Patel et al. 2004). Hence, in pharmacological immobilisation with DMB, the muscle is contracted but fails to move, undergoing isometric muscle contraction and static loading, but losing dynamic muscle loading. In contrast, immobilisation with a non-depolarising neuromuscular blocking agent such as pancuronium bromide leads to flaccid paralysis, whereby the muscle losing both static and dynamic loading upon the developing joint (Speight and Avery 1972). In *splotch-delayed* mutant mice, muscle progenitors fail to migrate to the limb, so the embryonic mouse lacks limb muscle (Franz 1993, Tremblay, Dietrich et al. 1998). In *Myf5*$^{-/-}$*Myod*$^{-/-}$ mutant mice, muscle progenitors migrate into the limb, but fail to commit to fate, hence myofibrils are absent (Rot-Nikcevic, Reddy et al. 2006, Rot-Nikcevic, Downing et al. 2007).

These are both known as muscleless limb mutants. In the absence of functioning, contractile muscle *in utero*, joint reaction forces would also be absent. However, in mammalian models there may be extrinsic sources of mechanical stimulation, such as the movements of the mother and non-mutant littermates.

In vitro methods have also been used to explore changing joint forces. As previously mentioned, e7 chick hindlimbs were cultured onto porous foam, with applied cyclic compression to induce flexion of the knee joint and observe morphological and cellular change (Chandaria, McGinty et al. 2016, Parisi, Chandaria et al. 2018). These complex experiments attempted to define a physiological angle of flexion and replicate this, by using a movement regime most representative of physiological fetal movements. They replicated aspects of activity-inactivity cycles in normal chick fetal development, attempting to best mimic normal kinematics (Chambers, Bradley et al. 1995). However, these studies note that the model does not allow for extension of the knee, only flexion. Computational modelling would be an ideal way to explore the joint reaction force and kinetics in a complex system such as the bioreactor, with previous embryonic musculoskeletal simulations predicting joint forces in the growing limb (Giorgi, Carriero et al. 2014, Giorgi, Carriero et al. 2015, Verbruggen, Kainz et al. 2018).

2.7 Summary

This chapter has presented a review of skeletogenesis, synovial joint formation, clinical conditions and the use of animal models in joint cavitation and morphogenesis. Adult cartilage and bone are mechanically sensitive and can adapt to environmental stimuli to regulate localised growth and remodelling. Developing cartilaginous rudiments are also mechanically sensitive, with processes such as morphogenesis, cavitation and mineralisation abnormal under altered or absent prenatal limb movements. However, much is still unknown about the timing of embryonic movement on early joint development, and critical periods of mechanosensitive events. Early interventions for joint recovery remain few and far between, with no known studies in the mammalian embryo.

In this thesis, I present research that builds upon knowledge of movement during skeletal development. Specifically, the research in this thesis focused on identifying a critical time period for movement leading to cavitation in the chick, analysing the effects of externally applied mechanical stimulation in the *in ovo* chick embryo, and exploring the effects of mechanical stimulation in an *in vitro* murine model.

Chapter 3

3. Materials and Methods

Materials and methods broadly used throughout this thesis are discussed in detail within this chapter. More specific materials and methods are presented within their own chapters.

3.1 Chick

3.1.1 Incubation

Experiments using the embryonic chick were performed in the first half of this PhD. Fertilised DeKalb White eggs (Henry Stewart & Co Ltd, UK) were refrigerated upon arrival at 13° to suspend embryonic development. Prior to incubation, eggs were disinfected with 70% ethanol, and then placed along their horizontal axis into Corti Semi-Automatic incubators (The Incubator Shop, UK), which were preheated to 37.5°C.

Eggs were rotated 180° along the horizontal axis on embryonic days (e) 1 and 2, to ensure even heating and prevent adherence of the embryo to the inner shell. For all immobilisation and manipulation experiments, eggs were disinfected once more at e3, in preparation for albumen removal. A small hole was created using sterilised curved blade scissors in the blunt side of the egg, into which a sterile 17-gauge needle was guided contiguous to the bottom of the inner shell, to avoid damage to the embryo or yolk. 3ml of albumen was removed using a sterile 20ml syringe, and eggs were sealed with brown sellotape to minimise infection risk and leakage.

Subsequently, eggs were windowed to allow access to the developing embryo. At e3, eggs can be safely windowed to avoid fatal damage to blood vessels or developing membranes. After disinfection with 70% ethanol, a 3cm by 4cm rectangle of brown tape was stuck to the top of the shell, and sterile curved blade scissors used to cut an oval hole, exposing the embryo. Embryos were sealed with tape once more, and placed back into the incubator to continue development until further experimentation was needed.

Immobilisation regimes are detailed in Chapters 4 and 5.

3.1.2 Immobilisation

Sham-immobilised control embryos were administered with 100µl of 1% penicillin streptomycin (Penicillin Streptomycin, Gibco), in 1x sterile phosphate buffered saline (PBS; P4417, Sigma-Aldrich) in distilled water. Experimental embryos were treated with 100µl of 0.5% decamethonium bromide (DMB; 30520, Fluka) in 1% pencillin streptomycin/PBS solution. All solutions were warmed to 37.5°C to minimise shock to the embryo. Solutions were pipetted onto the chorioallatonic membrane, above the densest arrangement of blood vessels to promote drug uptake. Windows were sealed with sellotape and returned to incubate. DMB was administered every 24 hours according to the immobilisation protocol, to ensure immobilisation persisted. Sham immobilisation matched the treatment time of experimental embryos.

3.1.3 Membrane dissection and manipulation

Access of the late-stage chick embryo becomes hindered by the growth of vital membranes which, if penetrated incorrectly, results in death. A modified approach to membrane dissection was used (Spurlin and Lwigale 2013). At e7, sterilised curved and pointed forceps were used to carefully tear a hole in the chorion above the forelimb. Below this, a hole was then made in the amnion above the spine of the chick embryo (Figure 3.1a). The membranes were dissected sufficiently to expose the torso and hind limb. From observation, the chick embryo has the tendency to lie on its left-hand side. The right hind limb was therefore selected for manipulation (Figure 3.1b). Eggs were then sealed with brown tape, and on e8, sterilised rounded forceps were inserted between the body cavity and resting limb. The forceps were then opened, adducting the limb away from the body between a 40° and 45° angle (Figure 3.1c). As this experiment had not been previously performed, adduction between 40° and 45° was chosen to induce maximal change, based off Lelkes' 1958 paper (Lelkes 1958). The limb was then returned to the rest position, and was adducted a total of five times. Membranes were replaced over the embryo, and eggs were sealed, returned to the incubator, and harvested at e9.

3.1.4 Harvesting

Embryos were humanely harvested for morphological or histological analysis. At the end of the experiment, embryos were removed via the windowed shell using a perforated spoon. Attached blood vessels and membranes were cut away using curved blade scissors, and embryos were placed in ice-cold PBS within 9cm dishes to stun. The heart of the embryo was removed using straight forceps, and staged according to the Hamburger-Hamilton staging system (Hamburger and Hamilton 1951). A Leica EZ4HD dissecting microscope was using throughout to aid staging

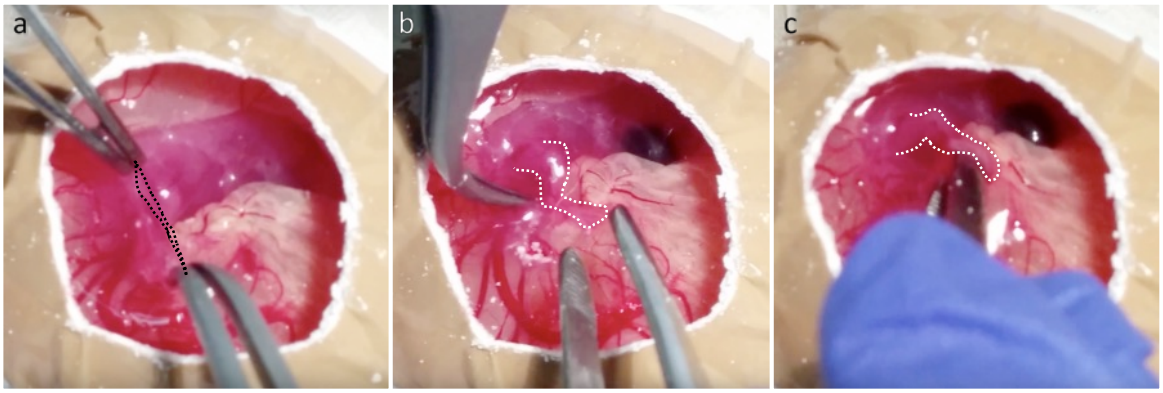


Figure 3.1: Membrane dissection and manipulation of the chick hind limb: (a) dissection of the amnion at e7 (black dotted line), (b) right hind limb of the chick pre-manipulation at e8 (white dotted line), (c) adduction of the hind limb at e8 (white dotted line)

and dissection. Heads were removed using straight forceps, and embryos placed on their ventral surface. Hind limbs were harvested by inserting the curved forceps between the spine and the medial pelvis, and gently pulling away the limb. The left-hand side were processed for OPT, and the right-hand side were processed for histology (see section 3.6).

3.2 Mouse

Experiments using embryonic mice were performed in the second half of this thesis. Embryonic hind limb and forelimb explants were cultured in a bioreactor system, with applied loading regimes.

3.2.1 Breeding

Splotch-delayed ($Pax3^{Sp\text{-}d/Sp\text{-}d}$) mice have a point mutation in the *Pax3* gene, which leads to a loss in migration of muscle progenitor cells to the developing limb (Franz 1993, Tremblay, Dietrich et al. 1998). These mice were chosen for investigation using the bioreactor culture system, as $Pax3^{Sp\text{-}d/Sp\text{-}d}$ mice show a loss in joint formation in many joints, including the elbow and the knee. $Pax3^{Sp\text{-}d/Sp\text{-}d}$ mice also display abnormal morphogenesis, with the loss of specific, interlocking shape (Kahn, Shwartz et al. 2009). Additionally, Splotch homozygotes die *in utero* at e13 or e14, whereas splotch-delayed homozygotes survive until birth, making them ideal for this thesis (Auerbach 1954, Moase and Trasler 1992). Heterozygous Splotch-delayed mice were purchased from JAX Labs, and the colony bred and maintained at Imperial College London. Both heterozygous and wild-type mice were housed within Imperial College London. Heterozygous mice conveniently have the phenotype of a white belly splotch, avoiding the need for polymerase chain reaction. Heterozygous Splotch-delayed mice were paired in triads, and were observed for plugs overnight. Mice were assumed to be pregnant if a plug was found, and gestation was estimated at e0.5 the morning after. Timed mated wild-type mice were used to supplement the breeding mice. All mice had a background of C57/BL6.

3.2.2 Harvesting

At the appropriate point in embryonic development, pregnant females were culled using cervical dislocation. After cessation of heartbeat, secondary confirmation of death by permanent cessation of circulation using femoral dissection was performed. The abdomen of the female was opened up using curved blade scissors, and both uterine horns removed. Embryos were carefully removed from individual amniotic sacs using curved and pointed forceps, and detached from individual placentae. Embryos were humanely culled by decapitation, and immediately stored in warmed media (see section 3.4.2).

3.2.3 Dissection

Embryos were staged according to Theiler Staging, then rapidly dissected. Embryos were placed on their ventral side in 9cm dishes with a 2mm layer of warmed media to prevent dehydration. A Leica EZ4HD dissecting microscope was used throughout to aid in staging and dissection. Curved forceps were inserted between the medial side of the pelvis and spine, and hind limbs gently pulled away. Curved forceps were then inserted between the scapula and ribcage, and the forelimb gently pulled away. The left-hand side was reserved for bioreactor culture and stored in 37.5°C media, and the right-hand side was reserved as a baseline measure of morphology.

3.3 Development of mammalian culture system

3.3.1 The bioreactor, and current culture set-up

A biological reactor, or, bioreactor, provides a controllable, closed environment which supports biological growth. The Ebers TC-3 bioreactor (Don Whitley Scientific, UK) was used throughout this thesis. The TC-3 is composed of autoclavable materials, with optical grade window glass at the top of the chamber, allowing for easy inspection of samples. The TC-3 bioreactor can apply a uniaxial compressive loading regime into individual bioreactor culture chambers. Up to three culture chambers can be actuated simultaneously upon the bioreactor, with compressive loads distributed equally. The force is applied through a single driving arm, attached to each chamber. Complex loading profiles can be applied upon culture samples through control software (Ebers T-3). The TC-3 can be configured in both horizontal and vertical configurations, allowing for air-liquid interface or fully-submerged cultures.

Previous work in our group has established an optimised embryonic chick hind limb culture model, including the explant support system (Chandaria 2017). In brief, the ideal support system would fit within the culture chambers, allow the perfusion of culture media and nutrients to tissue explants, have a consistent support factor with minimal fatigue, and would prevent tissue explants from slipping (Figure 3.2)

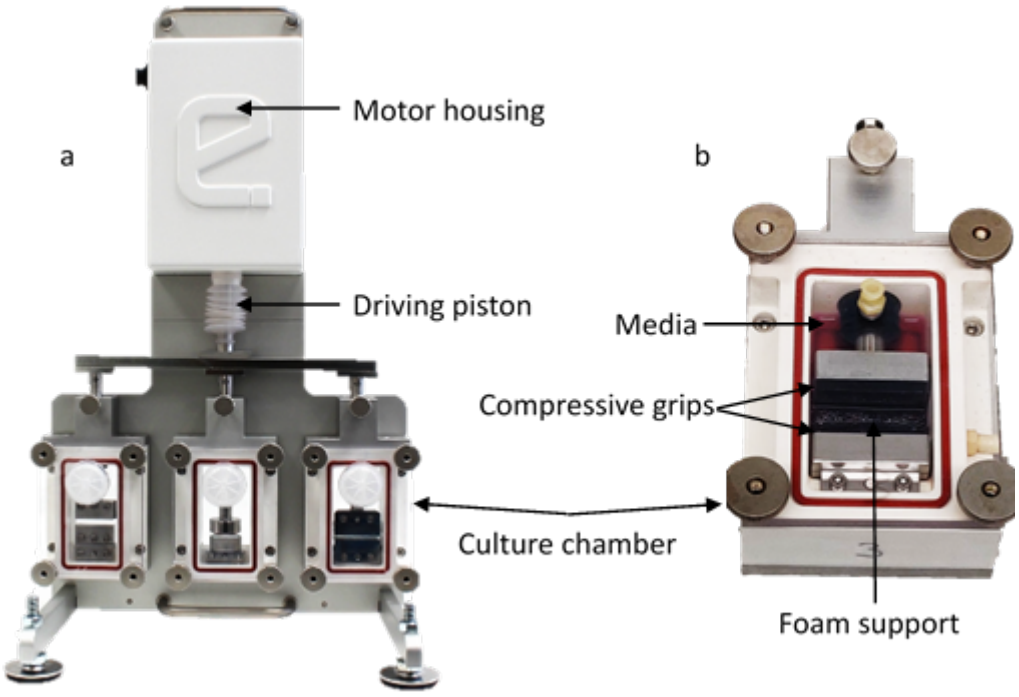


Figure 3.2: (a) Ebers TC-3 bioreactor system and (b) compression culture chambers with foam support and culture media (Ebers Med Tech SL, 2019).

Mechanical tests revealed that 45 pore per inch (PPI) polyurethane foam scaffolds with a step cut into them provided the best support with the least fatigue, and allowed for physiological flexion in the chick knee (Chandaria 2017). Foams, along with chambers, were autoclavable.

Chick hind limb explant culture conditions such as methods of nutrient delivery, presence of soft tissue, and culture have also been explored. Culture at air-liquid interface, with explants stripped of soft tissue, and for up to six days was found to favour more normal knee joint development (Chandaria 2017).

Due to previous validation, it was decided to use the same foam and 'step' set-up for the mouse hind limbs and forelimbs (Figure 3.3). Culture conditions to maximise nutrient delivery were also chosen, with explants cultured at an air-liquid interface with soft tissue stripped. An air-liquid interface allows for improved gas exchange, and has been reported to enhance viability and ability for bone formation (Smith, Locke et al. 2010), increase oxygen tension in cultured tissue (Smith, Locke et al. 2010), and increase bone development in cultured chick femora (Kanczler, Smith et al. 2012). Soft tissue on chick explants statically cultured for three days became necrotic, the presence of which is thought to be a limiting factor for rudiment development (Chandaria 2017).

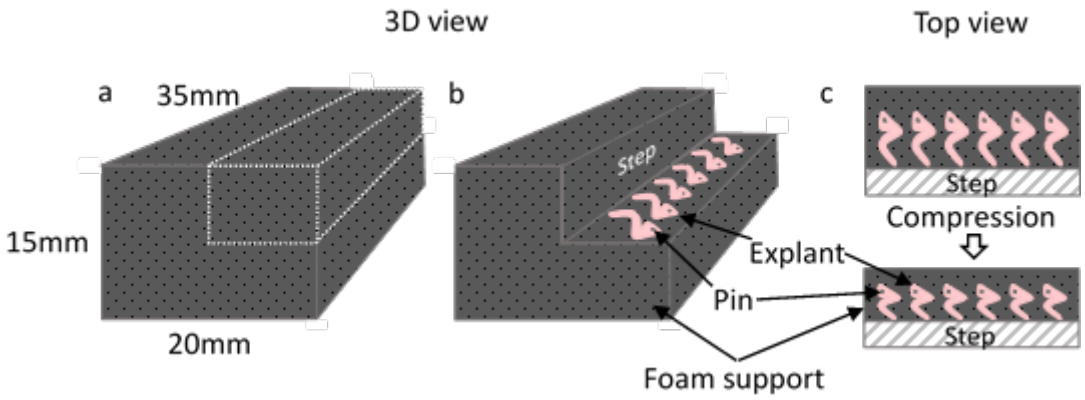


Figure 3.3: Current bioreactor set up

As the mouse hind limbs and forelimbs are of different morphologies and dimensions compared to the chick, it was decided to test for the viability of longer culture durations, decide on the age of the embryonic limbs to be harvested and cultured, and to optimise for physiological flexion.

Media used previously, consisting of alpha-minimum essential medium (αMEM) GlutaMAX (Gibco, UK) supplemented with 1% penicillin/streptomycin (Sigma-Aldrich, UK) and 100mM ascorbic acid (Sigma-Aldrich, UK) was not able to promote osteogenesis (Chandaria 2017). Hence, a modified osteogenic media was used to promote osteogenesis and, and to test whether Alizarin red staining would last long enough to be imaged. All optimisation cultures were performed under static loading conditions, so that any variation introduced by mechanical stimulation would be removed.

3.3.2 Age of limb explants

Mesenchymal precartilaginous condensations form at around e12 within the limbs, and are almost fully replaced by cartilage by e13.5–14 (Kaufman and Bard 1999). Mineralisation of osteoid is first present in the humerus at e14, and in the femur at e14.5, with more distal rudiments commencing ossification slightly later in time (Flaherty and Richtsmeier 2018). To explore the earliest stainable periods of mineralisation, it was decided to harvest and culture mouse embryonic hind limbs and forelimbs at e13.5, e14.5, and e15.5 for three days, and decide the earliest age feasible to handle and culture mouse limbs.

Hind limbs and forelimbs were harvested and prepared according to section 3.3. Dissected limbs were kept, for a maximum of one hour, in 1ml 37˚c basal media consisting of α-MEM GlutaMAX (Gibco, UK), supplemented with 1% penicillin/streptomycin (Sigma-Aldrich, UK), and 100mM L-ascorbic acid (Sigma-Aldrich, UK). This media was also used for culture. Soft tissues surrounding the explants were removed, by carefully lifting the explant with curved forceps and placing on

sterile filter paper. The explant was then rolled laterally using the same curved forceps, to carefully strip away the skin and soft tissue from the cartilage rudiment (Henstock, Rotherham et al. 2013). Explants were then returned to warmed media.

Under sterile working conditions, sterilised 45PPI foam scaffolds were saturated with sterile basal media. Explants were then placed medial side down onto the scaffolds, within sterile 6cm petri dishes. Basal media was then pipetted to a level to create an air-liquid interface, leaving the medial side of the hind limb in contact with media, and the lateral side exposed to the culture atmosphere. The petri dish lid was replaced, and placed in a 5% humidified CO_2 incubator (Sanyo, MCO-18AC(UV)). Explants were cultured for three days, with daily media changes. After culture, explants were examined visually.

The culture of e13.5 hind limbs and forelimbs for three days was deemed unviable. At e13.5, cultured explants had sunk into the foam scaffold (Figure 3.4a, d). Explants were thin and grey, and had become pulpy and soft in texture. These were very difficult to remove without breaking the tissue. The culture of explants harvested at e14.5 and e15.5 was more promising, as tissue was pink and flushed with media. Hence, it was decided to culture using hind limbs and forelimbs harvested at e14.5 and e15.5.

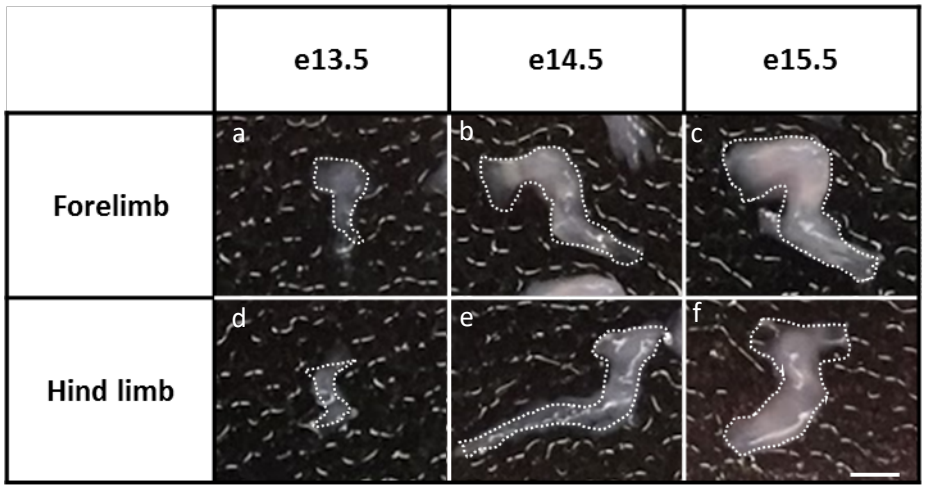


Figure 3.4: Limb explants harvested at different ages after 3 days of static culture. Scale bar=200μm

3.3.3 Culture duration, and osteogenic media

As the culture of explants aged e14.5 and e15.5 was feasible, it was next aimed to extend the culture duration from three days to six, and to examine the resulting morphology in mammalian cultures. Previous work in the chick knee has shown that joint shape changes only emerge after six days of static culture (Lelkes 1958). Additionally, chick hind limbs cultured in basal media with ascorbic acid failed to ossify (Chandaria 2017). The standard procedure for osteogenesis in cell and tissue culture is culture with 100nM dexamethasone, 2mM β-glycerophosphate and 100mM L-ascorbic acid (Langenbach and Handschel 2013). Hence, glycerophosphate, dexamethasone, and L-ascorbic acid were added to basal media to promote osteogenesis.

Previous work demonstrated that pinning each chick hind limb explant through the pelvis with a 27 gauge needle was necessary to keep rudiments in place during loading (Chandaria 2017). As murine limbs are notably smaller than chick limbs, 30 gauge needles were used instead to minimise damage to the delicate tissue. Hind limbs and forelimbs were harvested and processed as in section 3.4.2. The scapula was pinned to the foam explant close to the medial border, and the pelvis through the body of the ilium. Media was changed daily for three days or six days, dependent on culture duration. As in section 3.5, explants were stained with 0.01% Alizarin red and 0.015% Alcian blue (Figure 3.5), and imaged with OPT. Elbow and knee measurements were performed to analyse for joint shape changes (Figures 3.12 and 3.13). Mineralisation ratio was calculated for the long bones of the forelimb and the hind limb, by diving rudiment length by vertical length of reconstructed mineralised cartilage (Figures 3.12 and 3.13). Student's *t*-test was performed to assess for significant differences between three and six days of culture.

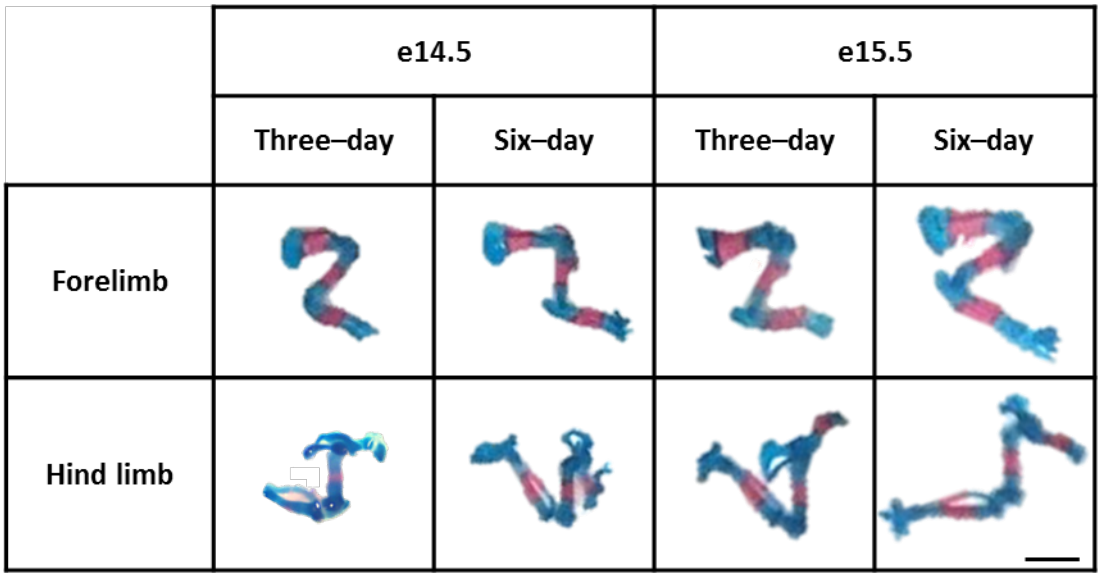


Figure 3.5: Limb explants after 3 and 6 days of static culture, stained with 0.015% Alcian blue and 0.01% Alizarin red for cartilage (blue) and mineralisation (red). Scale bar=200μm

A trend was present in the static forelimb cultures at both e14.5 and e15.5. In general, the longer, six–day period of culture led to an increase in joint measurements compared to the shorter, three–day period of culture. In the e14.5 elbows cultured for six days, six out of 13 measurements were significantly increased compared to the three–day cultures (Figure 3.6a, b, d, e). In the e14.5 elbows cultured for six days, six out of 13 measurements were also significantly increased compared to the three–day cultures (Figure 3.6a', b', d', e'). A similar trend was present in the hind limb cultures. 13 out of 18 measurements were significantly increased in the six–day e14.5 knee cultures, compared to the three–day e14.5 knee cultures (Figure 3.7a–d, f–h). In the six–day e15.5 knees, 8 out of 18 measurements were also significantly increased compared to the three–day e15.5 cultures (Figure 3.7a', b', d'–h'). In all measurements where no significant differences were calculated, trends suggested an increase in measurement length when cultured for six days compared to three days.

Compared to a three–day culture, a six–day period of culture also led to an increase in the mineralisation ratio in the long bones of the forelimb and hind limb. In the e14.5 forelimb cultures, the mineralisation ratio of the humerus was significantly increased when the culture duration was extended from a three–day period to a six–day period (Figure 3.8a). At e15.5, the mineralisation ratio of all three rudiments, the humerus, radius and ulna, increases significantly with an extended culture duration (Figure 3.8b). In the e14.5 hind limb cultures, although not significant, trends suggest a six–day period of culture increases mineralisation ratio (Figure 3.8c). By e15.5, a six–day culture of the hind limb leads to a significantly increased mineralisation ratio in all three rudiments, compared to a three–day period of culture (Figure 3.8d).

A six–day period of culture allowed for significantly larger knee and elbow joint rudiments at both e14.5 and e15.5, along with a significantly larger mineralisation ratio at e15.5 of the long bones, compared to three–day cultures. However, joint shape and mineralisation ratio changes after culture compared to baseline are still unknown. Hence, as six days of murine culture was feasible, I decided that future cultures would be carried out for six days, with a baseline against which to measure joint shape and mineralisation ratio changes.

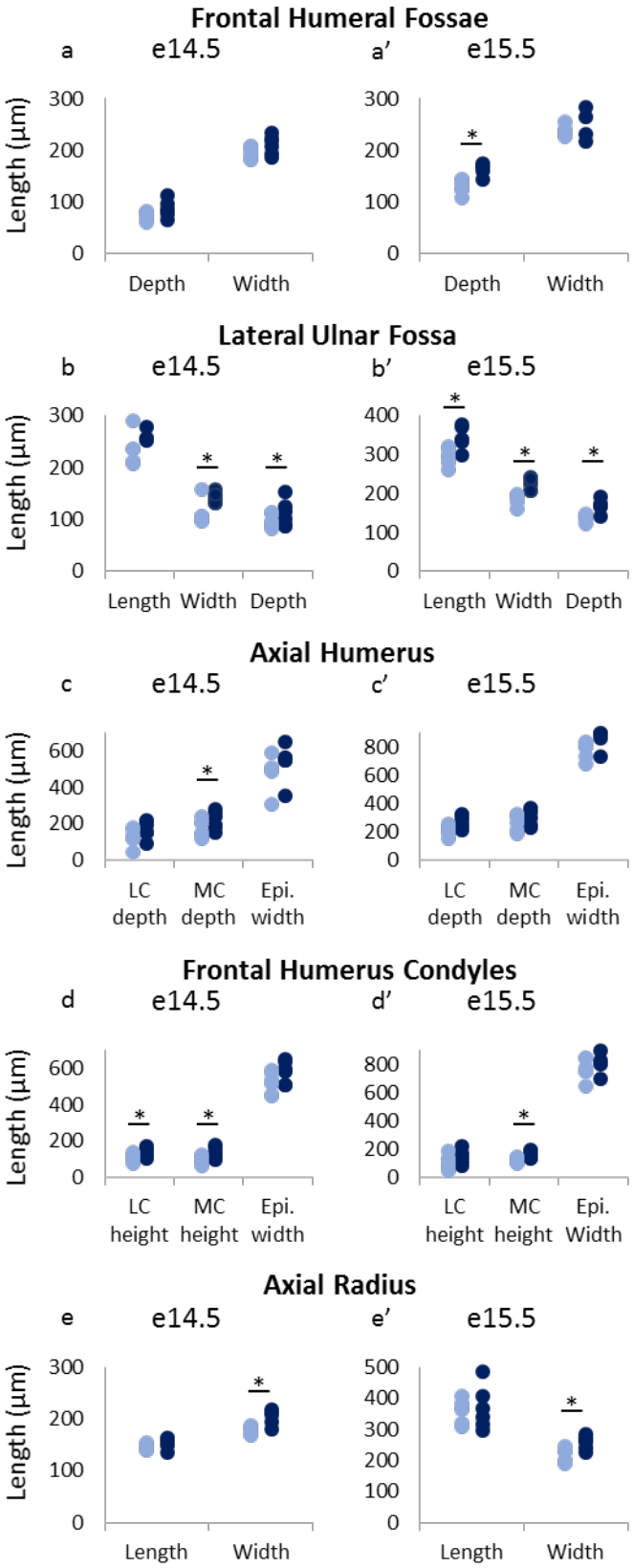


Figure 3.6: Dot plots of measurements of the murine elbow joints. Embryos were harvested at e14.5 or e15.5, and cultured for three (light blue) or six (dark blue) days of static culture. LC, lateral condyle; MC, medial condyle; Epi., epicondylar. A six–day period of culture led to a general increase in joint measurements compared to the shorter, three–day period of culture. n=6 per group

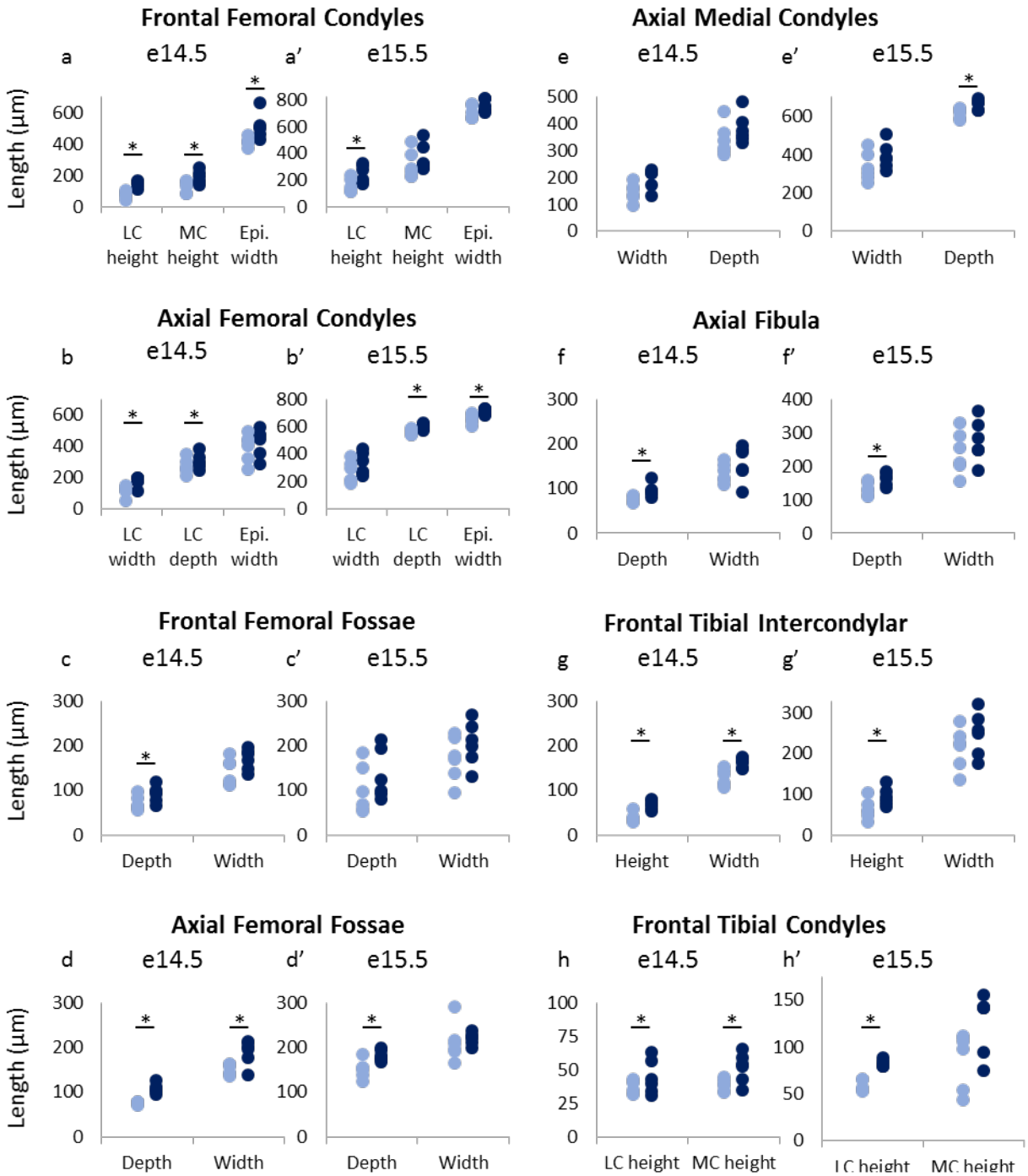


Figure 3.7: Dot plots of measurements of the murine knee joints. Embryos were harvested at e14.5 or e15.5, and cultured for three (light blue) or six (dark blue) days of static culture. LC, lateral condyle; MC, medial condyle; Epi., epicondylar. A six–day period of culture led to a general increase in joint measurements compared to the shorter, three–day period of culture. n=6 per group

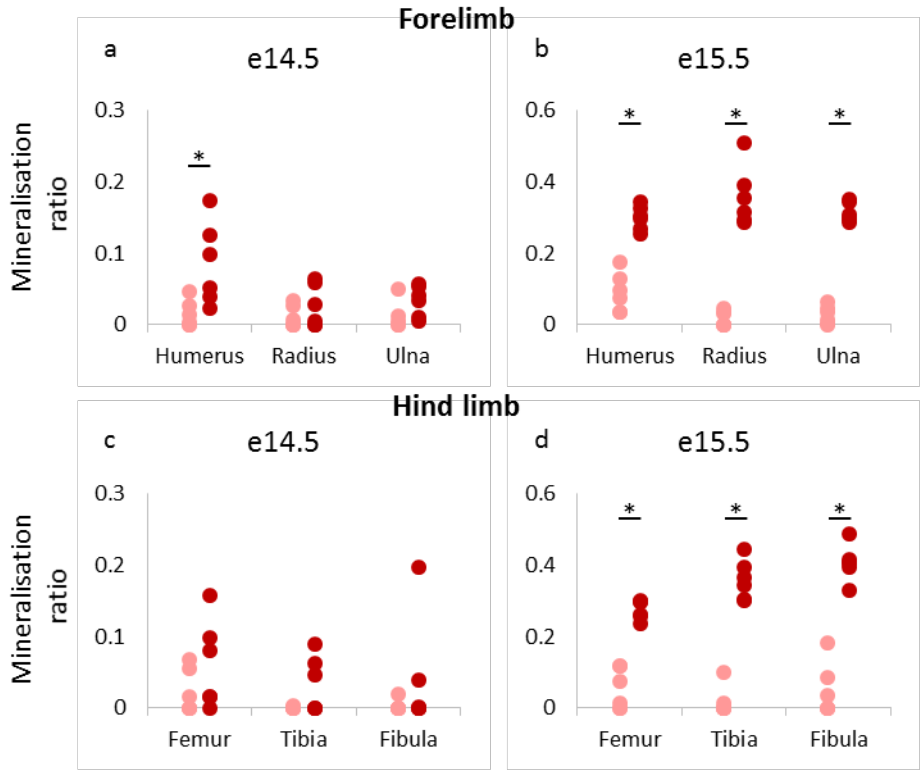


Figure 3.8: Dot plots of mineralisation ratio of the murine forelimb and hind limb rudiments, Embryos were harvested at e14.5 or e15.5, and cultured for three (light red) or six (dark red) days of static culture. A six–day period of culture led to a general increase in mineralisation ratio compared to the shorter, three–day period of culture. n=6 per group

3.3.4 Validation and calibration of mechanical stimulation

The pregnant mouse presents more challenges than the chick when quantifying fetal movement. Unlike the embryonic chick, where it is possible to window and observe movement (Hamburger and Balaban 1963), harvesting of the murine embryo rapidly leads to death. To best knowledge, analysis of typical, physiological murine knee and elbow flexion and extension movements *in utero* does not exist. Previous work has aimed for a 14˚ angle of flexion in the chick knee (Chandaria 2017), based on a 12±4˚ mean chick knee flexion from rest at e9 (Watson and Bekoff 1990). It was decided to aim for a single displacement regime which would lead to a flexion angle of between 12-18˚ for both the elbow and the knee, to best approximate physiological flexion. Initial validation tests focused on e14.5 mouse forelimbs and hind limbs. A total of 14 e14.5 freshly harvested limbs (seven forelimbs, seven hind limbs) were processed and pinned as described in section 3.4.2, with warmed media added to saturate the foams during displacement. Explants were subjected to 1, 1.5, 2, 2.5, 3, 3.5, and 4mm of cyclic compression for 60 seconds, with a rest period of five minutes between each compressive regime to allow both the explant and foam to fully recover. A loading rate of 4mm/s was used for all tests. The flexion of limb explants was validated and calibrated using video recording. Internal joint angles were measured

using the angle tool in ImageJ (Schneider, Rasband et al. 2012). Angles were measured from single frames of minimum and maximum compression, with frames selected between 45–60 seconds of loading. The difference in flexion before and after loading was calculated as the change in flexion, and averaged for the elbow and knee.

Analysis of the frames validated the flexion of both the elbow and the knee, and additionally validated the pinning position of the 30 gauge needle to hold the explant in place without damage during displacement (Figure 3.9).

In the elbow joint, the bioreactor induced 11.8±5.3˚ (mean±SD) of flexion at 1mm of displacement, to a maximum of 48.8±3.8˚ using 4mm of displacement (Figure 3.10a). In the knee, the bioreactor induced an average of 2.0±0.6˚ (mean±SD) at 1mm of displacement, to a maximum average of 51±4.9˚ using 4mm of displacement (Figure 3.10b). At e14.5, 2mm of displacement produced an average of 14.4±2.4° of flexion in the knee, and an average of 18.576±3.4° of flexion in the elbow. The average of 16.5±3.7° was considered as 'physiological' flexion for e14.5 explants. Linear regression analysis found a strong relationship between the magnitude of applied compression and angle of flexion in the elbow (R^2=0.9758) and knee (R^2=0.978) joints.

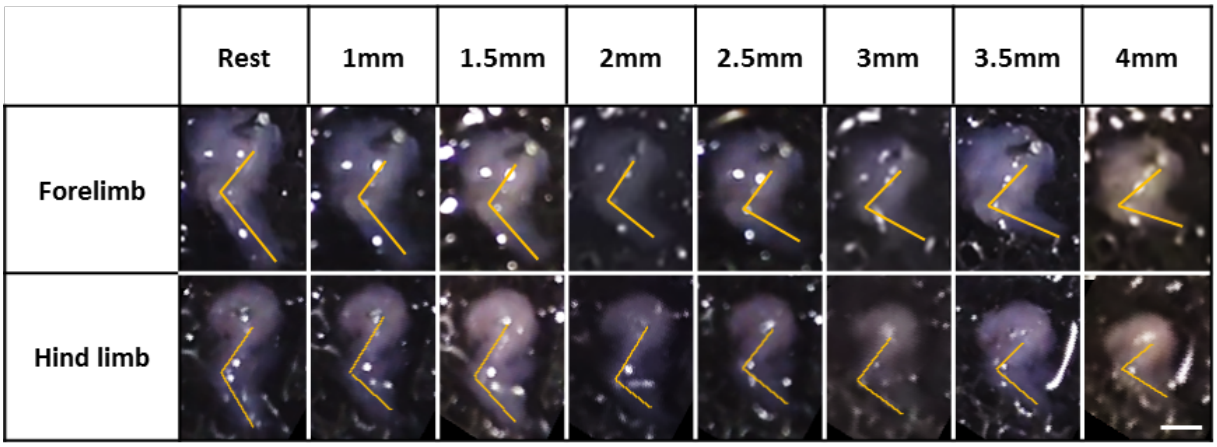


Figure 3.9: Increasing compression of the foam support resulting in a bending action at the murine elbow and knee joint at e14.5, as shown by the decrease in internal joint flexion angle. n=6 per group; scale bar=200µm

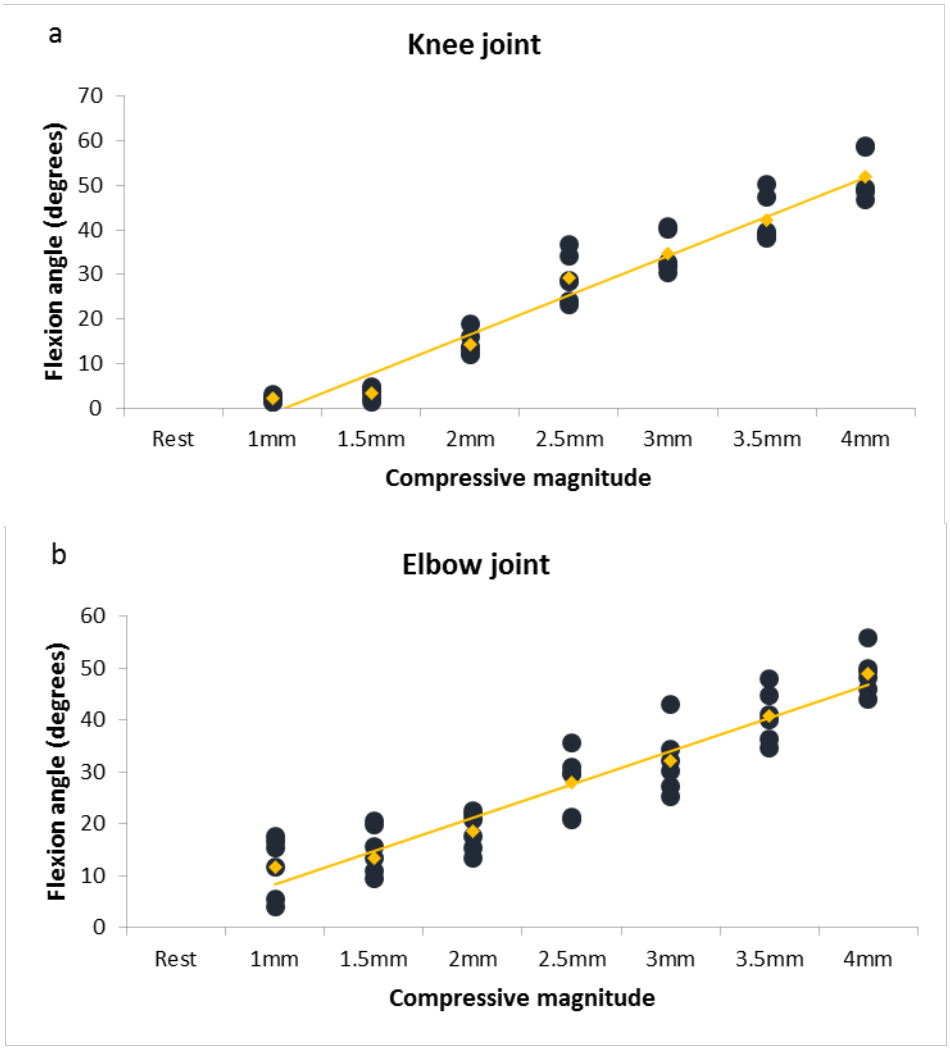


Figure 3.10: Flexion angle increased linearly (trend line and averages in yellow) with compressive magnitude. Flexion angles of developing e14.5 (a) elbow and (b) knee joints in explants undergoing 1–4mm of uniaxial compression. n=6 per group

Based on these results, validation of stimulation was also performed for e15.5 forelimbs and hind limbs for 2mm of displacement (data not shown). At e15.5, 2mm displacement produces an average of 17.9±1.7° of flexion in the elbow, and an average of 14.6±1.9° of flexion in the knee. Therefore, a displacement of 2mm was chosen for all dynamic explants.

3.4 3D shape analysis

Limbs designated for 3D shape analysis were processed for staining, embedded into agarose, and imaged using OPT. 3D renders were then created using Mimics (Materialise), with shape and statistical analyses performed upon these renders. The following protocols were optimised from Quintana and Sharpe (Quintana and Sharpe 2011).

3.4.1 Staining

All steps occurred at room temperature, unless otherwise stated (Hogan, Beddington et al. 1994). Limbs first underwent a stepwise dehydration protocol, in order to remove water from tissue. Limbs were submerged in increasing concentrations of ethanol diluted in distilled water (25%, 50%, 75%, 95%), for 15 minutes per step. Limbs were then washed in fresh 95% ethanol, and placed on a rocker for 24 hours (Stuart mini gyro-rocker SSM3). Limbs were then stained with filtered 0.015% Alcian blue solution in 95% ethanol with 20% glacial acetic acid, made up at least 24 hours prior to use. Alcian blue is a cationic stain, which stains acidic glycosaminoglycans within cartilage. Chick limbs were stained for between six to eight hours, due to bigger size and fattier thighs, and mouse limbs for between four to six hours. Limbs were carefully monitored by eye to prevent over-staining. Stained limbs were then washed in 95% ethanol overnight, and cleared in 1% potassium hydroxide (KOH) solution in distilled water for between 15 to 30 minutes, until clearing was deemed sufficient. After washing in PBS, limbs were stained with 0.01% Alizarin red solution in 1% KOH solution. Alizarin red is a fluorescent marker which binds to free calcium and certain calcium compounds, and is used to define mineralised cartilage. Limbs were stained for between one to two hours, and after adequate stain penetration, were cleared once more in 1% KOH. Care was taken whilst changing solutions, as the tissue becomes very delicate through clearing. Once samples were fully stained, they were fixed overnight in 4% paraformaldehyde dissolved in 1x PBS at 4°C. Fixation crosslinks proteins and anchors soluble proteins to the cytoskeleton, thus increasing the mechanical strength of the tissue. Post-fixation, tissue was washed in 95% ethanol, and stored at 4°C in 95% ethanol for a maximum of one week prior to embedding.

3.4.2 Embedding and trimming limbs

Low gelling temperature agarose (Sigma-Aldrich) was used to embed the stained limbs (Quintana and Sharpe 2011). A 1% solution was made by heating distilled water to 100°C using a heated magnetic stirring plate. Powdered agarose was tipped in, stirring continuously with a magnetic stirrer until fully dissolved. The agarose was filtered using 0.4µm filter paper to remove dust and undissolved agarose, and cooled to 45°C. Once cool, the filtered agarose was poured into labelled 6cm petri dishes, to a depth of 8mm. Limbs were then briefly washed in distilled water, then coated in agarose. Limbs were then submerged into the poured agarose and, as the agarose cooled and gelated, were lifted using curved forceps and suspended mid-depth in the agarose, so as the frontal plane of the limb was parallel to the top and bottom of the agarose. Agarose blocks were then refrigerated at 4°C for three hours to solidify. A scalpel was used to cut within the perimeter of the petri dish to loosen the agarose, and the agarose transferred to a 9cm dish for trimming. Limbs were oriented so that the axis of rotation would run through the centres of the stylopod

and zeugopod, and trimmed parallel to the axis. A block of agarose at least 5mm was left below the sample, to allow the sample to be mounted. Trimmed samples were dehydrated in 100% methanol for 24 hours, with two changes of fresh methanol approximately eight hours apart. Dehydrated samples were cleared in a 50:50 mix of benzyl alcohol and benzyl benzoate (BABB) for 24 hours, and stored in glass vials.

3.4.3 Imaging limbs with optical projection tomography

Cleared samples were removed from BABB, and the bottom of the sample dried carefully (Quintana and Sharpe 2011). Samples were attached to magnetic cylindrical mounts using superglue, and attached to a rotating arm, suspended upside down into a glass cuvette containing BABB. The lens was adjusted to focus on the sample. The sample was then scanned at 0.01s and 0.001s of exposure for Alcian blue, and 0.01s and 0.05s of exposure for Alizarin red. 400 images were taken at 0.9° rotational increments over 360° of rotation. The 400 images per scan were reconstructed into a stack of 2D tomographic images using NRecon by SkyScan (Brucker microCT, 2011). Mimics (Mimics, v18.0, Materialise NV, Belgium) was used to create 3D models of rudiments of interest from the tomographic stack, which were rendered into a 3D object, saved as .stl files. Different 3D models were created for different model organisms. For the chick, due to the prominent interest of the hip, the pelvis and femur was segmented out. For the mouse, the humerus, radius and ulna, and femur, tibia and fibula were segmented out.

3.4.4 Joint shape and mineralisation ratio analysis

.stl files were imported into ParaView (Ahrens 2005), and orientated systematically. In the chick hind limb, the proximal femur was orientated in the frontal plane, and the pelvis in the lateral and frontal planes (Figure 3.11). In the mouse forelimb, the distal humerus was orientated in the frontal, lateral and axial planes, the ulna in the lateral plane, and the radius in the frontal and axial planes (Figure 3.12). In the mouse hind limb, the distal femur was orientated in the frontal, lateral, and axial planes, the tibia in the frontal plane, and the fibula in the frontal and axial planes (Figure 3.13). Regions to be measured were selected based on anatomical landmarks.

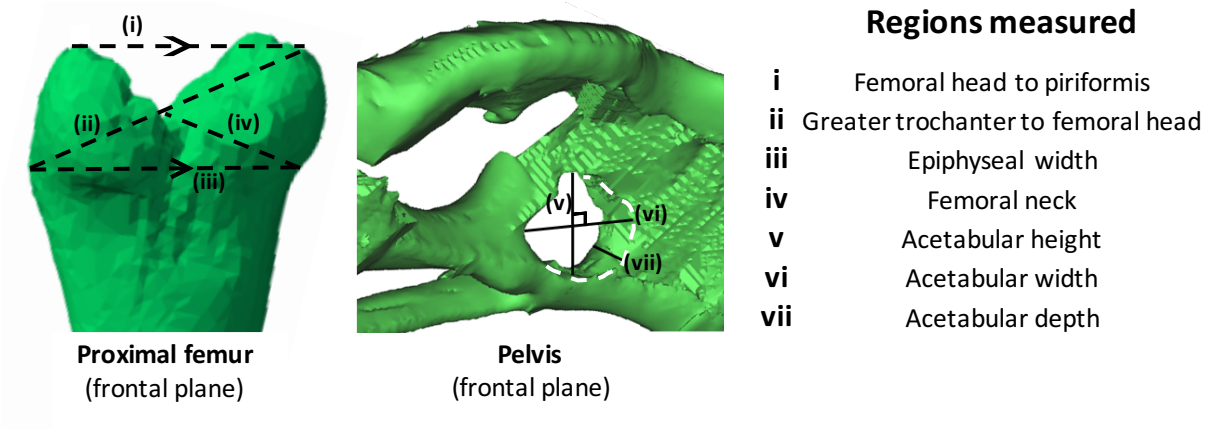
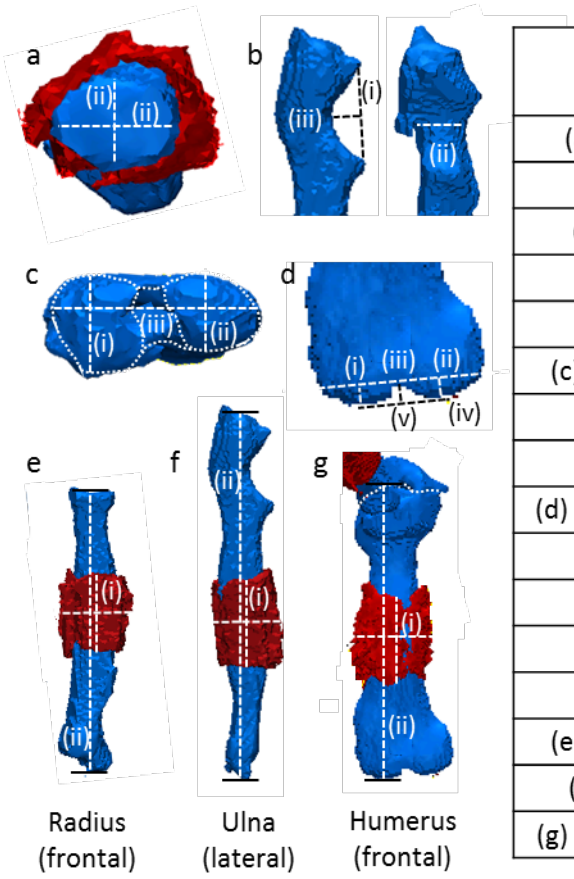
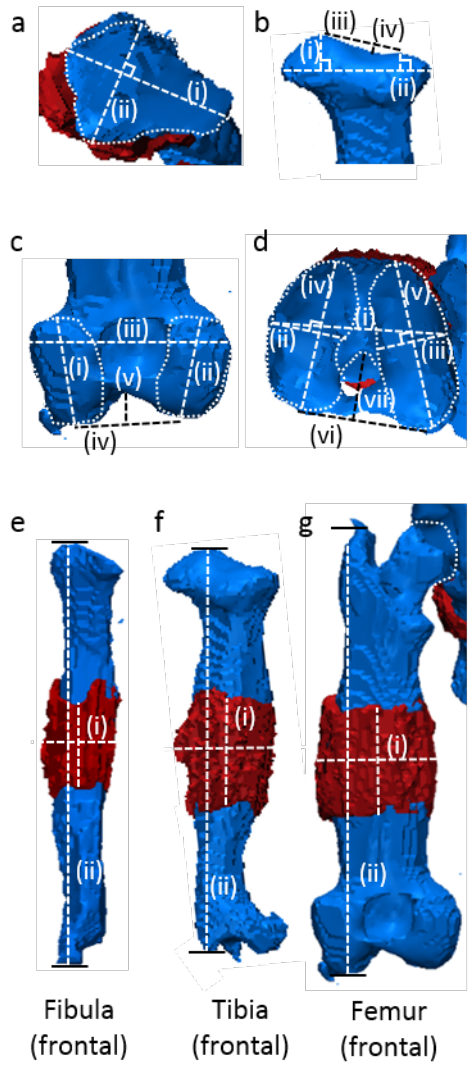


Figure 3.11: Representative image of chick hip measurements based on anatomical landmarks. Seven joint morphological parameters were selected according to anatomical landmarks present on the femoral head (a) and acetabulum (b) at e9. Proximal femurs were orientated frontally, and measurements taken in triplicate in Paraview. The pelvises were orientated in the frontal plane and lateral, and acetabular height, width and depth measured in triplicate. White dotted line indicates depth of the acetabulum.



Rudiment (orientation)	Regions measured	
(a) Radius (axial)	i	Length
	ii	Width
(b) Ulna (fossa)	i	Length
	ii	Width
	iii	Depth
(c) Humerus (axial)	i	Epicondylar width
	ii	Medial condyle depth
	iii	Lateral condyle depth
(d) Humerus (frontal)	i	Medial condyle height
	ii	Lateral condyle height
	iii	Epicondylar width
	iv	Fossa width
	v	Fossa depth
(e) Radius (frontal)	i/ii	Mineralisation ratio
(f) Ulna (lateral)	i/ii	Mineralisation ratio
(g) Humerus (frontal)	i/ii	Mineralisation ratio

Figure 3.12: Representative image of murine elbow measurements based on anatomical landmarks. 13 joint morphological parameters were selected according to anatomical landmarks present on the radius (a), ulna (b), and humeri (c, d). Radii were orientated in the axial plane, ulnae in the lateral and frontal planes, and the humerus in the axial and frontal planes. Mineralisation ratio was calculated as centred length of mineralised region divided by rudiment length (e–g). Measurements were taken in triplicate in Paraview.



Rudiment (orientation)	Regions measured	
(a) Fibula (axial)	**i**	Length
	ii	Width
(b) Tibia (frontal)	**i**	Medial condyle height
	ii	Lateral condyle height
	iii	Intercondylar height
	iv	Intercondylar width
(c) Femur (frontal)	**i**	Lateral condyle height
	ii	Medial condyle height
	iii	Epicondylar width
	iv	Fossa width
	v	Fossa depth
(d) Femur (axial)	**i**	Epicondylar width
	ii	Lateral condyle width
	iii	Medial condyle width
	iv	Lateral condyle depth
	v	Medial condyle depth
	vi	Fossa width
	vii	Fossa depth
(e) Fibula (frontal)	**i/ii**	Mineralisation ratio
(f) Tibia (frontal)	**i/ii**	Mineralisation ratio
(g) Femur (frontal)	**i/ii**	Mineralisation ratio

Figure 3.13: Representative image of murine knee measurements based on anatomical landmarks. 18 joint morphological parameters were selected according to anatomical landmarks present on the fibula (a), tibia (b), and femur (c, d). Fibulae were orientated in the axial plane, tibiae in the frontal plane, and femora in the axial and frontal planes. Mineralisation ratio was calculated as centred length of mineralised region divided by rudiment length (e–g). Measurements were taken in triplicate in Paraview.

To visually compare joint shape profiles of the chick hip, and mouse elbow and knee, 3D reconstructions of joints made using Mimics were virtually aligned in Paraview. For the chick hip, the femoral heads were aligned into the frontal plane such that the femoral neck was viewed in its longest plane, and virtual sections were taken through the lateral plane of the acetabulum such that the full depth of the acetabulum with the full ridge of the labrum were visible. Shape profiles were then traced around the orientated reconstructions at 4x magnification to ensure for accuracy (PowerPoint, Microsoft Office, 2017). Acetabular outlines were traced along the joint space, tracing a 'closed' acetabulum. Femoral profiles were aligned with the base of the femoral

neck, and acetabular profiles with the superior-most point of the labrum. For the mouse elbow, the distal humeri were first orientated into the frontal plane, and then rotated orthogonally to obtain medial and lateral views of the medial and lateral humeral condyles respectively. The radii were orientated frontally, and the ulnae laterally. For the mouse knee, the distal femora were first orientated into the frontal plane, and similarly to the humeri, rotated orthogonally to obtain medial and lateral views of the medial and lateral femoral condyles respectively. The tibiae were orientated frontally, and the fibulae laterally. Shape profiles were traced around the aligned joints in PowerPoint, pooled according to group, and overlaid. Frontal humeri and femora were aligned to the fossa depth, perpendicular to the midpoint of the frontal fossa width. Medial and lateral humeral and femoral condyles were aligned to the junction of condylar outgrowth relative to the shaft of the diaphysis. Frontal radial and fibular outlines were aligned to the midpoint of respective frontal width. Lateral ulnar outlines were aligned to the fossa depth, perpendicular to the midpoint of fossa length. Frontal tibial outlines were aligned to the midpoint of intercondylar width, perpendicular to intercondylar height.

Seven measurements of the chick hip, 13 measurements of the mouse elbow, and 18 measurements of the mouse knee were taken in triplicate from individually orientated reconstructions (Figures 3.11-13). Mineralisation of the mouse limb rudiments was measured as a ratio: length of mineralised region divided by the total length of bone.

3.5 Histology

3.5.1 Embedding and sectioning

In order to assess for cavitation status which cannot be assessed by OPT, chick limbs were prepared for cryosectioning and for histological analysis. Cultured avian limbs are known to present with multiple unstained areas surrounding the joint rudiment, which cannot be ruled out as an experimental artefact (Chandaria 2017). Hence, assessment of cavitation status in cultured murine limbs was not carried out. After harvest, limbs were immediately submerged at room temperature into 15% sucrose in PBS. After the sample had sunk, normally after two hours, the sample was resubmerged in 30% sucrose in PBS for two hours, followed by a final submersion in a 50:50 mix of 30% sucrose in PBS (OCT-30% sucrose), and optimum cutting temperature compound (OCT compound), until the sample had sunk. OCT is a water-soluble blend of glycols and resins used to embed tissue prior to sectioning on a cryostat. Once the tissue was fully infiltrated with OCT-30% sucrose, the sample was embedded into fresh OCT-30% sucrose. Samples were placed with their lateral sides on the bottom of the cryo moulds, and OCT-30% sucrose pipetted over, taking care to avoid bubbles. Samples were then flash-frozen upon a bed of dry ice, and stored at -80°C until sectioned. Embedded samples were sectioned using a cryostat

(NX70 Cryostat, Cryostar™, Thermo Fisher Scientific, UK) at 8µm, and mounted onto Superfrost™ Plus slides (Thermo Fisher Scientific, UK).

3.5.2 Staining

Histological staining was performed using 1% Toluidine blue in distilled water. Toluidine blue is a basic metachromatic dye, and binds to glycosaminoglycans in cartilage (Sridharan and Shankar 2012). Frozen sections on slides were rehydrated for five minutes in PBS, and then immersed in 1% Toluidine blue for three minutes. Slides were then rinsed with tap water, dried, and imaged using a XYZ microscope at 10x magnification. Stained, sectioned hip joints were examined for cavitational failure. A points system was used to determine the extent of cavitational failure. A single point was awarded for the following three individual markers of cavitational failure: (1) no clear separation between joint rudiments due to lack of tissue clearing, (2) decreased joint space between joint rudiments, and (3) fusion between rudiments. A score of zero points led to the section being classed as "successful cavitation", a score of one point led to the section being classed as "hindered cavitation", a score of two points led to the section being classed as "severely hindered cavitation", and a score of three points led to the section being classed as "failed cavitation".

3.6 Licensing

All chick experiments were performed in accordance with European Legislation (Directive 86/609/EEC), under which no license is necessary when working with embryos younger than two thirds of the way through gestation. All mouse experiments were carried out under Project Licence P39D18B9C, under Personal Licence I50EC1DF8.

Chapter 4

4. Early Chick Hip Development: A Critical Period of Movement

4.1 Introduction

There is a large body of evidence that strongly implicates the role of mechanical stimulation upon normal, healthy, bone and joint development, evidenced by the various post-natal conditions and syndromes associated with absent or reduced fetal movement, such as arthrogryposis multiplex congenita (AMC), or developmental dysplasia of the hip (DDH) (reviewed in section 2.5). It has been demonstrated in many animal models of abnormal fetal movement that immobilisation hinders the morphological development of major synovial joints, and cause cavitational failure across the joint space (reviewed in section 2.6).

Previous chick studies examined cavitation, and to a lesser extent, morphogenesis, in embryonic synovial joints immobilised for durations as long as fifteen days, from time points e3 to e21, and harvested from e6 to post-hatching (Fell and Canti 1934, Hamburger and Waugh 1940, Lelkes 1958, Drachman and Coulombre 1962, Drachman and Sokoloff 1966, Murray and Drachman 1969, Mitrovic 1982, Osborne, Lamb et al. 2002, Roddy, Prendergast et al. 2011, Nowlan, Chandaria et al. 2014, Nowlan and Sharpe 2014, Singh, Shea et al. 2018). In the chick hip joint, morphogenesis commences prior to cavitation, with major hip anatomical features present prior to cavitation at e8.5–9 (Nowlan and Sharpe 2014). A previous study from our group showed that in chicks immobilised from e4-8, hips assessed at pre-cavitation stages were morphologically indistinct from non-immobilised controls. However, after 'failed cavitation' in the immobilised hips, multiple shape abnormalities were present (Nowlan, Chandaria et al. 2014). There therefore appears to be an intrinsic link between movements, cavitation and morphogenesis, but there are several gaps in our understanding of the sequential and consequential events of these aspects of joint development. It is known that movement is important for cavitation and morphogenesis, and that abnormal morphogenesis succeeds abnormal cavitation. However, it is unknown when,

or for how long, the embryo must be active for normal cavitation or morphogenesis to occur. It is also unknown whether cavitation is sufficient for early joint morphogenesis.

In the research described in this chapter, I aimed to fill some of the gaps in knowledge of the temporal effects of pre-cavitational movement on joint cavitation and morphogenesis, and of the dependency of later morphogenesis on the presence or absence of a joint cavity. This study is the first systematic investigation on the cavitational and morphological effects of immobility induced at varying time points, for varying durations, harvested immediately after hip joint cavitation. It was hypothesised that there would be a time period of defined length and duration critical for normal cavitation and morphogenesis. To investigate this hypothesis, chick embryos were immobilised for varying time periods and durations between e3 and e8. The effects of different timings and durations on hip cavitation and morphogenesis at e9 were then assessed.

4.2 Materials and Methods

4.2.1 Immobilisation regimes – windowing and paralysis

Fertilised eggs were incubated, removed of albumen, and windowed, as described in section 3.1.1. A range of immobilisation regimes using 0.5% decamethonium bromide (DMB) were performed, in order to elucidate a critical time period for morphogenesis and/or cavitation, and were termed 'cumulative' (varying day of initiation of immobilisation and continuing until harvest), 'single–day' (varying day of initiation of immobilisation for a single 24–hour period prior to harvest), 'two–day' (varying day of initiation of immobilisation for a single 48–hour period prior to harvest), and 'three–day' (varying day of initiation of immobilisation for a single 72–hour period prior to harvest), as detailed in Figure 4.1. A naming convention was defined, where immobilisation from days 3–4 was group I3–4, immobilisation on day 3 was group I3, etc. Embryos were immobilised at the same time of day as the start of incubation, according to regime.

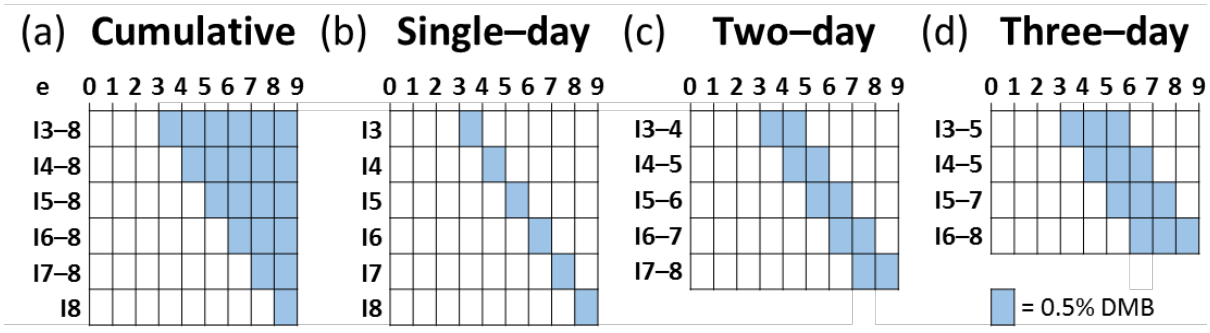


Figure 4.1: Four different immobilisation regimes were used: (a) cumulative, (b) single, (c) two–day, and (d) three–day. Groups within immobilisation regimes are named to the left of the graphs (e.g. I3–8 denotes immobilisation from e3–8). Embryonic days of development are numbered along the top of the graphs, and when shaded in blue denote 24–hour period of immobilisation with 0.5% decamethonium bromide (DMB). All embryos were harvested at e9.

4.2.2 Controls

As embryos underwent three invasive experiment procedures during this experiment, it became of interest to quantify the effects of albumen removal, windowing, and the physical act of pipetting PBS directly onto embryonic membranes on skeletal development. Three different groups of controls were used. 1: a physiological control group, where albumen was not removed nor were eggs windowed; 2: an albumen removal group, where albumen was removed but eggs were not windowed, and 3: a sham-immobilisation group, where embryos underwent identical experimental steps as the cumulative immobilised regime, but with 100µl of sterilised 1x PBS dropped onto the embryonic membranes instead of 100µl of 0.5% DMB. Control groups and specimen numbers are detailed in Table 4.1. Measurement data was analysed by one-way ANOVA, with no significant differences shown between groups (detailed in Appendix II). As the control group with the most interventions, the 'prolonged' sham-immobilisation group (sham e3–8) was used as the control group.

4.2.3 Specimen numbers

Embryos were harvested from three experiments, and pooled. Hind limbs that were damaged at any point during processing were discarded and not included in the final analysis. Left hind limbs were processed for 3D shape analysis, and right hind limbs processed histologically for cavitation. A minimum of six hind limbs per group were analysed for morphology, and between two and four hind limbs analysed histologically, as detailed in Table 4.1.

4.2.4 Joint shape and cavitational analysis

Hind limbs for 3D shape analysis were stained with 0.015% Alcian blue and imaged with OPT, as detailed in section 3.4. Characteristics of joint morphogenesis were compared across immobilisation groups. Hind limbs for cavitational analysis were cryologically sectioned at 12µm, stained with 0.01% Toluidine blue, and examined for cavitational failure, as detailed in section 3.5.2.

(a)	Cumulative		(b)	Single–day		(c)	Two–day		(d)	Three–day		(e)	Controls	
	OPT	Histology		OPT	Histology		OPT	Histology		OPT	Histology		OPT	Histology
I3–8	8	3	I3	6	2	I3–4	6	2	I3–5	7	4	Phys	8	3
I4–8	7	3	I4	6	2	I4–5	6	3	I4–6	6	3	Alb	10	–
I5–8	8	3	I5	6	3	I5–6	7	3	I5–7	7	4	S3–8	10	–
I6–8	8	3	I6	6	3	I6–7	6	3	I6–8	8	3	S4–8	7	–
I7–8	7	3	I7	6	3	I7–8	7	3				S5–8	8	–
I8	7	3	I8	7	3							S6–8	7	–
												S7–8	7	–
												S8	7	–

Table 4.1: Number of chick hind limbs analysed for shape changes and histologically at e9. Limbs were pooled from three experiments. OPT, limbs processed for 3D shape analysis; Histology, limbs processed for cavitational analysis.

4.2.5 Statistical analysis

For all immobilised and control groups, measurements were taken based on anatomical landmarks, as described in section 3.3.3. Physiological, albumen removal and sham-immobilised control groups were tested for normality using the Shapiro-Wilks test. As all groups were normally distributed, a one-way ANOVA was used to test for significant differences between each control group for the seven regions measured (p-values of less than 0.05). As no significant differences existed, the 'prolonged' sham-immobilisation group (S3–8) was used as a control group compared to immobilised groups (Appendix 1). These tests were carried out in SPSS (IBM Corp. Released 2016, IBM SPSS Statistics for Windows, Version 24.0. Armonk, NY; IBM Corp).

Between immobilisation regimes, the statistical test for equivalence (the two one-sided *t*-test) was used for equivalence testing between immobilised groups. Specifically designed to test for bioequivalence, the two one-sided *t*-test validates the equivalence between two groups, and was used in order to identify equivalence between all immobilised groups and prolonged immobilisation (Limentani, Ringo et al. 2005). For each group, the upper 100(1-γ)% confidence limit for the standard deviation, *s**, was calculated as:

$$s* = s\sqrt{\frac{n-1}{\chi^2_{(\gamma,n-1)}}}$$

where *s* is the standard deviation, and $\chi^2_{(\gamma,n-1)}$is the 80th percentile of a distribution with *n*-1 degrees of freedom (Seely, Munyakazi *et al*. 2003). This accommodation for error in *s* helps to ensure that *s* adequately represents the true standard deviation (Limentani, Ringo et al. 2005).

For each pair of compared groups, an acceptance criterion (θ) was defined outside of which the difference in mean values was considered statistically significant. With the significance level (α)=0.05, probability for a Type II error (β)=0.05, *n* (for each group), absolute value of the observed difference between the groups' means values (δ)=0, and *s** values, theta was calculated by:

$$\theta = \delta + s * \left[t_{(1-\alpha,2n-2)} + t_{(1-\beta/2,2n-2)}\right]\sqrt{2}/n$$

A 100(1-2α)% confidence interval was then constructed for the difference between the two mean values, and compared to θ, using the following:

$$(\bar{y}_1 - \bar{y}_2) \pm t_{(1-\alpha,n_1+n_2-2)} \cdot \sqrt{s_p^2\,(\frac{1}{n_1}+\frac{1}{n_2})}$$

If the confidence interval was entirely within the acceptance interval [-θ, θ], the mean values of the two groups were considered equivalent (Limentani, Ringo et al. 2005). The two one-sided *t*-test was carried out in Jupyter using the TOSTER package (Lakens 2017).

4.3 Results

4.3.1 Cumulative immobilisation

Cumulative immobilisation experiments involved immobilisation for between one and six days prior to harvest at e9, with the longest period of immobilisation (I3–8, termed prolonged immobilisation) completely eliminating movement during development. As previously described, and replicated here, prolonged immobilisation led to a smaller, shallower acetabulum, and a smaller, dramatically stunted femoral head (Figure 4.2, compare control group (a, a') to prolonged immobilisation group (I3–8, g, g') (Nowlan, Chandaria et al. 2014). All seven measurements of the acetabulum and femoral head were non-equivalent between the control group and prolonged immobilisation groups (Figure 4.3). Assessing the effects on the femoral head between different groups, the effects were more severe depending on the duration of the immobility, but the effects on shape were not linearly related to the duration. Qualitatively, the femoral heads of the I4–8 and I5–8 groups had a similar lack of outgrowth as those of the prolonged immobilisation group (Figure 4.2, compare e' and f' to g'). Fossa depth and greater trochanter outgrowth and definition were similarly lost in the I4–8 and I5–8 groups, as in prolonged immobilisation (Figure 4.2, compare e' and f' to g'). From the shape profiles, a trend towards an increasingly normal femoral head was apparent as the duration of immobility decreased. The femoral head became more pronounced, the greater trochanter more prominent, and the width greater, as one looks from right to left (Figure 4.2), bottom row.

For all measurements of the femoral head, the statistics revealed an association within the groups immobilised for four or more days (I5–8, I4–8 and I3–8). In two out of four femoral head measurements, either the I4–8 group, the I5–8 group, or both groups, were statistically equivalent to the prolonged immobilisation group (Figure 4.3a, c, d). The I4–8 and I5–8 groups decreased in the measurement of femoral head to greater trochanter, but not to the extent of the prolonged immobilisation group (Figure 4.3c). The femoral neck was differentially affected, with equivalence between I6–8 and prolonged (Figure 4.3b).

The outlines indicated that even a short period of immobility could have an effect on acetabular width and depth, but the effects of immobilisation were quite variable from sample to sample (Figure 4.2, top row). Measurements of the acetabulum revealed a less dichotomous situation than for the femoral head, with a gradual trend towards decreased height, width, and depth of the acetabulum, in proportion to the duration of immobility (Figure 4.3e–g). However, there did again

seem to be a 'batching' effect, composed of the groups with four or more days of immobility (I5–8, I4–8 and I3–8), particularly for acetabular height and width (Figure 4.3e–f).

Statistical analysis revealed equivalence for two out of three acetabular measurements in either the I4–8 group, the I5–8 group, or both groups, to the prolonged immobilisation group (Figure 4.3e–f). The I8 group was equivalent to the control group for the measurement of acetabular depth (Figure 4.3g).

As expected, all control hip joints were cavitated at e9, as were hips in the I8 group (Figure 4.4a–f). With increasing immobilisation came an increase in cavitational failure. Hips immobilised for two to three days prior to harvest at e9 (I5–8 and I6–8) experienced cavitational failure in two of three hips examined, with decreased joint space and fusion at the joint interface. Even more severely, in hips immobilised for four or more days (I5–8, I4–8 and I3–8), there was a complete failure of successful cavitation in all hips examined (three out of three for all groups; Figure 4.4m–u). The failure of cavitation in hips immobilised for four or more days indicates that continuous immobility on or before e5 has the most severe effect on hip joint cavitation, with continuous immobility from e6 having less severe effects on cavitation.

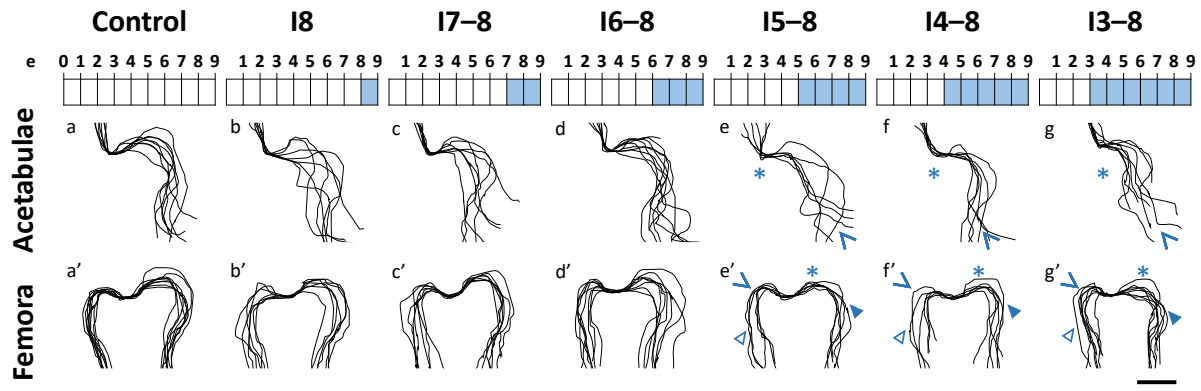


Figure 4.2: Shape profile outlines of the acetabulum (top row) and femoral head (bottom row) of the hip joint in embryonic chicks immobilised under the 'cumulative' immobilisation regime. Immobilisation regime: "I8", immobilised for e8; "I7–8", immobilised between e7 to 8, etc. Blue shading, treatment day. 0.5% DMB was administered once per treatment day to induce rigid paralysis. All chicks were harvested at e9. Observational findings: asterisk, decrease in acetabular or femoral head width compared to control; arrow, decrease in acetabular depth or femoral neck outgrowth compared to control; closed triangle, decrease in femoral head outgrowth compared to control; open triangle, decrease in greater trochanter outgrowth compared to control. Scale bar=200μm; n=6–8 per group.

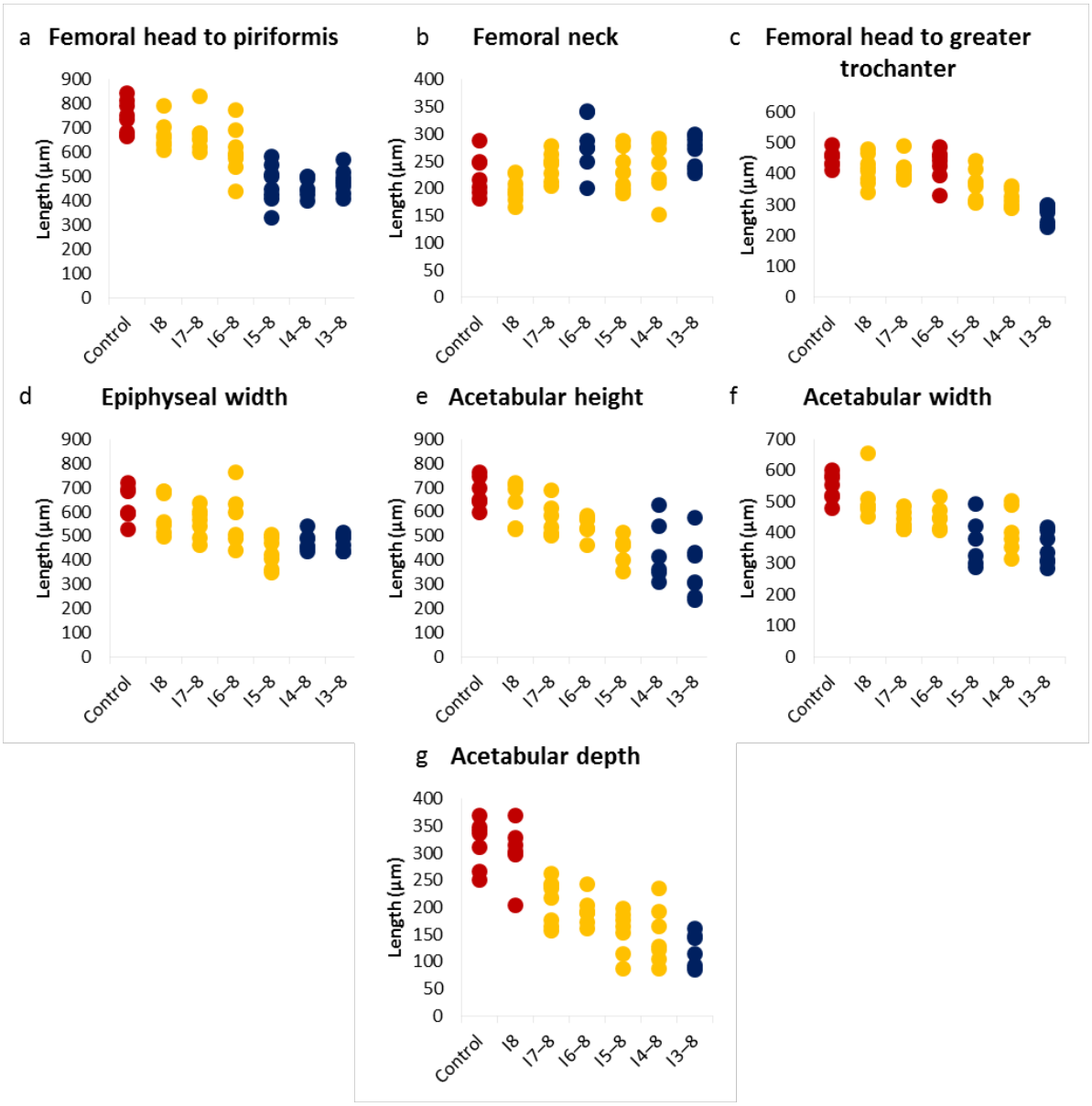


Figure 4.3: Dot plot graphs of measurements of the femoral head (a–d) and acetabulum (e–g) of the hip joint in embryonic chicks immobilised under the 'cumulative' immobilisation regime. 0.5% DMB was administered once per treatment day to induce rigid paralysis. All chicks were harvested at e9. Equivalence tests were used to test all groups for equivalence between prolonged immobilisation (I3–8), and between physiological controls (red, equivalent to control; blue, equivalent to prolonged immobilisation; yellow, equivalent to neither). n=6–8 per group.

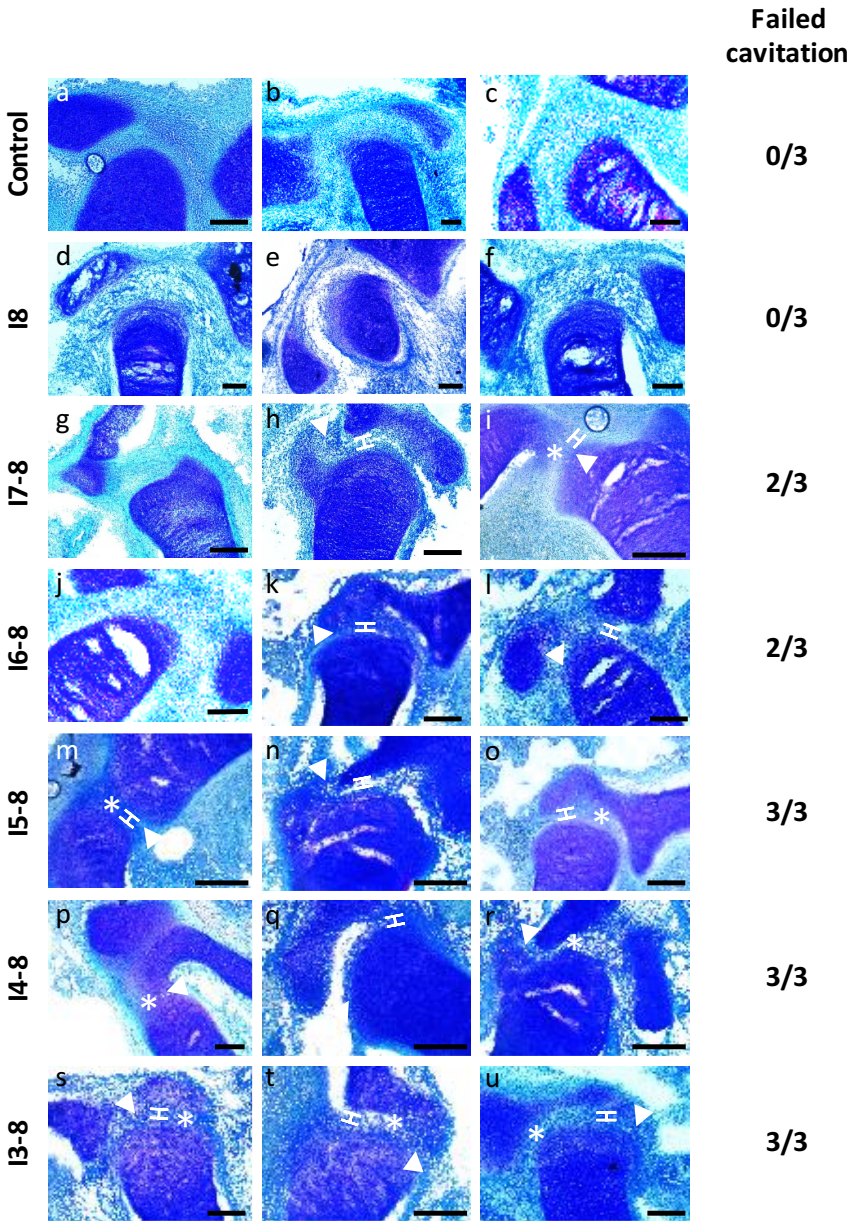


Figure 4.4: Histological sections of the femoral head and acetabulum of the hip joint in embryonic chicks immobilised under the 'cumulative' immobilisation regime. Immobilisation regime: 0.5% DMB was administered once per treatment day to induce rigid paralysis. All chicks were harvested at e9. Three markers for cavitational failure were used to grade samples (closed triangle, no clear separation between joint rudiments; I-bar, decrease in joint space between rudiments; asterisk, fusion between rudiments). A score of two or more was categorised as 'failed cavitation'. A score of one or less was categorised as 'cavitation'. Scale bar=200μm; n=3 per group.

4.3.2 Single–day immobilisation

Single–day immobilisation experiments involved immobilisation for a single 24–hour period between e3 and e8, prior to harvest at e9. A single day of immobilisation led to far fewer dramatic changes in shape and cavitation, compared to prolonged immobilisation. Shape profiles revealed more normal femoral head outgrowth throughout all single days of immobilisation, compared to the prolonged immobilisation group. Fossa depth was similarly deep throughout all single–day

groups compared to the control group, (Figure 4.5). Different features of the femoral head were slightly affected on different days of immobilisation. There was some variation in femoral head outgrowth in groups I8, I5, I4 and I3 (Figure 4.5, compare alignment of outlines of femoral heads in groups I8, I5, I4 and I3 to outlines of control group). Greater trochanter outgrowth and definition had increased variation in the I8 and I5 groups, compared to the control group. The width of the femoral head was similar in all immobilised groups, compared to the control group (Figure 4.5). No single–day period of immobilisation induced the severity of effects on outgrowth and morphology to the extent of the prolonged immobilisation group.

In three out of four measurements of the femoral head, a single day of immobilisation did not lead to effects as severe as prolonged immobilisation. A general trend showed a slight decrease in two measurements of the femoral head the earlier that immobilisation took place, but not equivalent to prolonged (Figure 4.6a, d). A single day of immobilisation between e5–8 led to little change in three out of four measurements of the femoral head, with some immobilisation groups equivalent to control (Figure 4.6c). The only exception to these trends was the femoral neck measurement. The femoral necks of the I3 group were equivalent to the prolonged immobilisation group, whilst the femoral necks of the I6 group was equivalent to the control group (Figure 4.6b).

Acetabular width and depth in groups I5, I4, and I3 was slightly decreased, corresponding with the loss of femoral head outgrowth in the I5, I4, and I3 groups (Figure 4.5). Qualitatively, acetabular depth was variable, with shape profiles aligned loosely in the I8, I5, I4 and I3 groups. The acetabulae in the prolonged immobilisation group were the most severely affected by immobilisation, compared to all single–day immobilisation groups. Statistical analysis revealed a

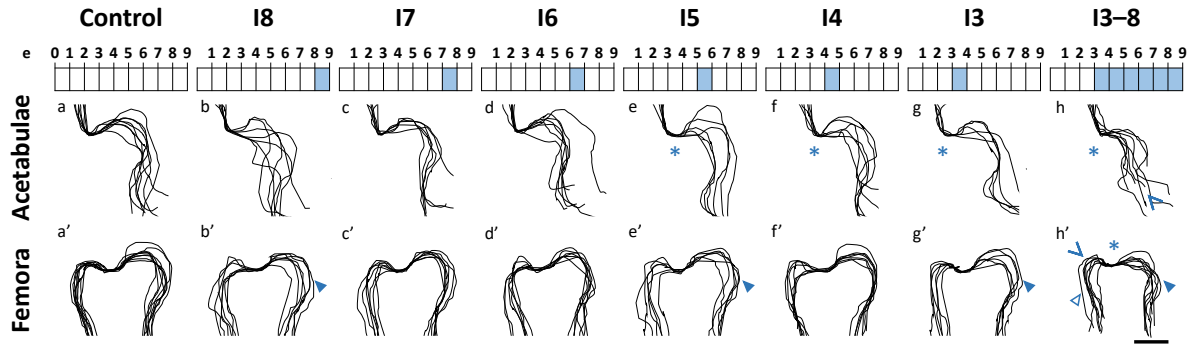


Figure 4.5: Shape profile outlines of the frontal femoral head and acetabulum of the hip joint in embryonic chicks immobilised for a single 24–hour period. Blue shading, treatment day. 0.5% DMB was administered once per treatment day to induce rigid paralysis. All chicks were harvested at e9. Observational findings: asterisk, decrease in acetabular or femoral head width compared to control; arrow, decrease in acetabular depth or femoral neck outgrowth compared to control; closed triangle, decrease in femoral head outgrowth compared to control; open triangle, decrease in greater trochanter outgrowth compared to control. Scale bar=200μm; n=6–8 per group.

general trend of decreased acetabular height and width the earlier that immobilisation occurred prior to harvest (Figure 4.6e, f, compare distribution of control group with distribution of single–day immobilisations, looking from left to right). Despite the slight trend of decreased measurements the earlier immobilisation occurred, immobilisation groups I8, I5, I4 and I3 for acetabular depth were statistically equivalent to control (Figure 4.6g).

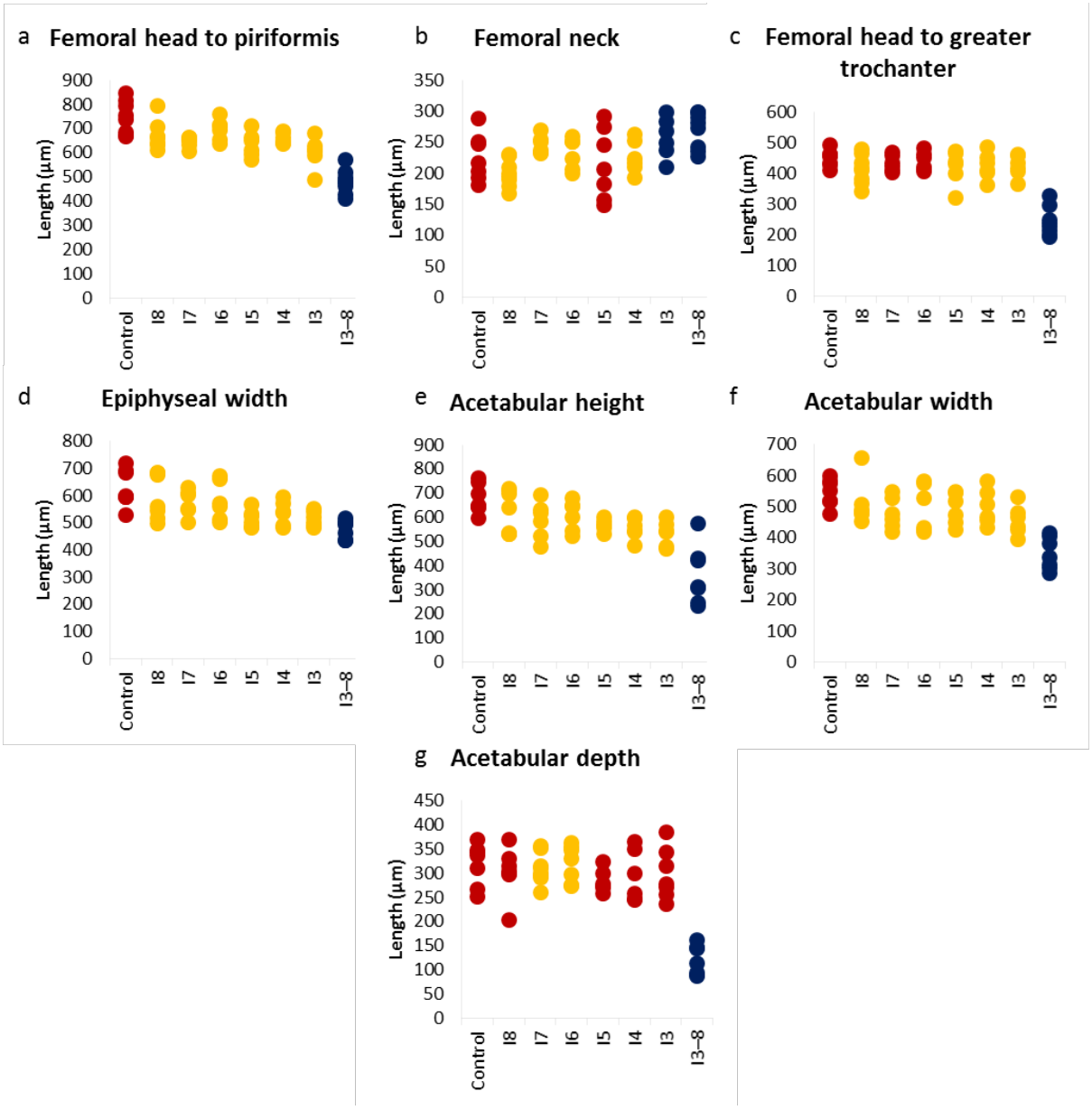


Figure 4.6: Dot plot graphs of measurements of the femoral head (a–d) and acetabulum (e–g) of the hip joint in embryonic chicks immobilised for a single 24–hour period. 0.5% DMB was administered once per treatment day to induce rigid paralysis. All chicks were harvested at e9. Equivalence tests were used to test all groups for equivalence between prolonged immobilisation (I3–8), and between physiological controls (red, equivalent to control; blue, equivalent to prolonged immobilisation; yellow, equivalent to neither). n=6–8 per group.

A single day of immobilisation did not affect cavitation, as in all hip joints examined, normal cavitation occurred (Figure 4.7, between two and three hips examined per group). These results indicate that a single 24–hour period of immobility between e3–8 was insufficient to affect cavitation at e9.

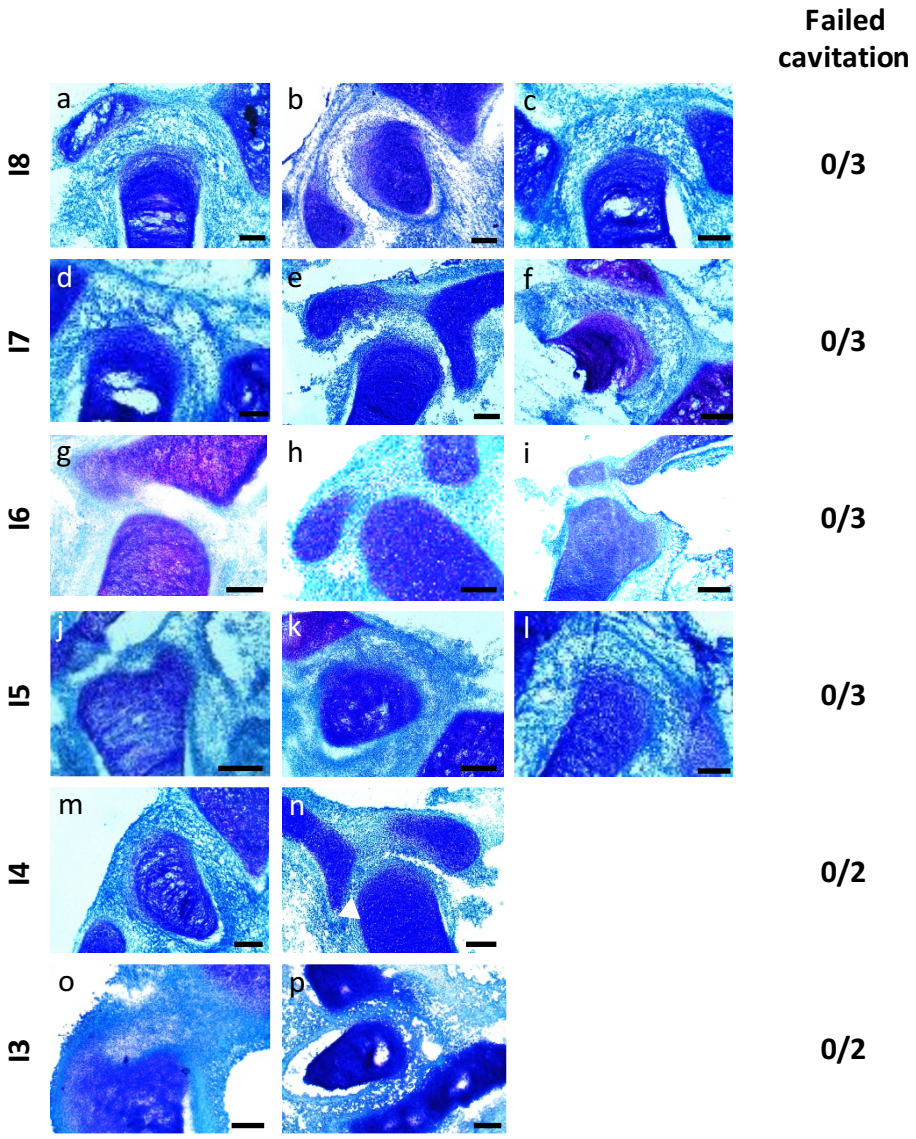


Figure 4.7: Histological sections of the femoral head and acetabulum of the hip joint in embryonic chicks immobilised for a single 24–hour period. 0.5% DMB was administered once per treatment day to induce rigid paralysis. All chicks were harvested at e9. Three markers for cavitational failure were used to grade samples (closed triangle, no clear separation between joint rudiments; I-bar, decrease in joint space between rudiments; asterisk, fusion between rudiments). A score of two or more was categorised as 'failed cavitation'. A score of one or less was categorised as 'cavitation'. Scale bar=200μm; n=2–3 per group.

4.3.3 Two–day immobilisation

Two–day immobilisation experiments involved immobilisation for a continuous 48–hour period prior to harvest at e9. A two–day period of immobilisation led to far more severe effects on the femoral head compared to a single–day period of immobilisation, but no two–day immobilisation group led to effects as severe as the prolonged immobilisation group. In hips immobilised for a two–day period earlier than e7 (I6–7, I5–6, I4–5, and I3–4), the femoral head flattened slightly and decreased in outgrowth compared to the control group (Figure 4.8c'–f', curly brackets). The earliest two–day period of immobilisation also decreased the width of the femoral head (I3–4; Figure 4.8f', square bracket) compared to the control group, with the greater trochanter less defined (I4–5, I3–4; Figure 4.8e'–f', compare open triangles with filled triangle). From the shape profiles, a two–day period of immobilisation did not affect fossa depth, with all fossa similarly deep (Figure 4.8, bottom row). Qualitatively, all two–day periods of immobilisation led to more variable outline profiles compared to control, with less tightly aligned profiles (Figure 4.8b'–f', open arrows).

The statistics revealed that in three out of four measurements of the femoral head, a two–day period of immobilisation led to a slight decrease in femoral head width compared to the control group. For all immobilisation groups, three out of four femoral head measurements were decreased compared to control, and also non-equivalent to control or prolonged immobilisation groups (Figure 4.9a, c, d; observe slightly sloping left to right gradient of individual measurements). Immobilisation at an earlier development stage generally led to the biggest decreases for three out of four measurements of the femoral head performed (Figure 4.9a, c, d; compare I3–4 group with other immobilised groups to the left).

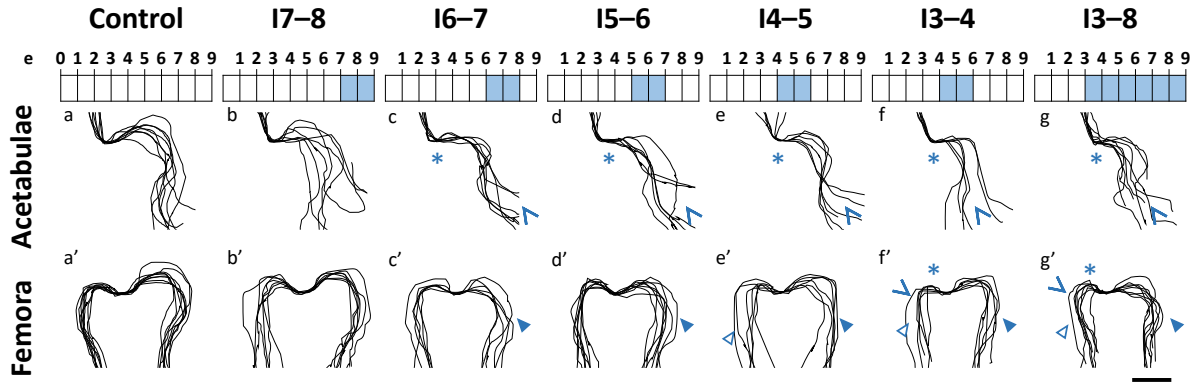


Figure 4.8: Shape profile outlines of the frontal femoral head and acetabulum of the hip joint in embryonic chicks immobilised for a single 48–hour period. Blue shading, treatment day. 0.5% DMB was administered once per treatment day to induce rigid paralysis. All chicks were harvested at e9. Observational findings: asterisk, decrease in acetabular or femoral head width compared to control; open arrow, decrease in acetabular depth or femoral neck outgrowth compared to control; closed triangle, decrease in femoral head outgrowth compared to control; open triangle, decrease in greater trochanter outgrowth. Scale bar=200μm; n=6–8 per group.

The femoral neck was affected differently to the other femoral head measurements. Femoral neck measurements in all two–day groups were in a similar range to both the control group and prolonged immobilisation group (Figure 4.9b). The I4–5 immobilisation group was statistically equivalent to control, and the I7–8, I6–7, I5–6, and I3–4 immobilisation groups equivalent to neither control nor prolonged group.

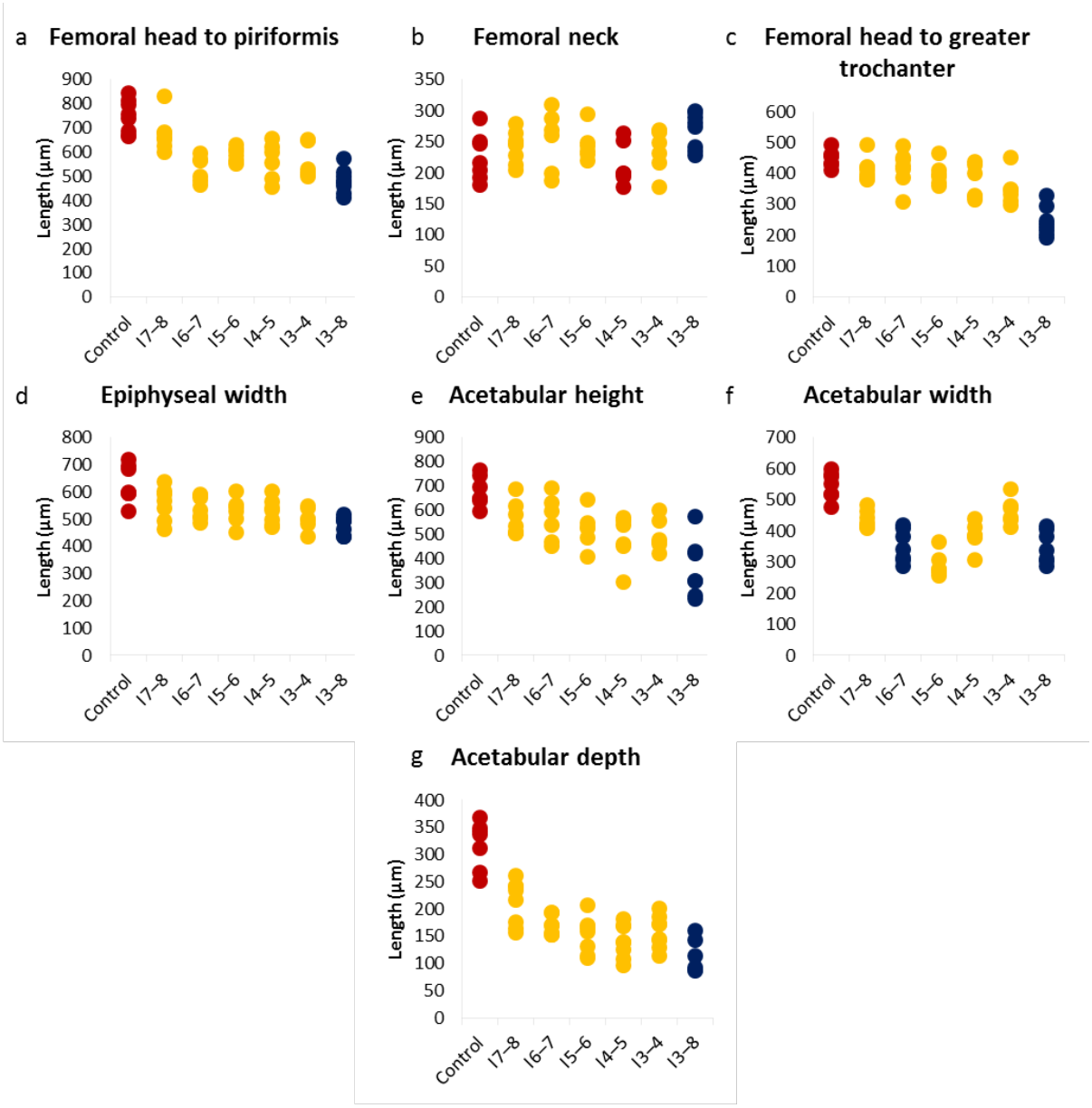


Figure 4.9: Dot plot graphs of measurements of the femoral head (a–d) and acetabulum (e–g) of the hip joint in embryonic chicks immobilised for a single 48–hour period. 0.5% DMB was administered once per treatment day to induce rigid paralysis. All chicks were harvested at e9. Equivalence tests were used to test all groups for equivalence between prolonged immobilisation (I3–8), and between physiological controls (red, equivalent to control; blue, equivalent to prolonged immobilisation; yellow, equivalent to neither). n=6–8 per group.

Acetabular outlines indicated that the later two-day periods of immobilisation had more severe effects on acetabular depth, which corresponded with smaller, flatter femoral heads in immobilisation groups I6–7, I5–6, I4–5, and I3–4. The same immobilisation groups had acetabulae which were almost as shallow as that of the prolonged group, and with less depth than the control group (I6–7, I5–6, I4–5, and I3–4; Figure 4.8c–f, open arrows). Acetabular width also was decreased compared to the control group in I6–7, I5–6, and I4–5, but less so in I3–4 (Figure 4.8, asterisks). Two days of immobilisation led to a greater variation in morphology compared to the control group, with shape profiles generally becoming less tightly aligned (Figure 4.8, top row, compare two–day groups with control).

Compared to measurements of the femoral head, acetabular height and depth decreased more dramatically that the control group, compared to measurements of the femoral head. Immobilisation at an earlier period decreased acetabular height and depth in a linear fashion until I4–5, for two out of three acetabular measurements. One immobilisation group (Figure 4.9f, I6–7 for acetabular width) was so severely affected by two days of immobilisation, that they were statistically equivalent to prolonged immobilisation. The I5–6 group was even more severely affected than prolonged immobilisation for acetabular width (Figure 4.9f). For acetabular width, the severity of effect of two days of immobilisation plateaued around I4–5. Immobilisation increased severity the earlier that hips were immobilised for, but not linearly. The severity of effect peaked at I4–5 for all three acetabular measurements, with severity even decreasing in the I3–4 group compared to I4–5, for acetabular width.

The increase in severity of morphological effects on the femoral head and acetabulum with an earlier two–day period of immobilisation does not reflect in the rates of cavitational failure histologically. Hips immobilised for the earliest two–day period prior to harvest at e9 (Figure 4.10m–n, I3–4) experienced no cavitational failure in two out of two hips examined. Hips immobilised for a two–day period between e4–6 (Figure 4.10g–l, I4–5 and I5–6) experienced cavitational failure in one out of three hips examined. Hips immobilised for a two–day period after e6 (Figure 4.10a–f, I6–7 and I7–8) experienced higher rates of cavitational failure, with two out of three examined hips failing to cavitate. These results indicate a differential effect between morphology and cavitation from immobilisation at different time points. Cavitation was more severely stunted when immobilisation occurs closer to physiological cavitation, whereas morphological aspects of the hip joint were more reduced the earlier that immobilisation occurs.

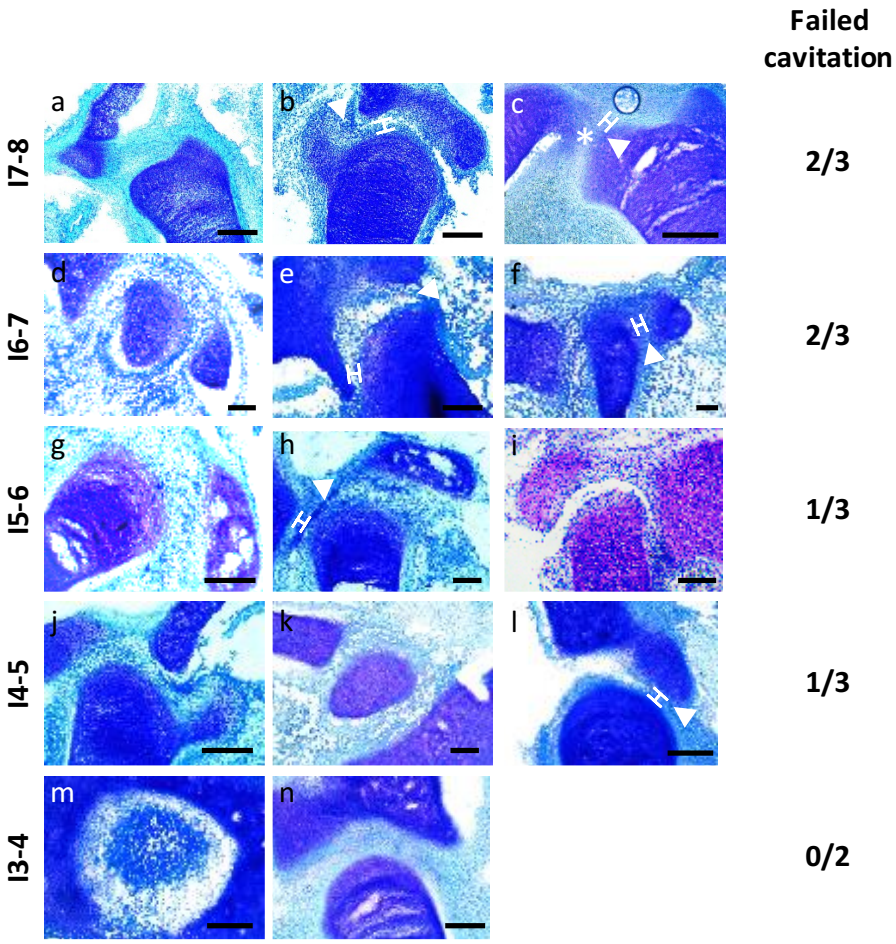


Figure 4.10: Histological sections of the femoral head and acetabulum of the hip joint in embryonic chicks immobilised for a single 48–hour period. 0.5% DMB was administered once per treatment day to induce rigid paralysis. All chicks were harvested at e9. Three markers for cavitational failure were used to grade samples (closed triangle, no clear separation between joint rudiments; I-bar, decrease in joint space between rudiments; asterisk, fusion between rudiments). A score of two or more was categorised as 'failed cavitation'. A score of one or less was categorised as 'cavitation'. Scale bar=200μm; n=2–3 per group.

4.3.4 Three–day immobilisation

Three–day immobilisation experiments involved immobilisation for a continuous 72–hour period prior to harvest at e9. The shape profiles of the femoral head revealed a loss of femoral head outgrowth with a three–day period of immobilisation between e3–7 (I3–5, I4–6, I5–7, Figure 4.11c'–e', closed triangles) compared to the control group, as well as a loss of femoral head width (I3–5, I4–6, I5–7, Figure 4.11c'–e', asterisks) compared to the control group. A three-day period of immobilisation between e3–7 led to a decrease in greater trochanter outgrowth, compared to the control group (I3–5, I4–6, I5–7, Figure 4.11c'–e'). The outgrowth of the greater trochanter in immobilisation group I6–8 was not particularly affected by immobilisation, and was comparable to the control group. A loss of fossa depth in I3–4 and I5–7 also occurred, with other groups displaying more normal fossa (Figure 4.11b'-e', open arrows). Any three–day period of

immobilisation between e3–8 led to a large variation in femoral head shape, with a large variation in shape profiles (Figure 4.11, bottom row, open arrow).

In three out of four femoral head measurements, an earlier three–day period of immobilisation from e5–7 (I5–7) more severely affected rudiment width than a later three–day period of immobilisation from e6–8 (I6–8) (Figure 4.12a, c, d). Immobilisation group I4–6 was also statistically equivalent in one out of four measurements to the prolonged immobilisation group (Figure 4.12d). In two out of four measurements of the femoral head, either the I5–7 group, the I4–6 group, or both, were statistically equivalent to the prolonged immobilisation group (Figure 4.12a, d). In two out of four measurements, measurements of the I5–7 group were lower than that of the prolonged immobilisation group (Figure 4.12a, d). A trend can be seen in three out of four measurements of the femoral head, where immobilisation on or prior to e4, group I3–4, and on or after e6, group I6–8, was less severe than a three–day period of immobilisation that includes e5, groups I4–6 and I5–7. These data points form a 'U' shaped graph, with the most severely affected measurements at the bottom of the 'U' (Figure 4.12a, c, d). Once more, the femoral neck was differentially affected by immobilisation. The I6–8 was statistically equivalent to the prolonged immobilisation group, whilst groups I3–5 and I5–7 were statistically equivalent to the control group. Group I4–6 was not equivalent to neither the control nor the prolonged immobilisation group.

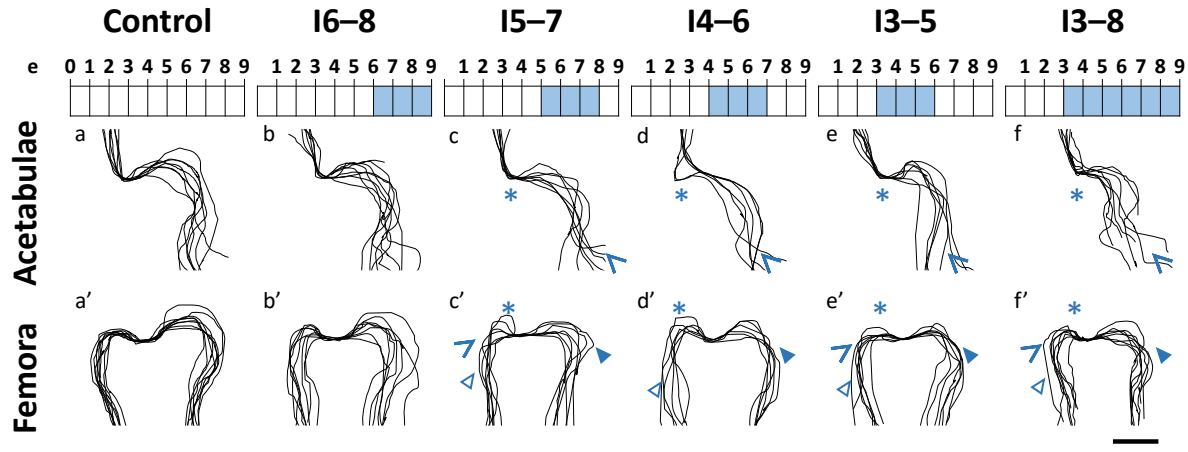


Figure 4.11: Shape profile outlines of the frontal femoral head and acetabulum of the hip joint in embryonic chicks immobilised for a single 72–hour period. Blue shading, treatment day. 0.5% DMB was administered once per treatment day to induce rigid paralysis. All chicks were harvested at e9. Observational findings: asterisk, decrease in acetabular or femoral head width compared to control; open arrow, decrease in acetabular depth or femoral neck outgrowth compared to control; closed triangle, decrease in femoral head outgrowth compared to control; open triangle, decrease in greater trochanter outgrowth. Scale bar=200μm; n=6–8 per group.

The acetabular shape outlines revealed that any three–day period of immobilisation from between e3–7 decrease acetabular width, comparable to that of the prolonged immobilisation group (Figure 4.11c–e, asterisks). Acetabular depth was similarly decreased, compared to the control group (Figure 4.11c–e, open arrows). As in the femoral head, any three–day period of immobilisation led to increased variation of the acetabular shape profiles (Figure 4.11b–e, open

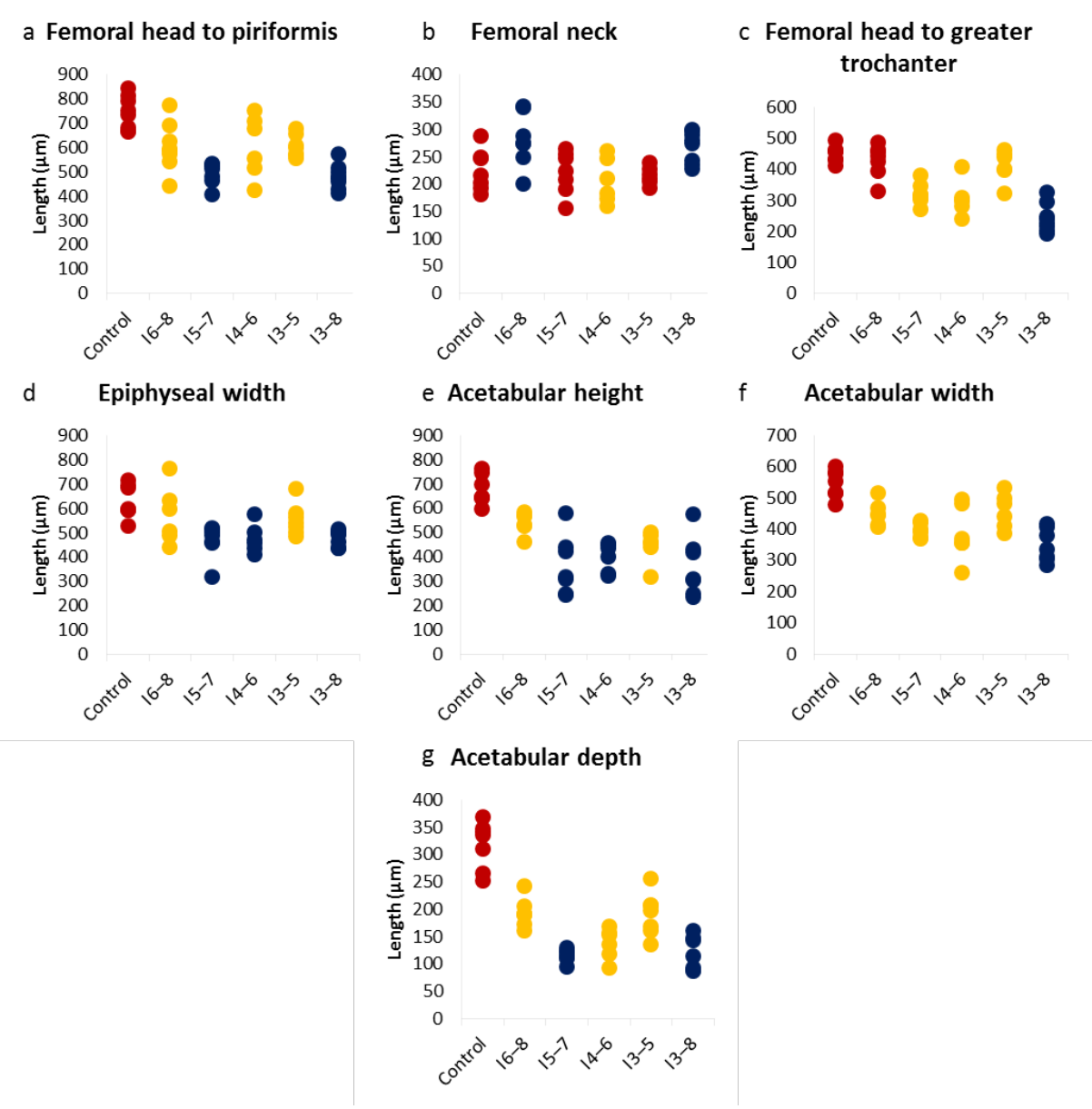


Figure 4.12: Dot plot graphs of measurements of the femoral head (a–d) and acetabulum (e–g) of the hip joint in embryonic chicks immobilised for a single 72–hour period. 0.5% DMB was administered once per treatment day to induce rigid paralysis. All chicks were harvested at e9. Equivalence tests were used to test all groups for equivalence between prolonged immobilisation (I3–8), and between physiological controls (red, equivalent to control; blue, equivalent to prolonged immobilisation; yellow, equivalent to neither). n=6–8 per group.

arrows). The 'U' shaped trend can also be seen in the measurements of the acetabular height, width and depth when immobilised for a three–day period. Groups I5–7 and I4–6 was most severely affected, at the bottom of the 'U shape (Figure 4.12e–g). For the acetabular height, width, and depth, groups I6–8 and I3–5 were non-equivalent to either the control or the prolonged immobilisation groups. One or both groups I5–7 and I4–6 were statistically equivalent to the prolonged immobilisation group in two out of three acetabular measurements (Figure 4.12e, g).

A three–day period of immobilisation severely affected the cavitation of immobilisation group I5–7, where three out of four hips examined failed to cavitate at e9 (Figure 4.13d–g). The hips immobilised either side of this three–day period, groups I6–8 and I4–6, were also affected by immobilisation, but not quite to the same extent, with two out of three hips examined failing to cavitate (Figure 4.13a–c, h–j). The earliest time period of immobilisation in group I3–5 led to two out of four hips examined failing to cavitate (Figure 4.13k–n).

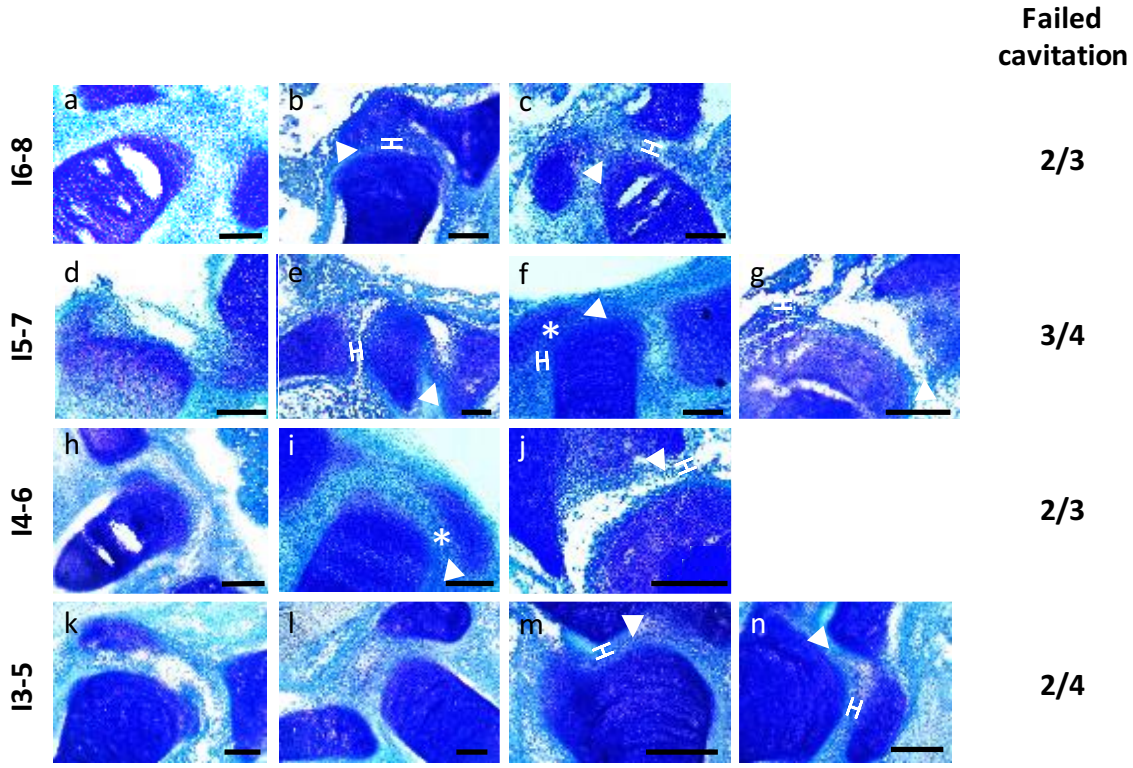


Figure 4.13: Histological sections of the femoral head and acetabulum of the hip joint in embryonic chicks immobilised for a single 72–hour period. 0.5% DMB was administered once per treatment day to induce rigid paralysis. All chicks were harvested at e9. Three markers for cavitational failure were used to grade samples (closed triangle, no clear separation between joint rudiments; I-bar, decrease in joint space between rudiments; asterisk, fusion between rudiments). A score of two or more was categorised as 'failed cavitation'. A score of one or less was categorised as 'cavitation'. Scale bar=200μm; n=2–3 per group.

4.4 Discussion

The results in this chapter describe the effects of varying timing and duration of pharmacological immobilisation on joint cavitation and morphogenesis, in order to identify a critical time period for spontaneous movement for normal early embryonic development of the chick hip. Cumulative immobilisation revealed that effects of immobilisation caused a trend of decreased joint size, in proportion to the duration of immobility. Immobilisation for four or more days led to failed cavitation in all hips examined. One day of immobilisation between e3–8 did not have a considerable impact on joint shape development or cavitation at e9. After two days of immobilisation, decreases in joint shape measurements were generally greater the earlier that immobilisation occurred, whilst immobilisation closer to e8, the point at which cavitation should occur, led to a greater rate of failed cavitation. Three days of immobilisation from e4–6 or e5–7 led to marked effects on both joint shape and cavitation, with the effects almost, but not quite, as severe as those of prolonged immobilisation (e3–8). These four immobilisation regimes combined indicate that a single day of immobilisation is not likely to drastically affect joint morphogenesis or cavitation, but immobilisation for three or more days significantly impedes joint development. The timing of the three–day period is relevant, with fetal movements most impactful upon major anatomical landmarks of the hip joint; namely: femoral head outgrowth, femoral head width, the outgrowth of the greater trochanter, and acetabular height, width, and depth, between e4–7. These morphological consequences due to a short period of immobilisation are almost as severe as the effects of long-term, prolonged immobilisation. Moreover, 72 hours of immobility during early fetal development induced between e5 and e7 severely impeded normal cavitation expected to occur at e8.5. The hypothesis that there is a time period of defined length and duration critical for normal cavitation and morphogenesis was corroborated.

Results from this study explore the complex interplay between movement, morphogenesis, and cavitation. The first fetal movements begin at e3.5, with a flexion of the neck to the left and right. By e4, these movements descend to the base of the limb buds. By e5, waves of movement occur from the neck to the tail of the embryo (Hamburger and Balaban 1963). Later, the first limb movements of the chick embryo occur at e6.5 (Hamburger and Balaban 1963). The severe morphological abnormalities which arise from immobilisation between e4–7, and failure of cavitation observed when immobilised from e5–7, are almost as severe as those resulting from prolonged immobilisation (from e3, prior to the very first fetal movements, to e9, after cavitation at e8.5). Immobilisation between e4–7 almost completely precedes the first few limb movements at e6.5. The paralytic effects of DMB last for approximately 24 hours, and all embryos which were treated between e3 and e7 were observed to be moving, with frequent limb movements and whole body movements at e9. Hence, it is therefore possible that an absence of whole-body

movements between e4–7 critically and irrecoverably interferes with one or more early mechanosensitive developmental processes during this window of time, moreso than later limb movements from e6.5 onwards.

In this study I investigated shape and cavitation parameters, and saw that neither increasing duration nor timing of immobilisation significantly affected the width of the femoral neck when examined at e9. The width of the femoral neck was measured diagonally across the height of the proximal growth plate, the only femoral head measurement to do so. The presence of the proximal growth plate introduces complexity. It is possible that if immobilisation confers morphological changes to the femoral neck, it may be too early in development for upstream mechanosensitive signalling events to become morphologically apparent in the cartilage rudiment. It may even be too early for cellular proliferative changes in the proximal growth plate, corroborated in experiments in immobilised mid- to late-embryonic chicks. Previous histological, immunological and cell proliferation studies were used to evaluate growth plate organisation, demonstrating that immobilisation regulates chondrocyte proliferation only in specific growth plates at certain timepoints. Immobilisation between e10–14 with harvest at e14, and e15–18 with harvest at e18 revealed that the proximal growth plate in the femoral neck showed no changes in the distribution of specific growth plate zones at any timepoint or immobilisation regime (Pollard, Charlton et al. 2017). However, the distal growth plate was affected at both timed immobilisations but moreso in the older embryos, with an expansion in the proliferative/maturing zone, and narrowing of the pre-hypertrophic zone in the distal femur. Alternatively, it may be that different skeletal elements are differentially affected by different periods of immobilisation, and the femoral neck may be less mechanosensitive than other developing rudiments.

Further morphological, cellular and molecular analyses are necessary to understand why there is an apparent difference in the response of the femoral neck to immobilisation compared to other proximal areas. Firstly, extending the embryonic chick immobilisation experiments and harvesting at later windows gives a longer time period for the potential effects to make themselves apparent morphologically, in that immobilisation would start at e3. Secondly, cellular analysis of the distribution of cell type and proliferation using the mitotic marker phosphohistone H3, and the S-phase marker proliferating cell nuclear antigen, within the proximal femur in all immobilisation regimes would reveal if immobilisation leads to quantitative proximal growth plate cellular differences. Thirdly, exploration of the molecular response to the absence of loading by RNA transcriptional profiling would help to better understand which genes may be involved specifically in different regions of the proximal growth plate.

Not only a non-competitive post-synaptic blocker of the neuromuscular junction, DMB is shown to inhibit the expression of skeletal myosin heavy chain in a concentration-dependent manner,

disrupting muscle development from e7, and cause subcutaneous oedema from e10 (Macharia, Patel et al. 2004). However, although DMB is known to cause cell death and apoptosis in the muscle, this is posited as due not to toxicity, but rather a secondary problem (Macharia, Patel et al. 2004). Additionally, DMB does not appear to have cytotoxic effects on cartilage, as TUNEL assays in chick femora reveal minimal apoptosis in control or immobilised cartilaginous rudiments (Pollard, Charlton et al. 2017). It is possible that morphological and cavitational changes seen in joint rudiments may be due to a yet-unknown effect of DMB causing muscle breakdown, leading to atrophy of blood vessels and peripheral nerves, rather than skeletal muscle immobilisation leading to loss of mechanical and chemical downstream effects. However, in limbs immobilised from e9 to e13, blood vessels and peripheral nerves were reported as 'very numerous throughout the limb' at e13 (Germiller and Goldstein 1997). This strengthens the argument that cartilage activity is more likely modulated by either cell signalling from muscle itself, or through mechanical signalling through mechanosensitive pathways.

From this study, questions arise: Which cellular and molecular mechanisms do pharmaceutical immobilisation alter in this study? And do these directly correlate with the joint cavitational and shape changes seen?

Chondrocyte proliferation and differentiation was not specifically investigated in this thesis. The immobilised femoral head demonstrated a reduction in greater trochanter outgrowth, a bone eminence and site of tendon attachment. A survey of the literature shows a corroboration in mammalian models, as loss of the humeral deltoid tuberosity was also noted in mutant mice with both reduced or absent limb muscle (Sotiriou, Rolfe et al. 2019). Bone eminence cells are not derived from the main cartilage template of the long bone, and only emerge after the primary cartilaginous template is laid down. A distinct pool of *Sox9*-positive, *Scx*-positive, *Col2a1*-negative cells was shown to form long bone eminences, under the regulation of TGFβ signalling, necessary for the specification of bone eminence progenitors, and the SCX/BMP4 pathway, necessary for the differentiation of these progenitors to eminence-forming cells (Blitz, Sharir et al. 2013). It is possible that growth of these bony eminences is regulated by conserved signalling patterns, as outgrowth of bone eminences is diminished in immobilised rudiments in both chick and mouse models. Additional transcriptional analyses of the chick model would confirm this.

In the present study, various joint shape features were reduced or deformed, such as the decrease in femoral head width and outgrowth, flattening of the femoral head, and decrease in acetabular dimensions. Similarly, in embryonic murine jaws which were sutured such that movement was prevented between e15.5 to e18.5, the mandibular condylar cartilage was reduced and deformed, and the volume and total cell number were reduced in the condylar cartilage. Subsequently, expression of Ihh and PTHrP and their related receptors, known mechanosensitive molecules

involved in regulating chondrocyte proliferation and differentiation, were decreased in condylar cartilage of the sutured group. A decrease in Ihh-positive cell proliferation in the mesenchymal and pre-hypertrophic cartilage zones were also decreased in the sutured group compared to the non-sutured group (Jahan, Matsumoto et al. 2014). Immobilisation was also seen to disrupt the normal expression pattern of PTHrP in the chick knee, so that it was no longer restricted to the periarticular regions, but instead expressed across the interzone (Roddy, Prendergast et al. 2011). Expression changes of mechanosensitive genes correlated with both morphological and proliferation changes in the knee joint. These results suggest that Ihh and PTHrP are involved in mechanotransduction pathways in developing cartilage. Changes in the expression of these molecules may well be observed in embryonic chicks in this study.

Previous experiments have immobilised the chick embryo for a continuous period of time, up until the point of harvest, therefore not allowing a resumption of movement (Roddy, Prendergast et al. 2011, Nowlan, Chandaria et al. 2014). These studies are comparable with conditions associated with sustained fetal immobility, such as fetal akinesia deformation sequence (FADS). However, some risk factors for AMC, such as oligohydramnios and reduced uterine space, are thought to be associated with reduced fetal movements at particular developmental stages, and not continuously (Nowlan 2015). Only one known study immobilised chicks for a brief window of time, and examined lower limb joints at e21, just after hatching. In this study, all embryonic chick hip joints immobilised for a single day cavitate normally at e9, with small decreases in joint shape measurements (Mitrovic 1982). Contrary to this, Drachman and Coulombre immobilised chick embryos between e7–9 for 24 or 48 hours, reporting joint ankyloses and altered ranges of movement in the toe, ankle, and knee at e21 (Drachman and Coulombre 1962). Immobilisation for 48 hours was also noted to be more severe than for a single day, a finding which was corroborated in terms of cavitation and morphogenesis in the current study. Although Drachman and Coulombre did not examine joint cavitation or morphology, it is possible that the minimal morphological effects seen after one day of immobilisation at e9 could lead to joint ankyloses and a more limited range of movement upon completion of fetal development. In our study, shape development was tightly linked with successful cavitation, as proposed previously (Nowlan, Chandaria et al. 2014). In no case where cavitation failed completely was there physiological morphogenesis, and vice versa.

This study was not without limitations. The chick is a valuable and well-explored model for skeletal development due to its broad similarities to mammalian skeletal development. However, differences in development, such as the perforated acetabulum, mineralisation, and eventual hollow bones, can limit the use of the chick model. Although all eggs delivered were between 55 to 65g, embryos were often slightly different sizes to each other, with different genetic

backgrounds, with the potential for slightly different morphologies. The slight variation in chick size and volume of egg may mean slightly different doses of DMB per day, which could account for variation in cavitation for some chicks immobilised for two to three days. As experiments were performed at different times of the year, the external temperature may have accelerated growth in some areas, which could also account for variation between groups I3–4 and I3–5, and high variation in general (Hamburger and Balaban 1963). Efforts were made to mitigate these differences, by having an n of at least 6 for all measurement groups. Post-hoc power calculations revealed a power of over 80% for all but two measurement groups. Additionally, some numbers of samples were low, particularly in assessment of cavitation. Tearing and folding artefacts were present in many sectioned samples contributing to the low number of examined hip joints. However, having identified the critical period of fetal movements for early joint development opens up many exciting avenues for future investigation. Other areas of interest which were beyond the scope of this study due to time-limitations were the changes that immobilisation may confer to cartilage and mineralised cartilage material properties, rate of mineralisation, and recently identified mechanosensitive gene expression (Nowlan, Prendergast et al. 2008, Rolfe, Nowlan et al. 2014).

From this study, an obvious question arises. I show that that even after a brief period of immobility, resumption of movement for the remainder of development is not sufficient to restore typical cavitation and morphogenesis. Is it therefore possible to externally manipulate the immobilised, developing chick *in ovo*, and ameliorate the effects of immobilisation upon cavitation and morphogenesis? External manipulation of the hind limb may add the critical mechanical stimulation necessary for normal cavitation, as cavitation appears to be a dose-dependent event. This idea is explored in the following chapter.

Chapter 5

5. Early Chick Hip Development: The Effect of External Manipulation

5.1 Introduction

As stated in the previous chapter, mechanical stimulation is necessary for physiological development of the skeletal system. The elimination of spontaneous movements in the chick embryo has long been known to hinder cavitation and morphogenesis of synovial joints, leading to joint fusion and incomplete or abnormal joint morphogenesis (Nowlan and Sharpe 2014). These effects are also seen during static culture of chick hind limb explants (Fell and Canti 1934, Lelkes 1958, Chandaria, McGinty et al. 2016). Few studies have been published detailing the changes in joint morphogenesis and cavitation of a developing joint experiencing applied mechanical stimulation. Lelkes demonstrated that external movement of *in vitro* hind limbs could counter the effects of immobilisation, and promote cavitation and articular surface development between the femur and tibia. Using compressive displacement bioreactor cultures, Chandaria *et al.* 2016 demonstrated that a physiological magnitude of movement *in vitro* promoted more normal progression of knee joint morphogenesis. To our knowledge, no studies have been published regarding the effects of externally applied mechanical stimulation on joint morphogenesis and cavitation during *in vivo* development.

In Chapter 4, later and longer periods of immobilisation more severely affected hip joint cavitation. Could a certain threshold of external mechanical stimulation be critical for hip joint cavitation? It is known that, under complete immobilisation, abnormal morphogenesis succeeds abnormal cavitation in the chick hip at e9 (Nowlan and Sharpe 2014). In Chapter 4, a 72–hour continual period of immobilisation between e4–7 led to pronounced effects on cavitation and

morphology of the hip joint at e9. Could external mechanical stimulation induce a cavitational event, and could this subsequently promote more normal morphogenesis?

It was hypothesised that external manipulation of the immobilised chick embryo hind limb, just prior to the point of cavitation, would allow for morphogenesis and cavitation of the hip joint to proceed more normally, even under continued immobilisation. To investigate this hypothesis, chick embryos were immobilised from e5–8. The hind limb was then manipulated at e8, around which point cavitation would normally occur. The effects of external manipulation on immobilised hip joint cavitation and morphogenesis at e9 were then assessed.

5.2 Materials and Methods

5.2.1 Chick treatment

Fertilised eggs were incubated, removed of albumen, and windowed, as described in section 3.1.1. One immobilisation regime was performed using 0.5% decamethonium bromide (DMB) based on the results of the last chapter. In the previous chapter, a 72–hour period of immobilisation was shown to be most critical for joint shape development and cavitation. Here, I immobilised from e5 rather than e4 in order to reduce high mortality, and continued to e8 to separate the influence of the resumption of natural movements, versus application of external movement. Embryos were immobilised at the same time as the start of incubation, according to regime. All embryos were harvested at e9.

5.2.2 Specimen numbers

Embryos were harvested from two manipulation experiments, and pooled. Hind limbs that were damaged at any point during processing were discarded and not included in the final analysis. As only the right hand side of an embryo was manipulated, the immobilised, unmanipulated left hand side acted as a contralateral control throughout this experiment. A total of 14 pairs of hind limbs were analysed for morphology, and six pairs of hind limbs were analysed for cavitation (Table 5.1).

Incubated	Harvested	OPT	Cryo
24 eggs	8 embryos	4 pairs	2 pairs
48 eggs	15 embryos	10 pairs	4 pairs

Table 5.1: Total number of paired chick hind limbs assessed for cavitation and morphology.

5.2.3 Joint shape and cavitational analysis

Hind limbs for 3D shape analysis were stained with 0.015% Alcian blue and imaged with OPT, and analysed, as detailed in section 3.3. Characteristics of joint morphogenesis were compared between manipulated and unmanipulated groups. Hind limbs for cavitational analysis were cryologically sectioned at 12μm, stained with 0.01% Toluidine blue, and examined for cavitational failure, as detailed in section 3.5.2.

5.2.4 Statistical analysis

Measurements were taken based on anatomical landmarks as in section 3.4. Power analyses were used to assess the power of each group, with a power of above 0.8 for each measurement comparison. The two-tailed, paired sample *t*-test was performed to assess for statistical differences between the manipulated and unmanipulated groups (Excel, Microsoft, 2018).

5.3 Results

5.3.1 Shape outlines

Immobilised femoral heads that experienced external manipulation had more features of normal joint development compared to the immobilised, unmanipulated femoral heads. The most striking difference in shape was noticed in the outgrowth of the femoral head. Qualitatively, the femoral heads of the manipulated group had more outgrowth than those of the unmanipulated femoral heads (Figure 5.1, compare a' to b', and observe in c'). Manipulated femoral heads were more rounded and pronounced, compared to unmanipulated femoral heads (Figure 5.1a', b'). Manipulated femoral heads also had an increased femoral width, and a deeper fossa, compared to the unmanipulated femoral heads (Figure 5.1a, b). From the shape profiles, external manipulation did not appear affect greater trochanter outgrowth, as the greater trochanters in both manipulated and unmanipulated limbs appeared similar. Both manipulated and unmanipulated shape profiles were variable (Figure 5.1, compare a' to b'). Externally manipulated acetabulae also had more normal features of joint development. The depth of externally manipulated acetabulae was particularly affected, which had greater depth compared to unmanipulated acetabulae. Externally manipulated acetabulae also increased slightly in width, compared to unmanipulated acetabulae (Figure 5.1, compare a to b). Again, shape profiles appeared variable in both manipulated and unmanipulated acetabulae (Figure 5.1c).

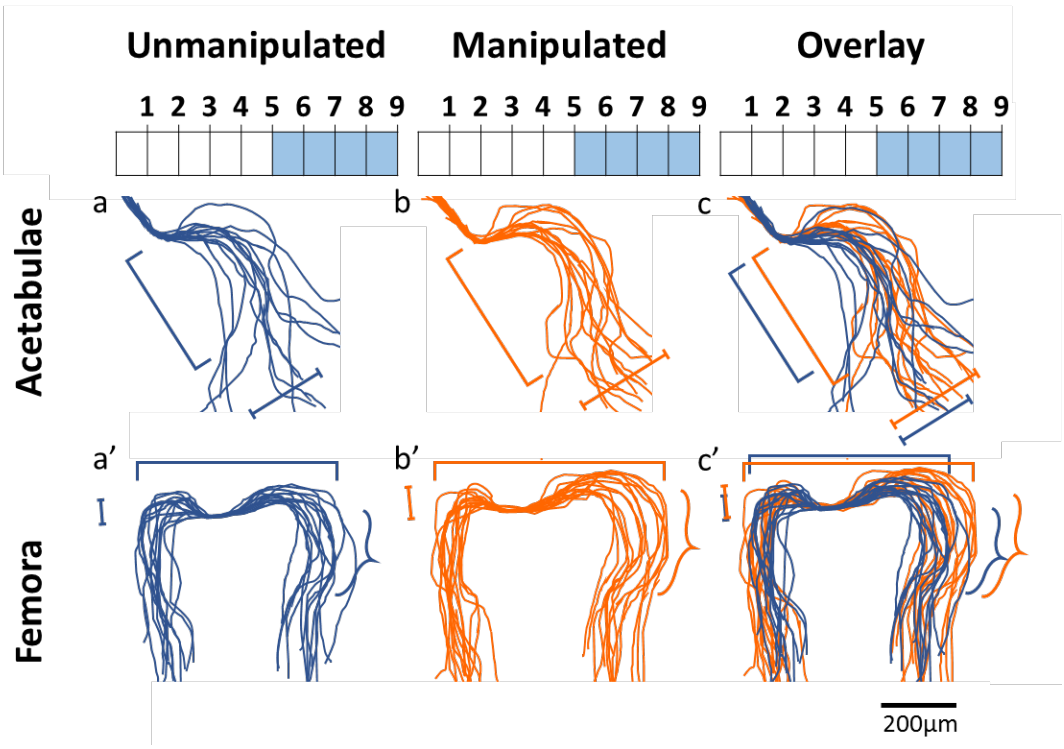


Figure 5.1: Shape profiles of the femoral head and acetabulum comparing unmanipulated (blue, n=14) and externally manipulated (orange, n=14) hip joints. Manipulated hip joints were larger than unmanipulated hip joints. Square brackets: acetabular or femoral width; curly brackets: femoral head outgrowth; I-bars: fossa depth.

5.3.2 Measurements

Statistically, externally manipulated femoral heads were significantly larger than unmanipulated femoral heads. Measurements of the femoral head to the piriformis, and the epiphyseal width in externally manipulated femora were significantly larger compared to unmanipulated femora (Figure 5.2a, d). The measurement of the femoral head to the greater trochanter was also significantly larger in the manipulated femora, compared to unmanipulated femora (Figure 5.2c). Statistically, external manipulation did not significantly affect the width of the femoral neck, and measurements did not reveal any such trend (Figure 5.2d). All three measurements of the acetabulae were larger with manipulation. Following external manipulation, acetabular height, width and depth were significantly larger compared to the unmanipulated acetabulae (Figure 5.2f–g).

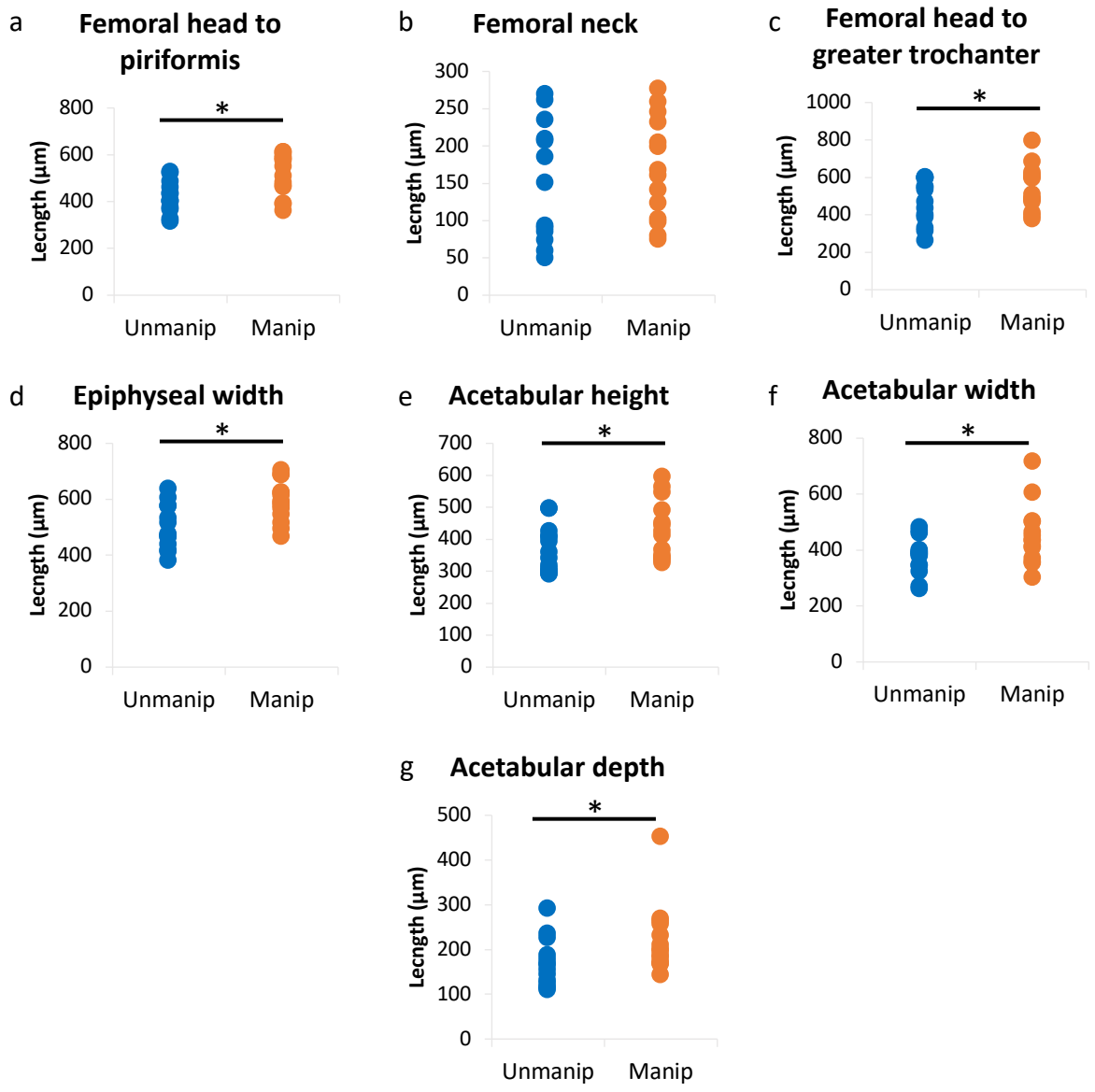


*Figure 5.2: Dot plot graphs of the femoral head and acetabulum comparing unmanipulated (blue, n=14) and externally manipulated (orange, n=14) hip joints. Manipulated hip joints were significantly larger than unmanipulated hip joints. *p-values < 0.05.*

5.3.3 Cavitation

Cavitation was assessed according to the scoring system in section 3.5.2. External manipulation of the immobilised chick hind limb partially ameliorated the effects of immobilisation from e5–8 in the hip joint. As seen in Chapter 4, immobilisation from e5–8 led to severely hindered cavitation (Figure 4.4m–o). In three out of six examined contralateral pairs, the externally manipulated hip joints were normally cavitated with increased joint space and tissue clearing around the hip joint (Figure 5.3b, d, f, score=0/3), compared to the unmanipulated hip joints with almost completely failed cavitation (Figure 5.3a, c, e, scores=1–2/3). In one out of six examined contralateral pairs, the externally manipulated joint was normally cavitated (Figure 5.3h, score=0/3) compared to the unmanipulated joint, which partially failed to cavitate (Figure 5.3g, score=1/3). In two out of

six examined contralateral pairs, both the manipulated and unmanipulated hip joints were severely affected by immobilisation with failed cavitation (Figure 5.3i–l, scores=2/3).

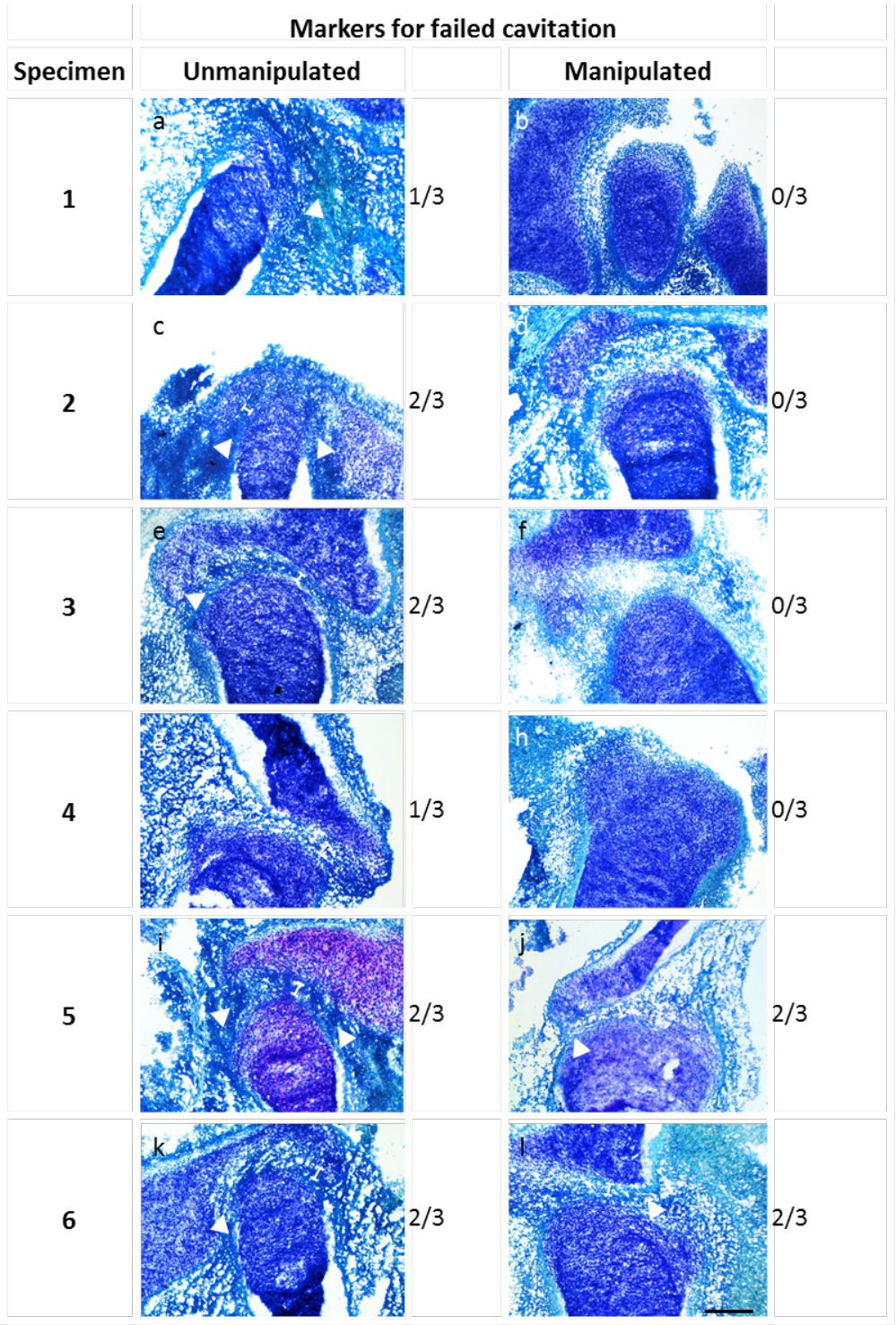


Figure 5.3: Histological sections of externally manipulated and unmanipulated paired hip joints. Unmanipulated hip joints had more signs of cavitational failure than manipulated hip joints (a–h). Cavitation was assessed and scored on a scale of zero to three according to the following criteria: closed triangle, no clear separation between joint rudiments due to lack of tissue clearing; I-bar, decreased joint space between joint rudiments; asterisk, fusion between rudiments.

5.4 Discussion

This research demonstrates for the first time that the effects of immobility on major hip anatomical landmarks during during early fetal development can be significantly ameliorated by a very short period of external manipulation *in ovo*. Femoral head outgrowth, femoral head width, and acetabular height, width and depth were all significantly increased compared to their unmanipulated counterparts. The effects of continual immobility on hip joint cavitation were also less severe in manipulated hip joints compared to unmanipulated hip joints. The hypothesis that applied, local movements would promote more normal joint development than contralateral controls was corroborated. A previous study in our group showed that morphology of the hip joint only became abnormal in immobilised chicks past the point at which cavitation should occur (Nowlan and Sharpe 2014). Here, despite continued immobility, manipulation led to more normal cavitation and more normal morphogenesis compared to unmanipulated contralateral rudiments. Hence, I purport that mechanical stimulation of the hip joint promotes cavitation of the joint rudiments, which is critical for the further morphogenesis and maturation of the hip joint.

Embryonic chicks were immobilised for four continuous days, from e5 until harvest at e9. The first independent movements of the chick limbs begin at e6.5, with slight adductions and abductions of the shoulder and hip, and increase in frequency by e9 (Hamburger and Balaban 1963). The external manipulation of the hip joint used in this chapter is not representative of physiological movement patterns of the chick embryo. However, repeated manipulation several times over development increases the risk of infection and causing tissue trauma to the delicate embryo. Previous studies moved the knee joint five times per 24–hour period (Lelkes 1958). Hence, manipulation of the hip joint five times at e8 was considered an appropriate single intervention on the hip joint *in ovo*.

During the course of this doctorate, the design of a culture system was published where embryonic chick hind limbs were encased in plastic grips and rotated, inducing plantarflexion of the ankle (Stein, Buckley et al. 2019). The loaded ankle was then placed back on top of the dissected chorioallantoic membrane. The youngest embryo that this culture system investigated was between e16–17, and the chick hatches between e20–21 (Hamburger and Hamilton 1951). Major morphological features of the hip joint emerge almost ten days prior to this (Nowlan, Chandaria et al. 2014). A simple manipulation of the hip joint was sufficient to investigate very early stages of joint development. Results from this study are not yet available, although survival appears similar to survival in the research in this chapter (~30%) (Stein, Buckley et al. 2019). Work in this chapter demonstrates that, despite a period of continual immobilisation, one well-timed intervention can promote more normal cavitation and morphogenesis.

The results presented in this chapter support the hypothesis that a threshold of pre-cavitational mechanical stimulation is necessary for cavitation and further morphogenesis of the developing joint. In the next chapter, I build upon these theories, and switch to a mammalian model of tissue culture. Using murine embryos, I explore the effects of increased mechanical loading in joints of the forelimb and hind limb.

Chapter 6

6. Early Mouse Limb Development: The Effects of Dynamic Loading

6.1 Introduction

As stated in Chapter 2, mechanical stimulation is necessary for physiological development of the skeletal system. Findings during *in vitro* culture of embryonic limbs are sparse, but also appear to support mechanical stimulation as important for joint development. Referenced in the previous chapter, culture of the embryonic chick showed that external flexion of explanted hind limbs led to more developed knee joint spaces (Lelkes 1958). Chapter 5 of this thesis demonstrated that external manipulation of the immobilised *in ovo* chick hind limb led to more developed joint morphology, as well as more developed joint cavities. Chandaria 2017 showed that a physiological magnitude of movement *in vitro* promoted a more normal progression of joint morphogenesis in the chick knee compared to under- or over-stimulation. The role of stretch-activated and voltage-gated calcium ion channels has also been implicated in the transduction of mechanical stimuli in the chick knee (Parisi, Chandaria et al. 2018). Access to the mammalian embryo is more difficult, although for example, daily subcutaneous injection of rat embryos with D-tubocurarine resulted in multiple articular contractures, alterations in femoral shape, and reduction of the absolute and relative volume of bone trabeculae (Rodriguez, Palacios et al. 1992). However, exploration of mechanical stimulation using surgical, pharmacological, or *in vitro* manipulation in the mammalian model is rare, and it remains unclear how static or dynamic cultures affect the growth and mineralisation of murine prenatal limbs, compared to uncultured limbs. The role of *in vitro* mechanical stimulation, or, absence of mechanical stimulation in growth and mineralisation of murine prenatal limbs is similarly unexplored.

Prior to examining these questions, it was necessary to quantify how much growth occurs over six days of *in vitro* culture. I hypothesised that six days of *in vitro* culture of murine prenatal limbs would lead to greater outgrowth and mineralisation of the murine limbs, compared to uncultured limbs. The mammalian bioreactor culture developed in Chapter 3 was used to culture two different mammalian joints, the elbow and knee, at two different developmental stages, e14.5 and e15.5. Growth and mineralisation were then characterised, compared to uncultured rudiments.

I then hypothesised that *in vitro* dynamic mechanical stimulation would lead to greater and more defined outgrowth of joint rudiments, and increased mineralisation, compared to statically-cultured murine limbs. Murine prenatal elbow and knee joints were cultured either dynamically or statically, as described in Chapter 3, and growth and mineralisation characterised.

The research described in the first half of this chapter hence aimed to explore two research questions:

- How do murine prenatal limbs grow *in vitro* compared to uncultured limbs?
- How does mechanical stimulation affect cartilage and mineralisation *in vitro?*

I next examined the subject of skeletal recovery due to applied movements, *in vitro*. In Chapter 5, external loading of the *in ovo* chick hind limb was seen to partially ameliorate the effects of immobility on joint morphogenesis and cavitation. Mutant murine models which lack limb muscle, or have absent or reduced muscle contraction during development, often show differential joint morphological and mineralisation profiles compared to their control littermates (reviewed in Chapter 2). As *in vivo* manipulation of the murine embryo was considered unfeasible, I decided to use the *in vitro* bioreactor system to explore whether external movement inducing mechanical forces upon *in vitro* prenatal cartilage would promote more normal shape and mineralisation, in the absence of muscle contraction due to a genetic mutation. The *Splotch-delayed* ($Pax3^{Sp\text{-}d/Sp\text{-}d}$) mouse, where muscle precursor cells do not migrate to the developing limbs and consequentially lack limb muscle, was chosen for investigation (Franz 1993, Vogan, Epstein *et al*. 1993). $Pax3^{Sp\text{-}d/Sp\text{-}d}$ mice have an altered mechanical environment due to their lack of appendicular muscle, which affects genes associated with development, differentiation, cell signalling, and cytoskeletal architecture (Rolfe, Nowlan et al. 2014). However, specific aspects of joint shape and mineralisation have not been characterised for the $Pax3^{Sp\text{-}d/Sp\text{-}d}$ mouse.

I hypothesised that six days of mechanostimulation from dynamic loading could promote more normal morphogenesis and mineralisation in $Pax3^{Sp\text{-}d/Sp\text{-}d}$ murine prenatal limbs, compared to unloaded $Pax3^{Sp\text{-}d/Sp\text{-}d}$ limbs. First, joint morphology and mineralisation profiles were characterised for the $Pax3^{Sp\text{-}d/Sp\text{-}d}$ mouse compared to control littermates at e14.5. Next, growth

and mineralisation of Pax3$^{Sp\text{-}d/Sp\text{-}d}$ and control littermates were dynamically-cultured, and growth and mineralisation characterised.

The research described in the second half of this chapter aimed to explore one research question:

- When muscleless limbs are cultured *in vitro*, can mechanical stimulation bring about more normal shape and mineralisation?

6.2 Materials and Methods

6.2.1 Harvest, culture, and number of limbs

To test for growth under static culture, and effect of mechanical stimulation *in vitro*, murine forelimbs and hind limbs were harvested at e14.5 and e15.5 and prepared for culture as described in Chapter 3. Right hind limbs and forelimbs of each embryo were subjected to dynamic or static culture, whilst left hind limbs and forelimbs were immediately processed for joint shape and mineralisation ratio analysis as a 'uncultured' measure of normal, physiological growth. Limbs were pooled from three separate cultures (Table 6.1). To test for shape and mineralisation recovery in muscleless mice, three Pax3$^{Sp\text{-}d/Sp\text{-}d}$ mutants and five control or heterozygous (control) embryos were harvested from one pregnant mouse at e14.5. Pax3$^{Sp\text{-}d/Sp\text{-}d}$ mice were identified by presence of curly tails and spina bifida in the lumbosacral region (Keller-Peck and Mullen 1996). Both mutant and control left and right hind limbs and forelimbs were subjected to dynamic loading. The e14.5 uncultured measure of normal growth from the previous experiment was used, as well as an e14.5 uncultured measure of five mutant forelimbs and four mutant hind limbs analysed from scans previously obtained in the Nowlan group (Table 6.2). Limbs were cultured as determined in section 3.1.2 and 3.1.3.

	(a) **Forelimb e14.5**		(b) **Forelimb e15.5**		(c) **Hind limb e14.5**		(d) **Hind limb e15.5**	
	Joint morphology	Mineralisation ratio	Joint morphology	Mineralisation ratio	Joint morphology	Mineralisation ratio	Joint morphology	Mineralisation ratio
Uncultured	6	6	6	6	7	7	7	7
Static	7	7	7	7	7	9	7	7
Dynamic	7	7	9	*	7	9	7	9

*Table 6.1: Number of control murine forelimbs and hind limbs analysed for elbow and knee joint morphology and mineralisation ratio (forelimb: humerus, radius and ulna; hindlimb: femur, tibia and fibula) of long rudiments. Limbs were pooled from three cultures. * For mineralisation ratio of the dynamically-cultured e15.5 forelimb, humerus n=14, radius n=10, ulna n=10.*

	(a) **Forelimb e14.5**		(b) **Hind limb e14.5**	
	Joint morphology	Mineralisation ratio	Joint morphology	Mineralisation ratio
Uncultured control	6	6	7	7
Uncultured Pax3$^{Sp\text{-}d/Sp\text{-}d}$	5	5	4	4
Dynamic control	4	7	4	9
Dynamic Pax3$^{Sp\text{-}d/Sp\text{-}d}$	5	5	5	5

Table 6.2: Number of control and Pax3$^{Sp\text{-}d/Sp\text{-}d}$ murine forelimbs and hind limbs analysed for elbow and knee joint morphology and mineralisation ratio (forelimb: humerus, radius and ulna; hindlimb: femur, tibia and fibula) of long rudiments.

6.2.2 Joint shape and mineralisation ratio analysis

Limbs for 3D shape analysis were stained with 0.015% Alcian blue and imaged with OPT, as detailed in section 3.4. Staining revealed an intact limb post-culture and loading, and no disintegration of the cartilaginous or mineralised tissue (Figure 6.1). Limbs damaged during processing were discarded. 3D reconstructions of joints were made using Mimics. Reconstructions of the elbow were virtually aligned to obtain views of the frontal humerus, lateral and medial humeral condyles, lateral ulna, and frontal radius. Reconstructions of the knee were virtually aligned to obtain views of the frontal distal femur, lateral and medial femoral condyles, frontal tibia, and frontal fibula (detailed in section 3.4.4). Outlines were then traced, and measurements (detailed in section 3.4.4) taken. Characteristics of skeletal development were then compared between uncultured, static, and dynamically loaded groups.



Figure 6.1: e15.5 hind limb dynamically cultured for 6 days and stained with Alcian blue/Alizarin red. Note limb is well-stained with no disintegration of rudiment.

6.2.3 Statistical analysis

For hind limb and forelimb uncultured, static, and dynamic groups, and hind limb and forelimb uncultured and dynamically-cultured Pax3$^{Sp\text{-}d/Sp\text{-}d}$ and control comparisons, joint measurements

were tested for normality using the Shapiro-Wilks test. In groups which were normally distributed, a one-way ANOVA was used to test for significant differences between uncultured, static, and dynamic groups. Where significant differences existed, Tukey's test was performed to identify groups which differed significantly (p-values of less than 0.05). In groups which were not normally distributed, the non-parametric Kruskal-Wallis test was used to test for significant differences between uncultured, static and dynamic groups. Dunn's post-hoc test was carried out, with the Bonferroni adjustment for multiple comparisons. Statistical tests were performed in SPSS (IBM Corp. Released 2016, IBM SPSS Statistics for Windows, Version 24.0. Armonk, NY; IBM Corp).

6.3 Results

6.3.1 Static growth of murine prenatal limbs *in vitro*

Forelimb

In both the e14.5 and e15.5 forelimbs, the medial condyle of the humerus was flatter and less bulbous, with the anterior curl of the medial condyle flattened and less prominent in the statically-cultured humerus, compared to the uncultured humerus (Figure 6.2, compare 6.2f to 6.2a and 6.2f' to 6.2a'). In the frontal humerus, static culture led to greater epicondylar width compared to uncultured humeri (Figure 6.2, square brackets). Humeral fossa depth also increased in e14.5 and e15.5 static cultures compared to uncultured humeri, as seen in the frontal humerus (Figure 6.2b, g, l, b', g', l, I bars). Again, the statically-cultured lateral condyle was less bulbous and prominent than the uncultured humeri. In both cultures, there were small increases in size and variation in statically-cultured radii compared to uncultured radii. (Figure 6.2n and 6.2n', open triangle). In both cultures, static culture of the ulna led to observed increased rudiment size, and led to a quantitative increase in length, depth and width of the ulnar fossa, compared to uncultured ulnae. (Figure 6.2e, j, o, e', j', o', I bars, arrow).

Qualitative analyses of the forelimb shapes reflected the quantitative measurement results. The height of the frontal lateral condyle showed no statistical differences or trends between uncultured and statically-cultured humeri in both e14.5 and e15.5 forelimbs (Figure 6.3d, d'). In the e14.5 forelimb, static culture led to significant increases in axial medial condylar depth and frontal epicondylar width, compared to measurements of the uncultured humeri (Figure 6.3c, d, c', d'). In the e15.5 forelimb, static culture led to significant increases in only frontal medial condylar height, compared to the uncultured humeri. Although not statistically significant, an

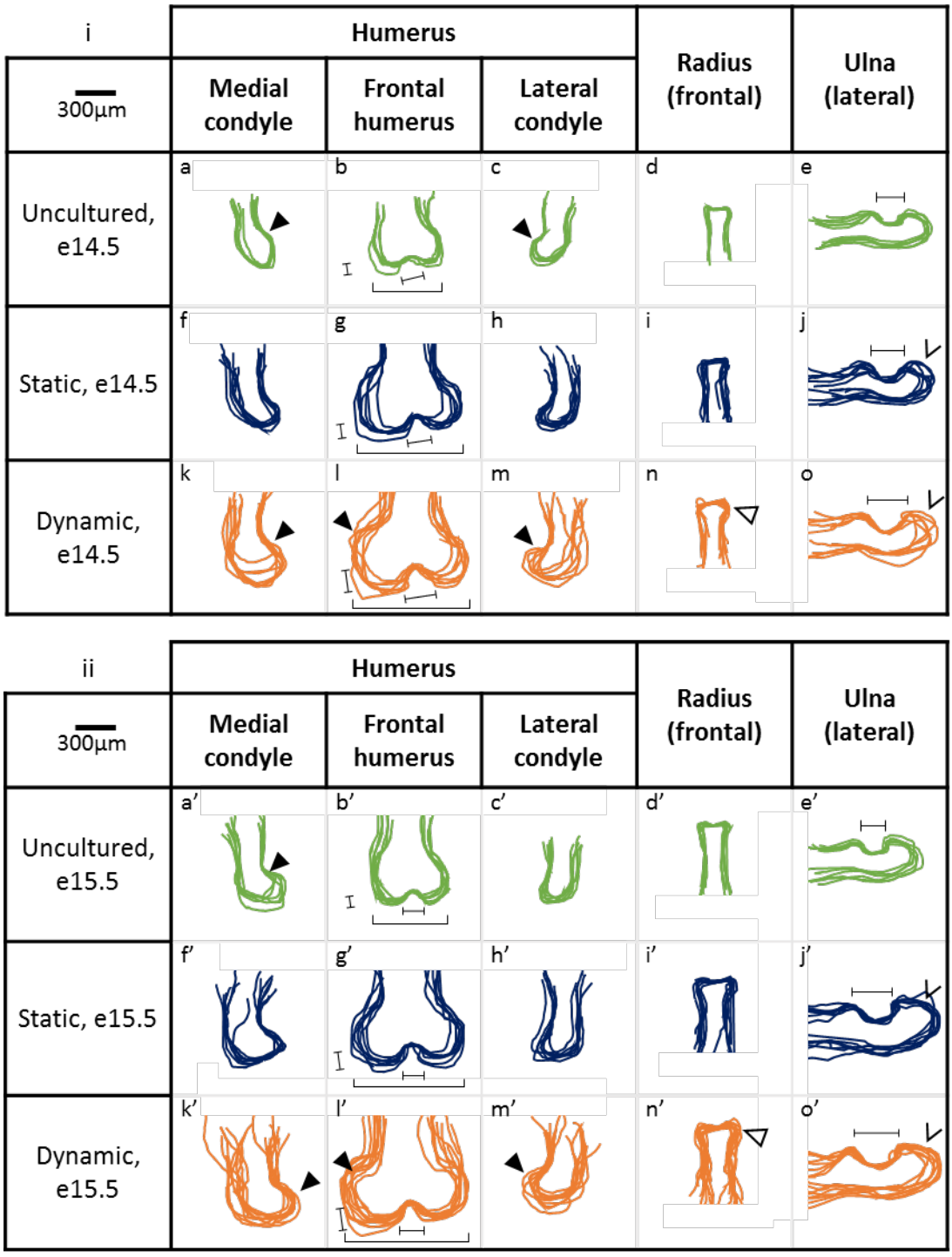


Figure 6.2: Shape profile outlines of the rudiments of the wild-type embryonic murine elbow joint. Embryos were harvested at (i) e14.5 or (ii) e15.5. Uncultured, outlines at e14.5 or e15.5. Static, limbs statically cultured for six days. Dynamic, limbs dynamically cultured for six days. Square brackets, epiphyseal width; I bars, fossa width and depth; filled triangle, anterior curl of condyle; open triangle, radial head protrusion; arrow, ulnar head protrusion. n=6–9 per group.

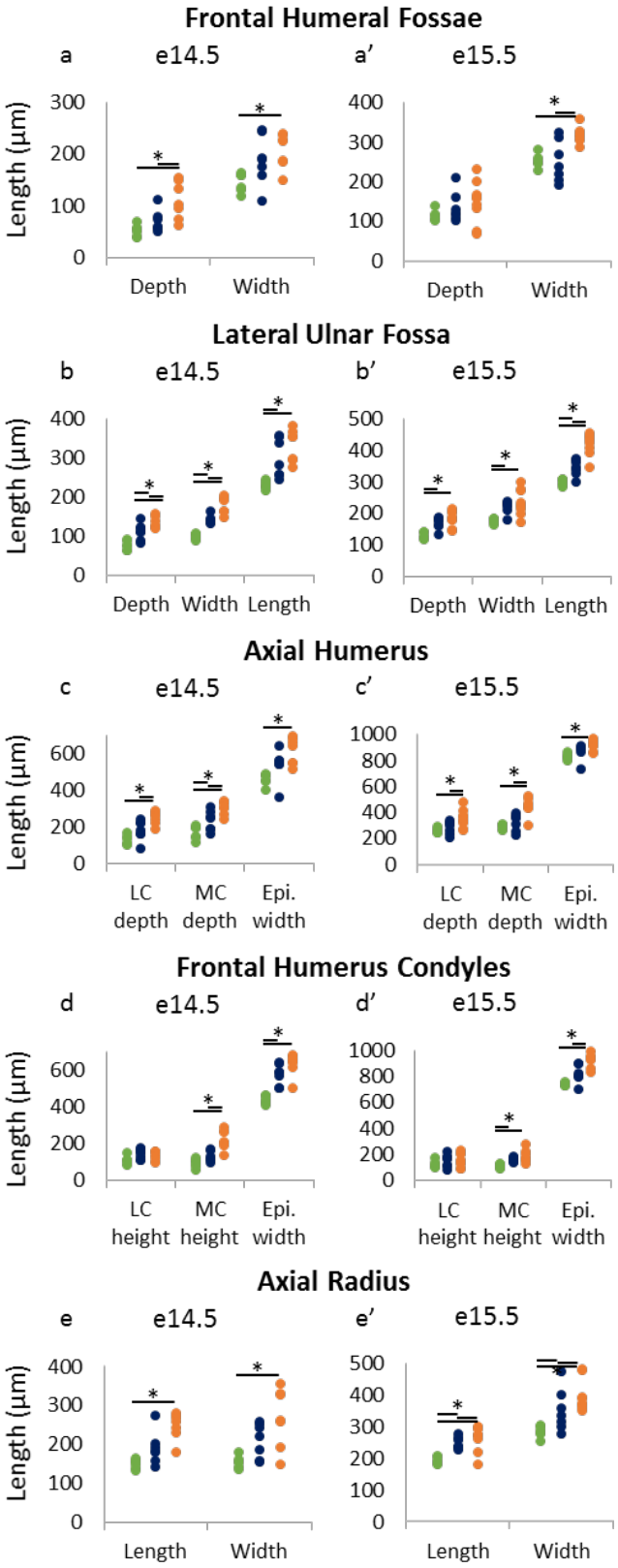


*Figure 6.3: Dot plot graphs of measurements of the wild-type embryonic murine elbow joint. Embryos were harvested at e14.5 or e15.5. LC, lateral condyle; MC, medial condyle; Epi., epicondylar. Uncultured (green), measurements at e14.5 or e15.5. Static (blue), limbs statically cultured for six days. Dynamic (orange), limbs dynamically cultured for six days. *=p-values <0.05. n = 6–9 per group.*

overall trend of static culture leading to increased growth was present in all measurements of the humerus in the e14.5 forelimbs, and in some measurements of the humerus, such as frontal humeral fossa depth, frontal and axial epicondylar width, and frontal medial condyle height for the e15.5 forelimbs (Figure 6.3a, c, d, a', c', d'). For both e14.5 and e15.5 forelimbs, there were statistically significant increases for all three measurements of the statically-cultured ulnae compared to the uncultured ulnae (Figure 6.3b, b'). Although not statistically significant, a general trend of static culture leading to increased growth compared to uncultured was present in the two e14.5 radial measurements. However, in the e15.5 forelimbs, static culture led to significant increases of radial width and depth compared to uncultured (Figure 6.3e, e').

Hind limb

Qualitatively, outlines for both statically-cultured e14.5 and e15.5 hind limbs were more varied, with outlines aligning less tightly compared to uncultured e14.5 hind limbs. Static culture of the femur led to both an increase in medial femoral condyle outgrowth and variation for both e14.5 and e15.5 hind limbs, compared to uncultured femora (Figure 6.4, compare 6.4a, f, k and 6.4a', f', k'). Static culture led to greater epicondylar width, as well as prominent medial and lateral condylar outgrowth seen frontally, compared to uncultured (Figure 6.4b, g, l, b', g', l', square brackets, filled triangle). For both e14.5 and e15.5 hind limbs, femoral fossa depth also increased with static culture, compared to uncultured femoral fossa depth (Figure 6.4b, g, l, b', g', l', I bars). Both medial and lateral condyles of the statically-cultured femora showed strong variation in morphology (Figure 6.4g, l, g', l'). Similarly to the femoral medial condyle; static culture led to more outgrowth of the lateral condyle compared to uncultured (Figure 6.4c, h, m, c', h', m', curly brackets). Statically-cultured tibiae and fibulae were larger than uncultured, with a protuberance of the tibial condyles and fibular head, respectively (Figure 6.4d, e, i, j, n, o, d', e', i', j', n', o').

Qualitative changes seen in the cultured hind limbs were again backed up by quantitative results. In both e14.5 and e15.5 hind limbs, static culture led to significant increases in the measurements of axial medial condyle depth, and axial fossa width and depth compared to measurements of the uncultured femora (Figure 6.5d, e, d', e'). Static culture also led to increases in axial lateral condyle depth, and frontal axial fossa with and depth compared to uncultured measurements in the e14.5 hind limbs, and increases in frontal medial condyle height, axial lateral condyle depth, and axial epicondylar width compared to uncultured measurements in the e15.5 hind limbs. (Figure 6.5b–e, a', b', d', e'). In both the e14.5 and e15.5 hind limbs, the intercondylar height of statically-cultured tibiae were on par with uncultured tibiae (Figure 6.5g, g').In the e14.5 statically-cultured tibiae, the intercondylar width increased significantly, and the medial and lateral height showed slight trends of increase compared to uncultured tibiae (Figure 6.5g–h). In the statically-cultured e15.5 tibiae, the lateral condyle height increased significantly, and intercondylar width slightly

increased compared to uncultured tibiae (Figure 6.5g'–h'). In both e14.5 and e15.5 hind limbs, static culture of the fibula led to increased fibular head depth and width compared to uncultured fibula, significantly so in the e15.5 fibular head depth (Figure 6.5f, f').

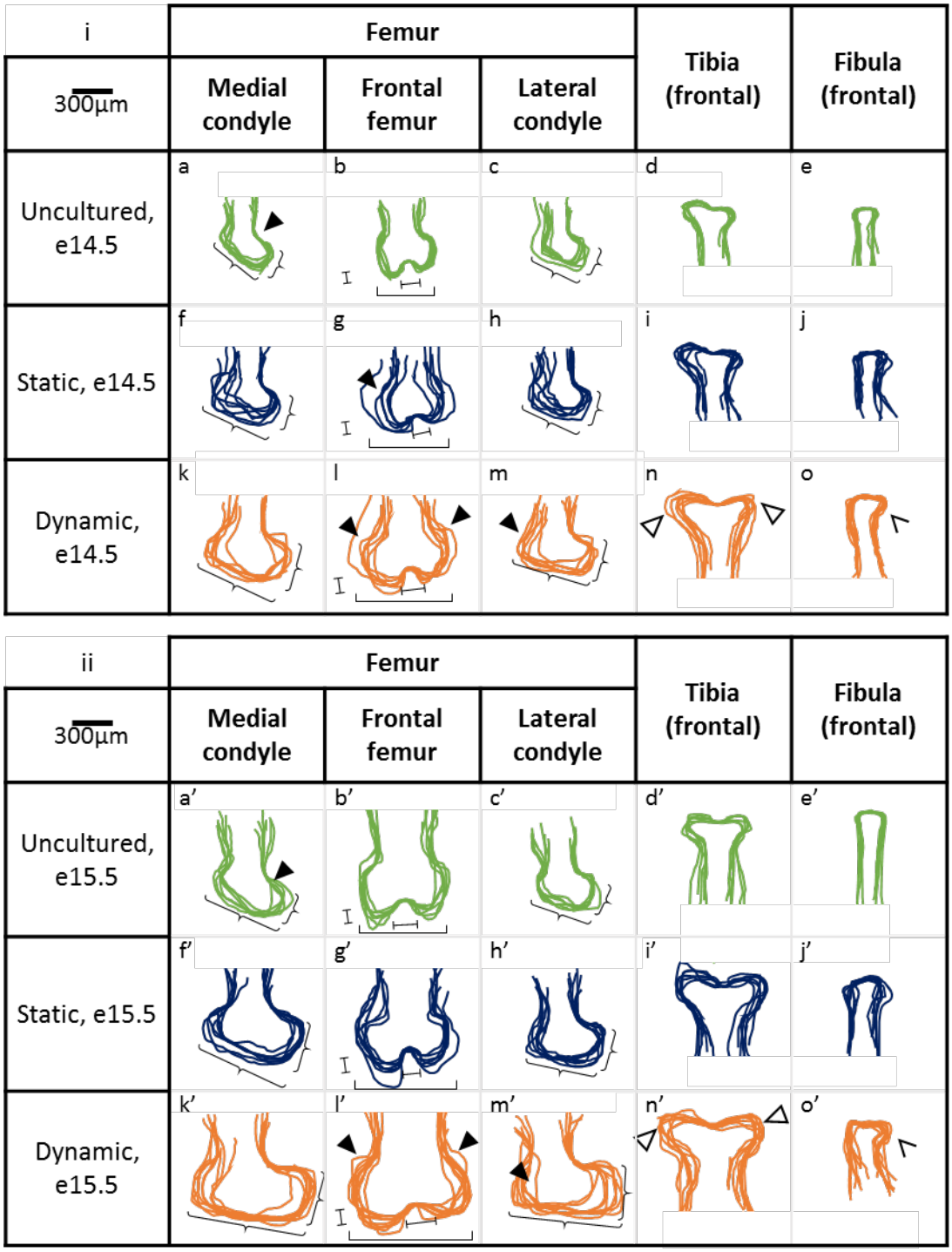


Figure 6.4: Shape profile outlines of the rudiments of the wild-type embryonic murine knee joint. Embryos were harvested at (i) e14.5 or (ii) e15.5. Uncultured, outlines at e14.5 or e15.5. Static, limbs statically cultured for six days. Dynamic, limbs dynamically cultured for six days. Square brackets, epiphyseal width; I bars, fossa width and depth; curly bracket, outgrowth of femoral condyle; filled triangle, epicondylar protuberance; open triangle, outgrowth of tibial condyle; arrow, fibular head protrusion. n=7 per group.

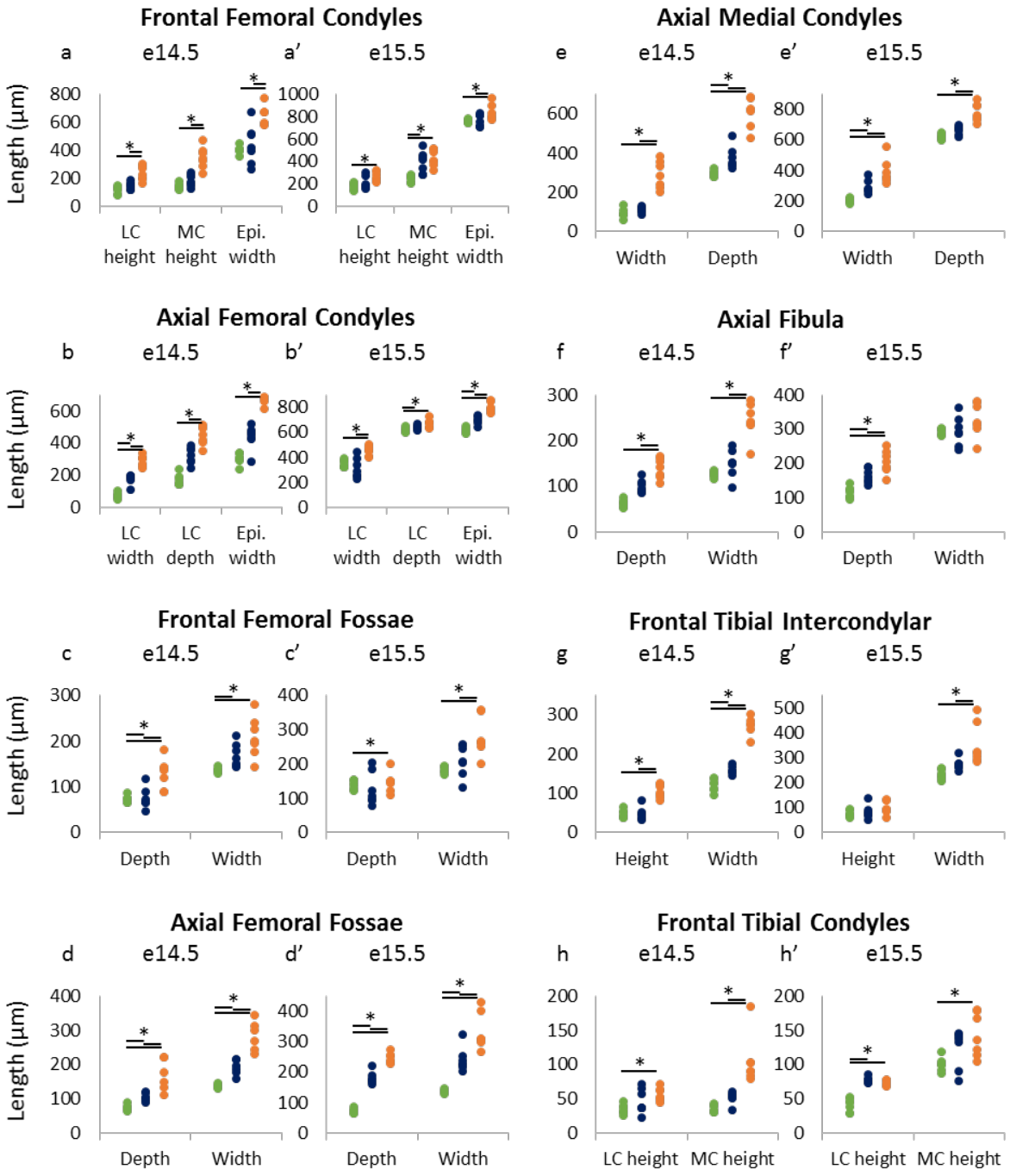


*Figure 6.5: Dot plot graphs of measurements of the wild-type embryonic murine knee joint. Embryos were harvested at e14.5 or e15.5. LC, lateral condyle; MC, medial condyle; Epi., epicondylar. Uncultured (green), measurements at e14.5 or e15.5. Static (blue), limbs statically cultured for six days. Dynamic (orange), limbs dynamically cultured for six days. *=p-values <0.05. n=7 per group.*

Mineralisation

There were no significant differences in mineralisation ratio between uncultured and statically-cultured forelimb long rudiments at e14.5 (Figure 6.6a). In the e15.5 forelimb, however, there were significant increases in mineralisation ratio in all rudiments of the forelimb when statically-cultured, compared to uncultured (Figure 6.6b). In the e14.5 hind limb, static cultured led to an increased mineralisation ratio in the femur alone (Figure 6.6c). In the e15.5 hind limb, however, there were significant increases in mineralisation ratio between static cultures and uncultured in all rudiments (Figure 6.6d).

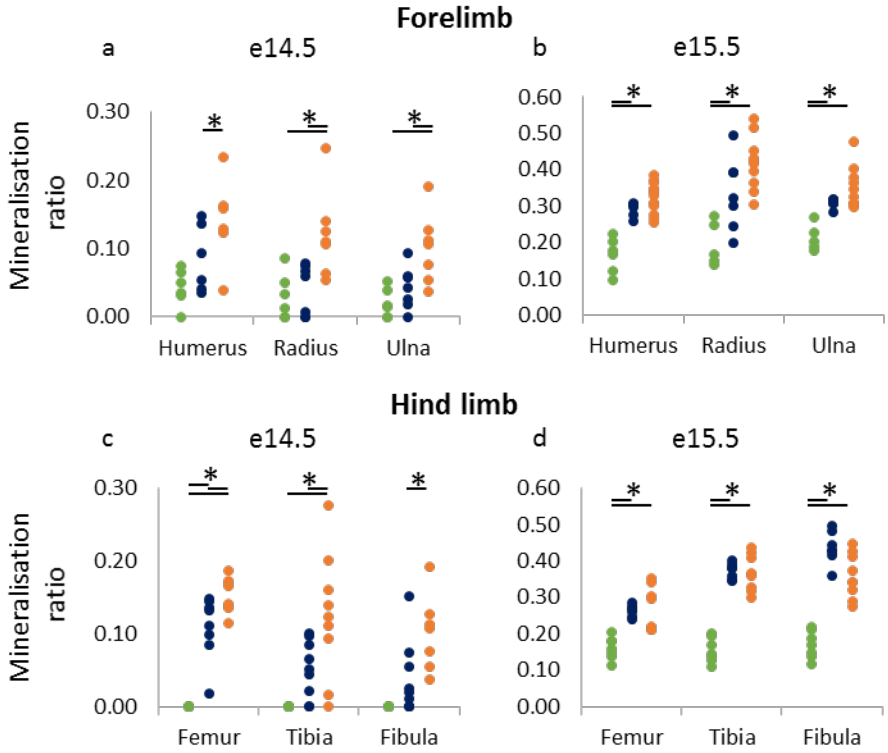


*Figure 6.6: Dot plot graphs of mineralisation ratio of the wild-type embryonic murine forelimb and hind limb rudiments. Embryos were harvested at e14.5 or e15.5. Uncultured (green), measurements at e14.5 or e15.5. Static (blue), limbs statically cultured for six days. Dynamic (orange), limbs dynamically cultured for six days. *=p-values <0.05. n=6–14 per group.*

6.3.2 Effect of mechanical stimulation on cartilage and mineralisation *in vitro*

Forelimb

Qualitatively, outlines for the e14.5 and e15.5 dynamic-cultured forelimbs were more varied and less tightly-aligned compared to statically-cultured forelimbs (Figure 6.2, compare 6.2f–j to 6.2k–o, and 6.2f'–j' to 6.2k'–o'). Humeri cultured under dynamic loading had a prominent anterior curl, which was rounder and larger compared to statically-cultured humeri (Figure 6.2k and 6.2k'). In the frontal humerus, dynamic culture led to greater epicondylar width compared to uncultured humeri (Figure 6.2, square brackets). Humeral fossa depth also increased in dynamic cultures compared to uncultured humeri, as seen in the frontal humerus (Figure 6.2, I bars). As in the e14.5 dynamically-cultured humeri, the dynamically-cultured e15.5 humeri also had the same protuberance on the frontal medial condyle compared to the statically-cultured humeri (Figure 6.2l and 6.2l', filled triangle). Again, the statically-cultured lateral condyle was less bulbous and prominent than the dynamically-cultured humeri. The lateral condyle of the e15.5 dynamically-cultured humeri in particular showed strong variation in morphology, with a far more prominent curl (Figure 6.4l'). In both e14.5 and e15.5 forelimbs, the radial head protruded more under dynamic culture compared to static culture (Figure 6.2n and n', open triangle). In both e14.5 and e15.5 forelimbs, dynamically-cultured ulnae had slightly larger fossae with a slight increase in ulnar length compared to statically-cultured ulnae (Figure 6.2j, o, j', o', I bars, arrow). From the shape profiles, a trend towards a larger joint with increased fossae depth and outgrowth of joint features was apparent, after dynamic culture. The medial and lateral condyles were more prominent, the humeral epiphyseal width greater, the radial head more prominent, and the fossae of the ulnae and humeri deeper in elbows which were dynamically-cultured for six days, compared to elbows which were statically-cultured.

Outlines revealed that dynamic culture of e14.5 and e15.5 forelimbs led to larger and more complex joint shapes compared to static culture. Quantitatively, this was reflected in the statistical analysis of joint measurements. In both e14.5 and e15.5 forelimbs, dynamic culture of the humerus led to significant increases in axial lateral and medial condylar depth, compared to measurements of statically cultured humeri (Figure 6.3c, c'). Dynamic culture of the e14.5 humerus also led to significant increases in frontal fossa depth and frontal medial condylar height, and trends of increase in frontal and axial epicondylar width, compared to e14.5 uncultured humeri (Figure 6.3a–d). Dynamic culture of the e15.5 humeri led to significant increases in frontal fossa and epicondylar width, with small trends of increase in three additional measurements of the humerus: fossa depth, axial epicondylar width, and medial condylar height (Figure 6.3a', c', d'). The height of the frontal lateral condyle in both e14.5 and e15.5 humeri, and depth of the frontal humeral fossa in the e15.5 humeri showed no statistical differences or trends between

statically- and dynamically-cultured humeri (Figure 6.3d, c', d'). In two of two measurements of the axial radius, dynamic culture led to trends of increase in the e14.5 radii, and significant increases in the e15.5 radii, in both radial width and depth compared to statically-cultured radii (Figure 6.3e, e'). In all three measurements of the e14.5 and e15.5 ulnae, there were statistically significant increases in the dynamically-cultured ulnae compared to the uncultured ulnae. In the measurements of ulnar fossa depth and width, dynamic culture led to statistically significant increases compared to the statically-cultured ulnae, with dynamic culture also leading to a trend of ulnar length increase compared to statically-cultured ulnae (Figure 6.3b, b').

Hind limb

Qualitatively, outlines for both statically- and dynamically-cultured e14.5 and e15.5 hind limbs were more varied, with outlines aligning loosely. Both static and dynamic culture of the e14.5 and e15.5 femur led to an increase in medial femoral condyle outgrowth, with the dynamically-cultured medial condyle in particular appearing much larger in width and depth (Figure 6.4f, k, f', k', curly brackets). The statically-cultured e14.5 medial condyle was varied in outgrowth, compared to dynamically-cultured femora (Figure 6.4f, k, f', k'). In both e14.5 and e15.5 femora, the femoral epicondylar width increased more after dynamic culture compared to statically-cultured femora (Figure 6.4g, l, g', l', square brackets). The e15.5 dynamically-cultured frontal femora were more curved and rounder compared to the e15.5 statically-cultured femora, with less prominent fossa (Figure 6.4g', l'). Dynamic culture also led to more outgrowth of the lateral condyle than static culture, with a variation in size and shape of the lateral condyle (Figure 6.4h, m, h', m'). Both medial and lateral condyles of the statically- and dynamically-cultured femora showed strong variation in morphology (Figure 6.4g, l, g', l'). A marked increase in tibial medial and lateral condylar size was seen when dynamically-cultured, compared to statically-cultured tibia (Figure 6.4i, n, i', n'). The dynamically-cultured medial and lateral tibial condyles were more pronounced and wider than statically-cultured tibial condyles (Figure 6.4i, n, i', n'). Dynamic culture led to a pronounced curl of the fibular head, as well as a notable increase in size, compared to statically-cultured fibulae (Figure 6.4j, o, j', o' arrow). From the shape profiles of the e14.5 and e15.5 hind limbs, a trend towards a larger joint with increased femoral fossae depth and outgrowth of joint features was apparent, after dynamic culture. The medial and lateral femoral condyles were more prominent, the femoral epiphyseal width greater, the tibial condyles more prominent, and the head of the fibula more curled and prominent in knees which were dynamically cultured for six days, compared to knees which were statically cultured.

Outlines revealed that dynamic culture led to larger and more complex knee joint shapes compared to statically-cultured hind limbs. Quantitatively, this was reflected in the statistical analysis of joint measurements. In all but one of the twelve measurements of the e14.5 femora,

dynamic culture of the femur led to significant increases, compared to measurements of statically-cultured femora (Figure 6.5a–e). Dynamic culture led to small trends of increase in one additional measurement of the e14.5 femur compared to static culture: frontal fossa width (Figure 6.5c). In the e15.5 femora, eight out of twelve measurements of dynamically-cultured femora led to significant increases in the frontal and axial epicondylar width, axial medial condylar depth and length, axial lateral condyle depth, frontal fossa width, and axial fossa width and depth, compared to measurements of statically cultured femora (Figure 6.5a'–e'). Dynamic culture led to small trends of increase in one additional measurement of the e15.5 femur compared to static culture: axial lateral condyle depth (Figure 6.5b'). In the measurements of tibial intercondylar height and width, and tibial medial condyle height, dynamic culture of the e14.5 tibiae led to statistically significant increases compared to the statically-cultured tibiae (Figure 6.5g–h). Dynamic culture of the e15.5 tibia led to significant increases in tibial intercondylar width compared to statically-cultured tibiae (Figure 6.5g'). However, there were no observable differences in tibial intercondylar height between the e15.5 static and dynamically-cultured tibiae (Figure 6.5g'). In both measurements of the e14.5 fibular head depth and width, and in the e15.5 fibular head depth, dynamic culture led to statistically significant increases compared to the statically-cultured fibulae (Figure 6.5f, f'). Fibular head width showed no statistical differences between static and dynamic fibulae, when cultured at e15.5 (Figure 6.5f').

Mineralisation

In the e14.5 forelimb and hind limb, all six dynamically-cultured long rudiments had significant increases in mineralisation ratio compared to static cultures. In the e15.5 forelimb, trends of mineralisation ratio increase were observed in all three dynamically-cultured rudiments compared to statically-cultured rudiments (Figure 6.6b). However, in the e15.5 hind limb, there were no trends of increased mineralisation in dynamically-cultured rudiments compared to statically-cultured rudiments, whilst the statically-cultured fibulae had a trend of greater mineralisation than the dynamically-cultured fibulae (Figure 6.6d).

6.3.3 Recovery of skeletal development in mechanically-stimulated rudiments

From one litter, e14.5 limbs from both Pax3$^{Sp\text{-}d/Sp\text{-}d}$ and control littermates were dynamically-cultured for six days. First, I compare uncultured Pax3$^{Sp\text{-}d/Sp\text{-}d}$ mutants to uncultured control littermates, using outlines, measurements and mineralisation ratio, in order to describe shape and mineralisation differences within the same litter. Then, I compare dynamically-cultured Pax3$^{Sp\text{-}d/Sp\text{-}d}$ mutants to the dynamically-cultured control littermates, to determine whether the genetic effects of immobility of the mutant can be ameliorated, and the extent of this.

Forelimb

In the uncultured Pax3$^{Sp\text{-}d/Sp\text{-}d}$ humerus, the medial condyle was much less pronounced and less bulbous compared to the control humerus (Figure 6.7a, f, filled triangle). The width of the frontal humerus was greatly reduced in the Pax3$^{Sp\text{-}d/Sp\text{-}d}$ mutant compared to the control, whilst humeral fossa depth was greater in the mutant (Figure 6.7b, g, square brackets, I bars). The Pax3$^{Sp\text{-}d/Sp\text{-}d}$ mutant lateral condyle was also reduced in size, lacking the curl and bulbous outgrowth seen in the control lateral condyle (Figure 6.7c, h, filled triangle). Some variation was seen in the Pax3$^{Sp\text{-}d/Sp\text{-}d}$ mutant medial and lateral condyles, with outlines aligning less neatly compared to the control medial and lateral condyles. Radial width appeared similar in both Pax3$^{Sp\text{-}d/Sp\text{-}d}$ mutant and control rudiments (Figure 6.7d, i). The head of the ulna was reduced in outgrowth in the Pax3$^{Sp\text{-}d/Sp\text{-}d}$ mutant with slightly shallower fossae, compared to the control ulnae (Figure 6.7e, j, I bars). In the dynamically-cultured Pax3$^{Sp\text{-}d/Sp\text{-}d}$ mutant medial condyle, the lack of outgrowth seen in the uncultured mutant appeared to recover, with more pronounced condylar growth (Figure 6.7f, p, filled triangle). Both the dynamically-cultured Pax3$^{Sp\text{-}d/Sp\text{-}d}$ and control medial condyles increase in size, with the mutant showing slightly more of a curl than the control (Figure 6.7k, p, filled triangles). Humeral epiphyseal width also recovered from uncultured in the dynamically-cultured mutant humeri, and humeral fossa width and depth was similar between the dynamically-cultured Pax3$^{Sp\text{-}d/Sp\text{-}d}$ mutants and controls (Figure 6.7b, l, q, square brackets, I bars). Some variation was seen in the dynamically-stimulated Pax3$^{Sp\text{-}d/Sp\text{-}d}$ lateral condyle, with a range of different condylar shapes and sizes compared to the control lateral condyle (Figure 6.7m, r). Again, the size and width of the radii appeared similar in both control and Pax3$^{Sp\text{-}d/Sp\text{-}d}$ dynamic cultures (Figure 6.7n, s). Ulnar head outgrowth again appeared smaller in the Pax3$^{Sp\text{-}d/Sp\text{-}d}$ mutant compared to the control ulnar head, with fossa depth also reduced (Figure 6.7o, t, arrow, I bars).

The qualitative forelimb joint shape changes in Figure 6.7 matched the quantitative measurements. Between the control and Pax3$^{Sp\text{-}d/Sp\text{-}d}$ unculturedS, trends indicated a general decrease of the mutant measurement compared to the control measurement, with significant decreases in the mutant ulnar fossa length and epicondylar width (Figure 6.8b, d). As expected, dynamic culture of both Pax3$^{Sp\text{-}d/Sp\text{-}d}$ mutant and control forelimbs generally appeared to increase measurements, compared to uncultured mutant and control measurements. Dynamic culture of control forelimbs led to the humeral fossa depth, axial and frontal epicondylar width, ulnar fossa depth, width and length, and axial radial length significantly increasing compared to the uncultured control forelimbs (Figure 6.8a–e). In total, seven out of 13 measurements significantly increased, with the humeral fossa width, ulnar fossa depth, medial condylar height and frontal epicondylar width also showing trends of increase compared to uncultured mutant forelimbs (Figure 6.8a, b, d). An exception was the radial width, which did not appear to differ much

between all groups (Figure 6.8e). Unlike the in measurements of uncultured control and uncultured Pax3$^{Sp\text{-}d/Sp\text{-}d}$ mutant, where a general decrease in size was seen in the mutant forelimb measurements, dynamic culture of the mutant forelimbs appeared to partially ameliorate the shape changes seen between uncultured mutant and uncultured control, as also seen in the outlines (Figure 6.7). Statistics revealed that in thirteen out of thirteen measurements, there were no significant differences between the dynamically-cultured control and Pax3$^{Sp\text{-}d/Sp\text{-}d}$ mutant forelimbs (Figure 6.8a–e). Comparison between dynamically-cultured mutant and controls showed that measurements appear nearly on par with one another. The lateral condyle depth and medial condyle height of the dynamically-cultured Pax3$^{Sp\text{-}d/Sp\text{-}d}$ mutant forelimbs were slightly increased compared to the dynamically-cultured control forelimbs (Figure 6.8c, d).

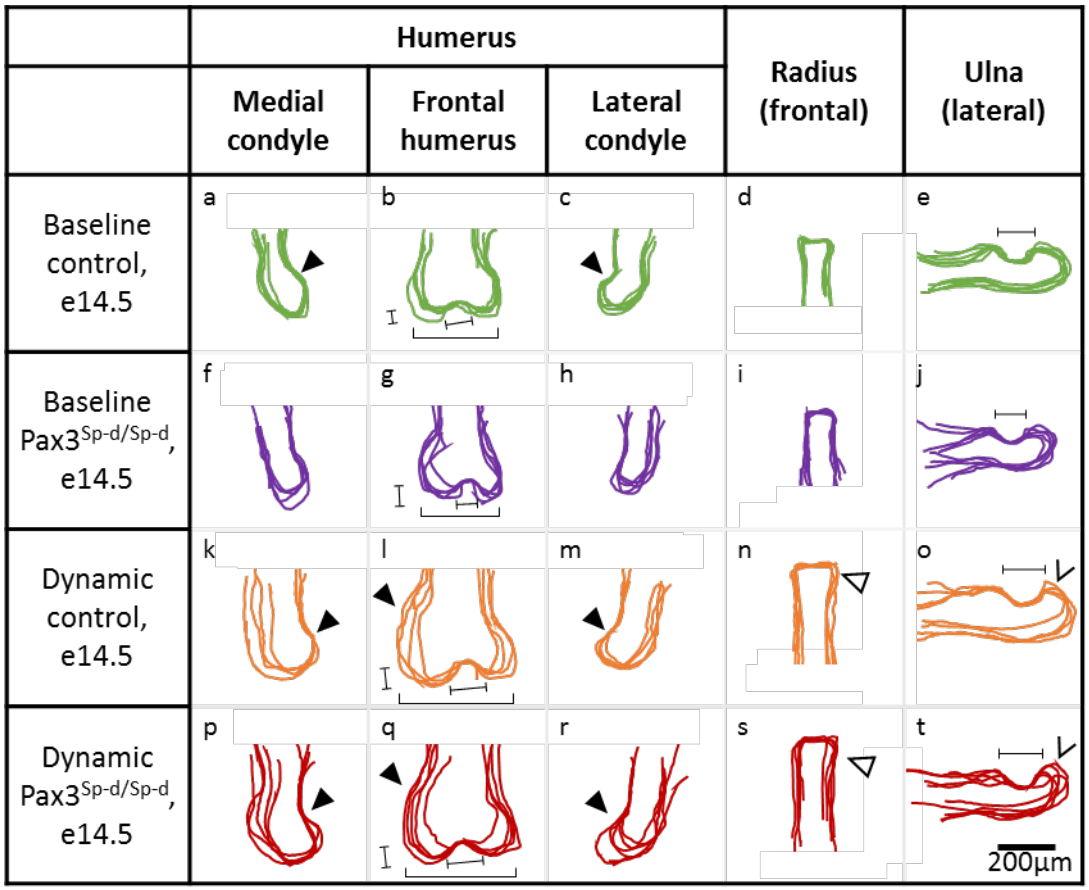


Figure 6.7: Shape profile outlines of the rudiments of the wild-type and Pax3$^{Sp\text{-}d/Sp\text{-}d}$ mutant embryonic murine elbow joint. All embryos were harvested at e14.5. Uncultured wild-type and uncultured Pax3$^{Sp\text{-}d/Sp\text{-}d}$, outlines at e14.5. Dynamic wild-type and dynamic Pax3$^{Sp\text{-}d/Sp\text{-}d}$, limbs dynamically cultured for six days. Square brackets, epiphyseal width; I bars, fossa width and depth; filled triangle, anterior curl of condyle; open triangle, radial head protrusion; arrow, ulnar head protrusion. n=4–6 per group.

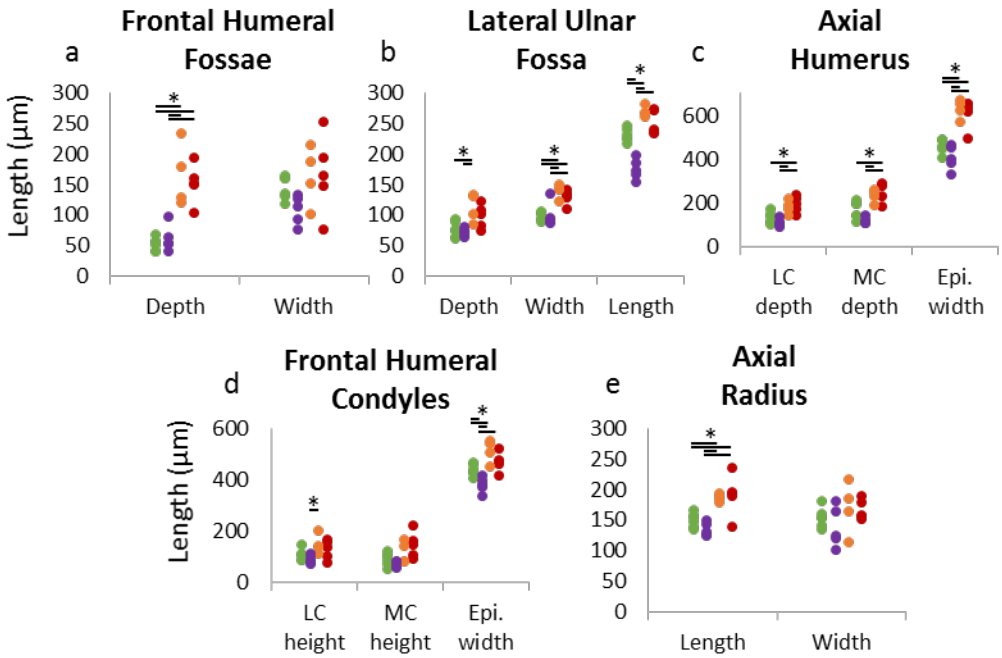


*Figure 6.8: Dot plot graphs of measurements of the wild-type and Pax3$^{Sp\text{-}d/Sp\text{-}d}$ mutant embryonic murine elbow joint. All embryos were harvested at e14.5. Uncultured wild-type (green) and uncultured Pax3$^{Sp\text{-}d/Sp\text{-}d}$), outlines at e14.5. Dynamic wild-type (orange) and dynamic Pax3$^{Sp\text{-}d/Sp\text{-}d}$ (red), limbs dynamically cultured for six days. *=p-values <0.05. n=4–6 per group.*

Hind limb

In the uncultured Pax3$^{Sp\text{-}d/Sp\text{-}d}$ mutant femora, the medial condyle was much more varied in size than shape compared to the uncultured control medial condyle, ranging from notably smaller, to approximately the same size as the control medial condyle. The medial condyle was only slightly less bulbous, and had more size variation, with outlines aligning less tightly compared to the control (Figure 6.9a, f). The epicondylar width of the frontal femur was reduced in the mutant compared to the control, whilst femoral fossa width and depth were similar (Figure 6.9, square brackets). As in the medial condyle, the mutant lateral condyle had less overall outgrowth, and was more varied in size than shape, with mutant outlines again aligning less tightly (Figure 6.9c, h, curly brackets). The frontal tibial plateau was slightly decreased in width, and the medial condyle less pronounced, in the uncultured mutant compared to the wildtype (Figure 6.9d, I, open triangles). Fibulae width was similar in both uncultured mutant and control specimens (Figure 6.9e, j). Both the dynamically-cultured control and Pax3$^{Sp\text{-}d/Sp\text{-}d}$ mutant knee joints increased substantially in size compared to their respective uncultureds. Some mutant condyle outlines were as large as the dynamically-cultured control outlines, but with a degree of shape and size variation, with mutant outlines not aligning as tightly (Figure 6.9k–t). Outgrowth in the medial condyle was partially restored in the dynamically-cultured mutant, appearing more bulbous in

shape compared to the mutant uncultured (Figure 6.9f, p, filled triangles). Femoral epiphyseal width also recovered in the dynamically-cultured mutant femora, with fossa width and depth similar between the mutant and control femora (Figure 6.9l, q, square brackets, I brackets). The lateral condyle in the dynamically-cultured mutant was lengthened yet narrower compared to the control (Figure 6.9l, q). Similarly to the uncultured femora, flaring out of the medial and lateral condyles reached a less defined point in the dynamically-cultured mutant femur, compared to the dynamically-cultured control femur (Figure 6.9l, q). In the dynamically-cultured femora, the frontal tibial plateau of some mutants was as wide as the control tibia, with the medial condyle varying in size (Figure 6.9n, s, open triangle). Again, fibulae width was similar in both mutant and control specimens (Figure 6.9o, t).

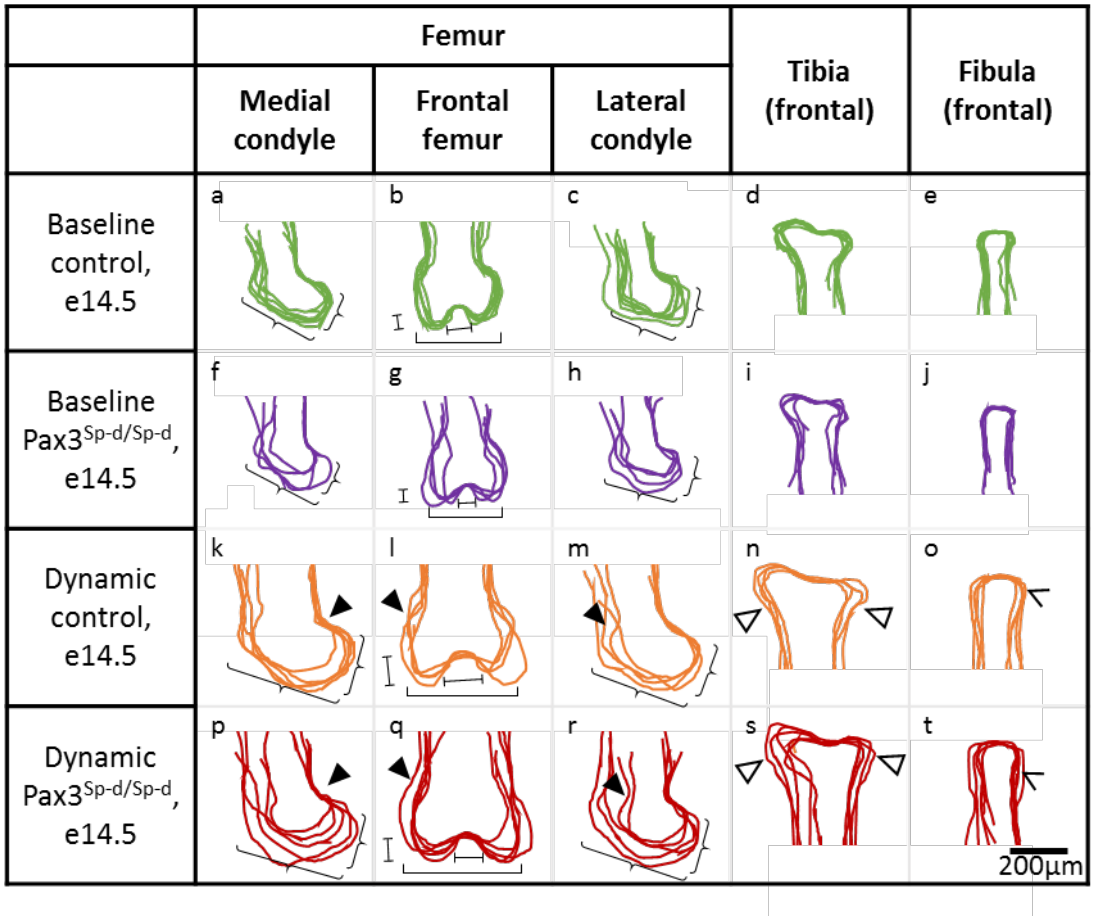


Figure 6.9: Shape profile outlines of the rudiments of the wild-type and Pax3$^{Sp\text{-}d/Sp\text{-}d}$ mutant embryonic murine knee joint. All embryos were harvested at e14.5. Uncultured wild-type and uncultured Pax3$^{Sp\text{-}d/Sp\text{-}d}$, outlines at e14.5. Dynamic wild-type and dynamic Pax3$^{Sp\text{-}d/Sp\text{-}d}$, limbs dynamically cultured for six days. Square brackets, epiphyseal width; I bars, fossa width and depth; curly bracket, outgrowth of femoral condyle; filled triangle, epicondylar protuberance; open triangle, outgrowth of tibial condyle; arrow, fibular head outgrowth. n=4–7 per group.

The qualitative shape changes seen in the Pax3$^{Sp\text{-}d/Sp\text{-}d}$ knee joints in Figure 6.9 match the quantitative statistical results. Between the control and Pax3$^{Sp\text{-}d/Sp\text{-}d}$ mutant uncultureds, trends indicated a general decrease in all eighteen mutant measurements compared to the control measurement, with significant decreases in the mutant axial medial condyle depth and fibula width (Figure 6.10e, f). As in the forelimb, dynamic culture of Pax3$^{Sp\text{-}d/Sp\text{-}d}$ mutant and control hind limbs increased measurement length compared to uncultured Pax3$^{Sp\text{-}d/Sp\text{-}d}$ mutants and controls, respectively. Dynamic culture of control hind limbs led to the frontal medial and lateral femoral condyle height, frontal femoral fossa width, frontal and axial femoral epicondylar width, axial femoral lateral condyle width and depth, axial femoral fossa depth and width, axial femoral medial condyle width and depth, axial fibular depth, frontal tibial medial and lateral condyle height, and frontal tibial intercondylar height and width increasing, compared to the uncultured control hind limb. In total, sixteen out of eighteen measurements of the dynamically-cultured wildtype hind limb significantly increased compared to the measurements of the uncultured control hind limbs (Figure 6.10a–h). Dynamic culture of mutant hind limbs led to the frontal medial and lateral femoral condyle height, frontal femoral fossa width, frontal and axial femoral epicondylar width, axial femoral lateral condyle width and depth, axial femoral fossa depth, axial femoral medial condyle width and depth, axial fibular depth and width, frontal tibial medial and lateral condyle height, and frontal tibial intercondylar height and width increasing, compared to the uncultured mutant hind limb (Figure 6.10a–h). Dynamic culture of Pax3$^{Sp\text{-}d/Sp\text{-}d}$ mutant hind limbs led to sixteen out of eighteen measurements significantly increasing compared to the uncultured Pax3$^{Sp\text{-}d/Sp\text{-}d}$ mutant hind limbs. Similarly to the dynamically-cultured mutant forelimb, dynamic culture of the Pax3$^{Sp\text{-}d/Sp\text{-}d}$ mutant hind limb also appeared to partially restore the shape changes seen between the uncultured Pax3$^{Sp\text{-}d/Sp\text{-}d}$ mutant and control hind limb measurements, as observed in the outlines. Statistics revealed that in all eighteen out of eighteen measurements, there were no significant differences between the dynamically-cultured control and dynamically-cultured Pax3$^{Sp\text{-}d/Sp\text{-}d}$ mutant hind limbs. The frontal and axial epicondylar widths, axial lateral condyle depth, frontal femoral fossa width, axial femoral fossa width and depth, axial medial condyle depth, and frontal tibial intercondylar height and width Pax3$^{Sp\text{-}d/Sp\text{-}d}$ mutant measurements were slightly decreased compared to the control measurement, but not significantly so (Figure 6.10a–e, h).

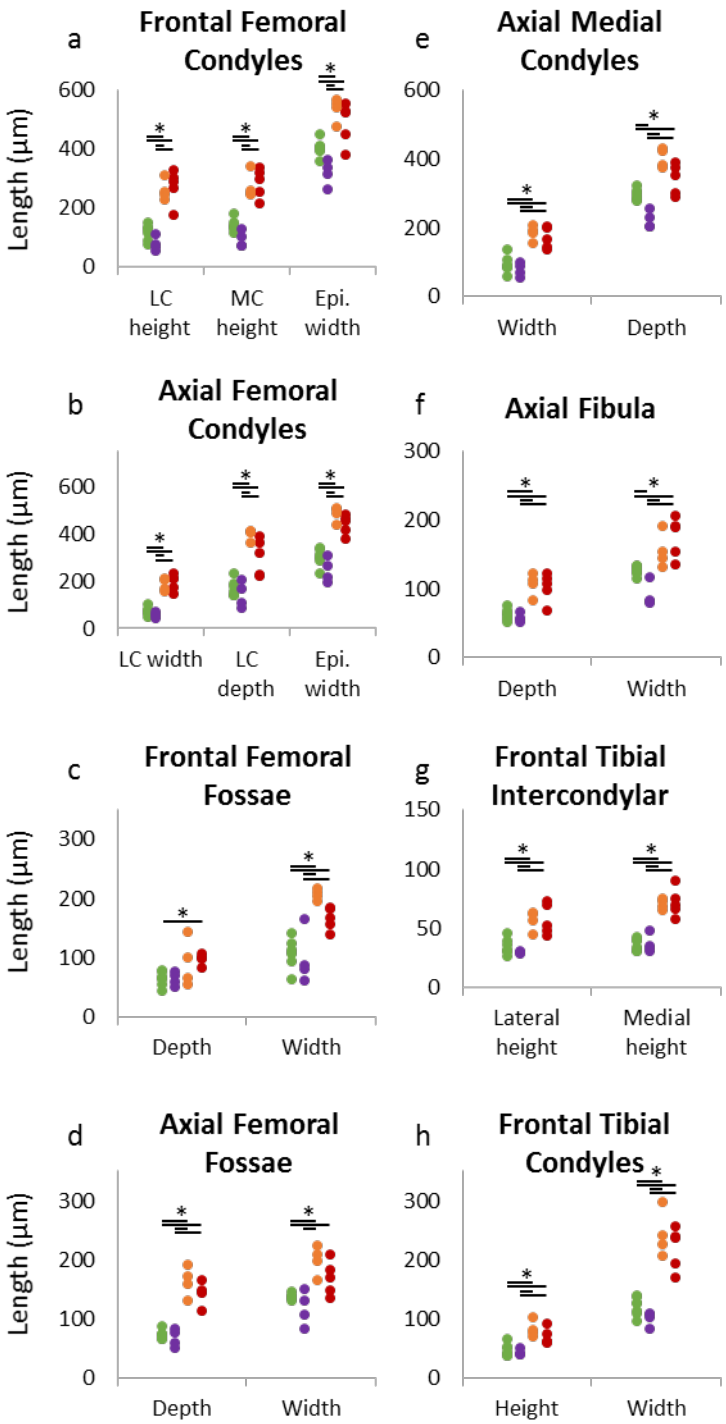


*Figure 6.10: Dot plot graphs of measurements of the wild-type and Pax3$^{Sp\text{-}d/Sp\text{-}d}$ mutant embryonic murine knee joint. All embryos were harvested at e14.5. Uncultured wild-type (green) and uncultured Pax3$^{Sp\text{-}d/Sp\text{-}d}$), outlines at e14.5. Dynamic wild-type (orange) and dynamic Pax3$^{Sp\text{-}d/Sp\text{-}d}$ (red), limbs dynamically cultured for six days. *=p-values <0.05. n=4–7 per group.*

Mineralisation

In all the rudiments of the hind limb and forelimb, there were no significant differences between the mineralisation ratio of all uncultured control and Pax3$^{Sp\text{-}d/Sp\text{-}d}$ mutant rudiments. However, there was a trend of slight decrease in the mineralisation ratio of the Pax3$^{Sp\text{-}d/Sp\text{-}d}$ mutant humerus and ulna compared to their control counterparts (Figure 6.11a, b). Six days of dynamic stimulation led to an increase in mineralisation ratio in all rudiments, both control and mutant, compared to their uncultured counterparts. Additionally, there were no statistically significant differences between the dynamically cultured control and dynamically-cultured mutant mineralisation ratios of the forelimb and hind limb, with no trends of increase or decrease between the Pax3$^{Sp\text{-}d/Sp\text{-}d}$ mutant and control ratios (Figure 6.11a, b).

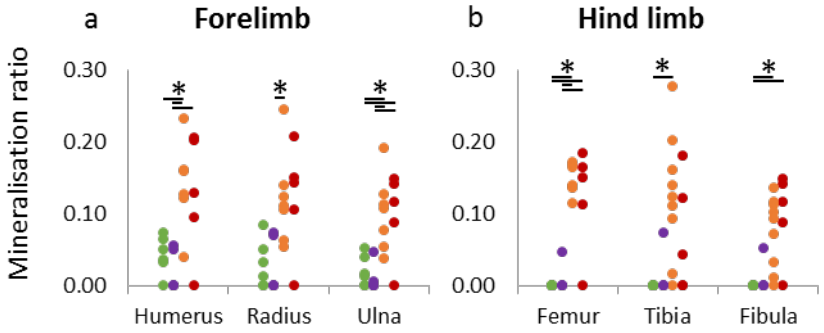


*Figure 6.11: Dot plot graphs of mineralisation ratio of the wild-type and Pax3$^{Sp\text{-}d/Sp\text{-}d}$ mutant embryonic murine forelimb and hind limb rudiments. All embryos were harvested at e14.5. Uncultured wild-type (green) and uncultured Pax3$^{Sp\text{-}d/Sp\text{-}d}$), outlines at e14.5. Dynamic wild-type (orange) and dynamic Pax3$^{Sp\text{-}d/Sp\text{-}d}$ (red), limbs dynamically cultured for six days. *=p-values <0.05. n=4–9 per group.*

6.4 Discussion

The results indicate that dynamic culture not only led to increased outgrowth of certain shape features of the joint compared to immobile limbs, but that movement itself was more important than the presence of muscle for early joint shape development and mineralisation. *In vitro* dynamic culture led to greater outgrowth of murine forelimb and hind limb knee and elbow rudiments compared to static culture at two different ages (e14.5 and e15.5), of which both were generally greater than uncultured joints. Dynamic culture also led to increased mineralisation ratio in the e14.5 and e15.5 forelimb, and e14.5 hind limb, compared to static cultures and uncultured joints. Importantly, *in vitro* dynamic culture of the Pax3$^{Sp\text{-}d/Sp\text{-}d}$ muscleless knee and elbow rudiments led to shape profiles and mineralisation ratios comparable with the dynamically-stimulated control rudiments.

The experiments in this research can be pooled into two different groups: early skeletal development under presence or absence of movement. Statically-cultured wild-type and uncultured Pax3$^{Sp\text{-}d/Sp\text{-}d}$ mutant embryos experienced an absence of moment during culture. Dynamically-cultured wild-type and dynamically–cultured Pax3$^{Sp\text{-}d/Sp\text{-}d}$ mutant embryos experienced applied movements for six days after harvest at e14.5. The statically- and dynamically-cultured wild-type embryos were harvested at e14.5 and e15.5, having experienced passive maternal movement, plus their first limb movements at e12.5, and then cultured for six days with or without loading. Uncultured Pax3$^{Sp\text{-}d/Sp\text{-}d}$ mutants were harvested at e14.5, with absent limb musculature, having only experienced the passive movements of their littermates from e12.5, plus maternal movements. Dynamically-cultured Pax3$^{Sp\text{-}d/Sp\text{-}d}$ mutants were cultured for six days with loading. Despite differences within moved and unmoved scenarios, specific features of joint development were consistently affected by the presence or absence of movement during development.

The mineralisation ratio of the uncultured Pax3$^{Sp\text{-}d/Sp\text{-}d}$ humerus, radius, and ulna decreased slightly compared to the uncultured control forelimb rudiments. This was in contrast to the mineralisation ratio of the uncultured Pax3$^{Sp\text{-}d/Sp\text{-}d}$ femur, tibia or fibula, which did not show any trends of increase or decrease compared to the uncultured control hind limb rudiments. When movement was applied *in vitro*, the mineralisation ratio of the dynamically-cultured mutants increased, comparable to cultured control rudiments. In the dynamically-cultured e14.5 and e15.5 humerus, radius, ulna, and the e14.5 femur, tibia, and fibula, all six rudiments had either significant increases, or trends of increase in mineralisation ratio compared to statically-cultured rudiments. However, in the femur and tibia of the e15.5 wild-type hind limb, there was no difference in mineralisation ratio between static and dynamic cultures, and a small increase in mineralisation of the e15.5 wild-type statically-cultured fibula compared to the dynamically-cultured fibula. The anterior curl of both the humeral medial and lateral condyles were flattened and less prominent in the uncultured Pax3$^{Sp\text{-}d/Sp\text{-}d}$ mutant and statically-cultured wild-type elbows; however, when *in vitro* movement was applied in both the dynamically-cultured wild-type and dynamically-cultured Pax3$^{Sp\text{-}d/Sp\text{-}d}$ elbow joints, these regions grew prominently. A similar effect was observed in the wild-type hind limb, where size and shape of the femoral medial and lateral condyles was reduced under static culture, and increased under dynamic culture. The size, more so than the shape of the femoral medial and lateral condyles in the Pax3$^{Sp\text{-}d/Sp\text{-}d}$ mutant were reduced, compared to their control counterparts. Humeral fossa depth and width also decreased in the uncultured mutant and statically-cultured wild-type elbows, and increased in size under applied movement *in vitro*. However, tibial medial condyle outgrowth, and width of the tibial plateau was only seen to significantly differ between static and dynamic culture of wild-

type embryos, with uncultured mutant tibiae having less severe effects compared to uncultured controls (key findings summarised in Figure 6.12).

A range of articular shape effects such as smaller, simpler, or malformed joint surfaces have been reported in several animal models of reduced or absent mobility (Drachman and Sokoloff 1966, Rot-Nikcevic, Reddy et al. 2006, Nowlan, Sharpe et al. 2010, Roddy, Prendergast et al. 2011, Brunt, Norton et al. 2015, Chandaria, McGinty et al. 2016, Sotiriou, Rolfe et al. 2019), along with disruption of rudiment mineralisation (Nowlan, Bourdon et al. 2010). Whilst almost all examined bones and joints of the immobilised chick are similarly affected by immobility, (Nowlan, Sharpe et al. 2010), previous papers have shown that in several mouse mutants where limb musculature fails to develop (*splotch-delayed Sp-d*, *Six1*$^{-/-}$*Six4*$^{-/}$ and *Myf5*$^{-/-}$*MyoD*$^{-/-}$), or where muscle is reduced, (*Myf5*$^{nlacZ/+}$*Myod*$^{-/-}$) the forelimb rudiments are more severely affected compared to the

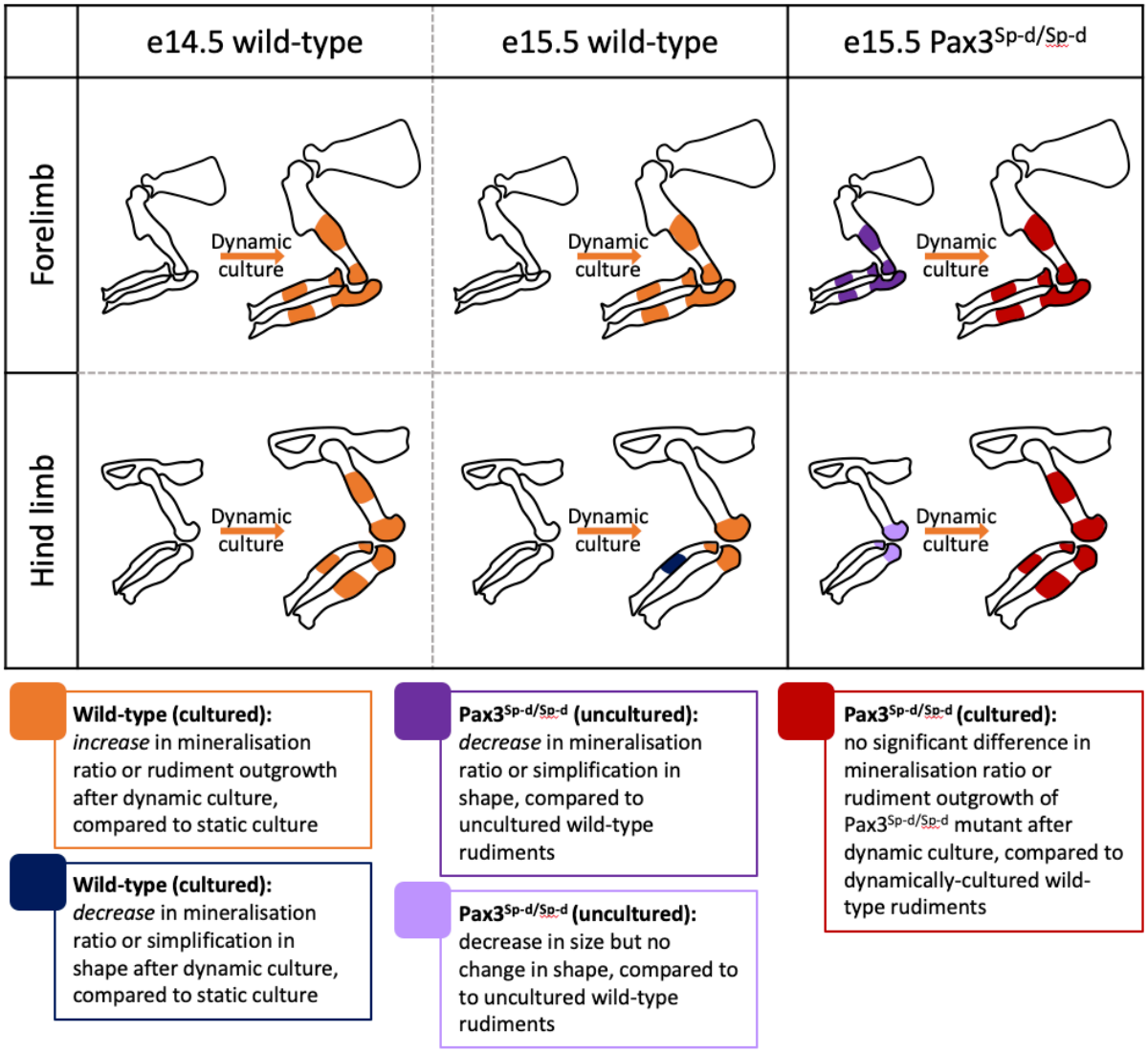


Figure 6.12: Summary of effects seen in murine forelimbs and hind limbs after six days of dynamic culture compared to static culture.

morphology of the elbow joint is more severely affected compared to the knee joint, which has few obvious shape abnormalities, along with no change in the progression of tibial mineralisation (Nowlan, Bourdon et al. 2010, Sotiriou, Rolfe et al. 2019). It has been proposed that different regions of the developing limbs may be exposed to different levels of passive movements from the gestating mother, littermates, or uterine contraction, and that these passive forces may be able to 'compensate' for the loss of movement due to muscle absence (Nowlan, Bourdon et al. 2010, Sotiriou, Rolfe et al. 2019). Muscle contraction is proposed to regulate β-catenin activation in the elbow, whereas in the fingers, muscle absence did not affect β-catenin activation, and the fingers were seen as normally cavitated (Kahn, Shwartz et al. 2009). Whilst I did not investigate genetic or molecular pathways, our results corroborate with previous murine work. In the elbow, the number of significant differences between the uncultured control and uncultured Pax3$^{Sp\text{-}d/Sp\text{-}d}$ mutant was two out of 13 (16%) measurements, compared to two out of 18 (11%) measurements in the knee. The uncultured mutant knee joint varied more in size, rather than shape, compared to the forelimb which had severely reduced outgrowth of the medial and lateral humeral condyles. Mineralisation ratio was also slightly reduced in the uncultured mutant forelimb rudiments, whereas in the hind limb, mineralisation of the femur, tibia and fibula were slightly increased in the mutant compared to control rudiments. Static culture of wild-type joints led to increased growth, but simplification of shape, compared to uncultured or dynamically-cultured joints. In contrast, despite the complete absence of limb muscle, *in vitro* dynamic stimulation of the Pax3$^{Sp\text{-}d/Sp\text{-}d}$ elbow and knee joints led to outgrowth of specific aspect of joint development, along with an increase in mineralisation ratio, comparable with dynamic stimulation of the wild-type control. Although the *in utero* mechanical environment experienced by elbow and knee joints is very different compared to the *in vitro* mechanical environment in the bioreactor, our results highlight the impact of external movements on early, localised joint outgrowth and mineralisation. I propose that mechanical forces exerted upon developing cartilage are necessary in the mechanoregulation of specific, early processes within developing skeletal rudiments, and that external forces are able to partially overcome aberrant joint shape changes and increase mineralisation as a consequence of reduced or absent limb muscle in early mammalian skeletal development.

It was observed that there was a marked difference in wild-type knee joint outgrowth, dependent on age of the limbs cultured. In the e14.5 and e15.5 wild-type elbows, the number of significant differences between dynamically-cultured and statically-cultured elbows was six out of 13 (46%) measurements at e14.5, compared to seven out of 13 measurements (54%) at e15.5. However, in the e14.5 and e15.5 wild-type knees, the number of significant differences between dynamically-cultured and statically-cultured knees was 16 out of 18 (89%) measurements at e14.5, compared

to only ten out of 18 (55%) measurements at e15.5. Additionally, in the femur and tibia of the wild-type e15.5 hind limbs, there was no difference in mineralisation ratio between static and dynamic cultures.

The difference between the age-dependent response of the forelimb and hind limb rudiments may be due to the amount of mechanical stimulation necessary for normal skeletal development. A recent spatiotemporal analysis of markers of joint, tendon, muscle, vascular, and cartilage development revealed similar patterning of these important limb processes (a) between the forelimb and hind limb, and (b) from e13.5 to e15.5, taking into account that the hind limb consistently lags half a day behind the forelimb (Martin 1990, Rafipay, Berg et al. 2018).

However, modelling of human fetal movements revealed that stress and strain in the fetal skeleton change over ontogeny and rise significantly over the latter half of gestation, with increased stress concentration in mineralised regions and increased strain concentrations in cartilage and articular surfaces over gestation (Verbruggen, Kainz et al. 2018). A previous chick bioreactor study in our group demonstrated a dose-dependent relationship between movement and morphogenesis in the developing knee, with a physiological level of flexion leading to the most normal progression of knee joint morphogenesis, compared to significantly smaller and less-developed rudiments in an under-flexed group, and large joint variation in an over-flexed group (Chandaria, McGinty et al. 2016). Taken together with the work in this chapter, these studies suggest that with an increase in rudiment size, comes the need for an increase in mechanical loading, and that the level of loading required for physiological growth during specific points in development varies between different joints, for example, the knee joint may need a larger increase in mechanical loading over gestation compared to the elbow joint. In the present study, some joint rudiments varied notably in size. This may be due to slight limb placement variation and small differences in embryonic age of the rudiment leading to shape changes and variation.

Research has explored the role of mechanical signalling, cell death and proliferation in mechanically-loaded cell and tissue cultures. The precise mechanism by which mechanical signals are sensed and then transduced into a functional chondrocyte response such as proliferation or differentiation remains unclear. Cyclic stretch-induced matrix deformation of 3D chondrocyte cultures was shown to significantly increase proliferation of immature chondrocytes over a six day period compared to non-deformed cultures, with cell doubling time greatly reduced (Wu and Chen 2000). However, differentiated chondrocytes did not increase in proliferation in response to mechanical stimulation, suggesting that for a proliferative response, chondrocytes need mechanical signalling in a specific window of time early on in the developmental period. Stretch-induced matrix deformation also up-regulated the expression of CMP/matrilin-1 and type X

collagen, markers of mature chondrocytes and hypertrophic cells respectively, suggesting that mechanical signalling plays a role in chondrocyte differentiation and maturation (Wu and Chen 2000). Cartilage matrix protein/matrilin-1 and type X collagen are also pericellular network-forming matrix proteins which directly interact with chondrocyte membranes, suggesting that mechanical signalling may be transduced through the extracellular matrix surrounding chondrocytes (Wu and Chen 2000). The question of cell death and proliferation during whole tissue culture arises. Light microscopy images reveal specimens that were well-stained and did not disintegrate even after dynamic loading, indicating that cell death did not play a major role in these findings (Figure 6.1). Previous research in the cultured embryonic chick knee reveals that culture in the dynamic bioreactor system leads to cell viability of greater than 95% with no significant differences in both statically and dynamically cultured distal femurs (Chandaria, McGinty et al. 2016). However, dynamically-loaded cultures led to significantly more proliferation than statically cultured femurs, suggesting that size and shape changes were due to mechanical stimulation upregulating proliferation rates. Future studies in this area should work to characterise the pattern of proliferation in the embryonic mouse in response to different loading regimes.

Recent research also suggests a role for stretch-activated and other ion channels in transduction of mechanical stimuli for a functional response in developing joint tissues. These ion channels are located in the plasma membrane surrounding developing chondrocytes. Blocking of the stretch-activated calcium ion channel during cyclical mechanical loading in an *in vitro* 3D chondrocyte culture was shown to prevent mechanical stimulation of chondrocyte proliferation, but did not block the up-regulation of CMP/matrilin-1 expression (Wu and Chen 2000). Blocking of voltage-gated calcium channels inhibited both CMP/matrilin-1 and chondrocyte proliferation, suggesting two different pathways for differentiation and proliferation (Wu and Chen 2000). Similar results were seen in whole embryonic chick limb culture. Blocking of either stretch-activated ion channels or voltage-gated calcium ion channels during cycling mechanical loading led to noticeable effects on growth and joint shape, inhibiting the morphological changes seen in dynamically loaded knee joints and leading to less complex knee joints (Parisi, Chandaria et al. 2018). The effects of mechanical loading on proliferation and differentiation on mammalian embryonic development were not explored in this study. Based on previous research, mechanical stimulation is necessary for proliferation and maturation of chondrocytes and is a likely avenue for future studies.

This work represents the first quantitative investigation into the contribution of applied flexion in the developing mammalian limb, highlighting differences in mechanoregulation of prenatal shape development and mineralisation between older and younger murine limbs, and between

the forelimb and hind limb. Fetal movements are known to play a significant role in healthy musculoskeletal development, and a decrease or absence of movements is implicated in conditions such as DDH, AMC, osteopenia, or FADS (reviewed in Nowlan 2015). The relevance of this research is that it may inform the timing and duration of possible future interventions to best restore joint structure and function, dependent on the joint involved. A potential intervention is prenatal vibroacoustic stimulation, which has been shown to evoke significantly increased fetal movement (Tan and Smyth 2001). Dependent on the joint involved, the timing of vibroacoustic stimulation may vary.

This study was not without limitations. The applied movement within the bioreactor is not considered physiological, as the murine elbow and knee can flex and extend, whereas in this culture system, they can only flex. Although dynamic culture does not replicate the full range of joint motion, as all limbs were cultured under 2mm of compressive loading, limbs can be compared relatively to each other. In dynamically-cultured explants, movement of the culture media has been proposed to induce fluid flow, increasing nutrient delivery in the otherwise-stagnant culture. The joint shape changes found between static and dynamic, as well as mutant and control cultures, match up with previous immobilisation studies (Drachman and Sokoloff 1966, Rot-Nikcevic, Reddy et al. 2006, Nowlan, Sharpe et al. 2010, Roddy, Prendergast et al. 2011, Brunt, Norton et al. 2015, Chandaria, McGinty et al. 2016, Sotiriou, Rolfe et al. 2019), giving confidence that changes in joint development were due to movement, and not increased nutrient delivery. The number of samples was as low as four samples in the uncultured Pax3$^{Sp\text{-}d/Sp\text{-}d}$ mutant hind limb, and dynamically-cultured controls. However, the use of just one litter in dynamically-cultured mutants and controls in this preliminary study allows for direct comparison between littermates and passive mechanical stimulation induced by just one mother, with intriguing results. The small number of mutants also meant that static culture of mutants could not be considered in the present study. However, the results from this study strengthen the hypothesis that dynamic loading leads to more normal joint shape and mineralisation, and if there were a possible translation to a human therapy, it would likely be an intervention leading to an increase in prenatal movement and joint movement.

The research in this demonstrates that specific aspects of joint development are promoted under loading, and fail to progress under absence of movement. This research also demonstrates that joint morphogenesis and mineralisation are age- and location-dependent processes. In the next chapter, a summary of key findings within this thesis, avenues for future research, and general conclusions are presented.

Chapter 7

7. Conclusions

7.1 Summary of Key Outcomes

Addressing the objectives highlighted in section 1.2, the key findings are summarised below.

The results of Chapter 4 showed that a single day of immobilisation is not likely to drastically affect joint morphogenesis or cavitation, but immobilisation for three or more days significantly impedes joint development. Fetal movements were shown to be most impactful upon hip joint morphology and cavitation between e4–7, and a short, three–day period of immobilisation leads to severe effects on morphology and cavitation. The hypothesis that there is a time period of defined length and duration for which movement is critical for normal cavitation and morphogenesis was corroborated. The findings in this chapter suggest that early whole-body movements may be more important than individual limb movements for early skeletal development.

The intervention in Chapter 5 demonstrated for the first time that the effects of immobility on major hip morphological landmarks and hip cavitation can be significantly ameliorated by a very short period of external manipulation *in ovo*, during early fetal development. The hypothesis that a threshold of pre-cavitational mechanical stimulation is necessary for cavitation and further morphogenesis of the developing joint was supported. These observations suggested that a single, well-timed pre-cavitational intervention could promote more normal joint development.

The novel murine culture methods developed and validated in (see Chapter 3) were applied to a series of experiments leading to a number of novel results, detailed below.

The studies in Chapter 6 indicated that dynamic loading led to increased outgrowth of certain anatomical features of the elbow and knee joints, compared to statically-cultured and uncultured

limbs. Dynamic loading also led to an increase in mineralisation ratio in certain long bone rudiments, compared to statically-cultured and uncultured limbs. The hypotheses that *in vitro* culture of murine prenatal limbs leads to greater outgrowth and mineralisation of the murine limbs, compared to uncultured limbs, and that *in vitro* dynamic mechanical stimulation leads to greater outgrowth and mineralisation, compared to statically-cultured murine limbs, were supported. Differences in morphological outgrowth and mineralisation ratio between e14.5 and e15.5 forelimb and hind limbs indicated that the level of mechanical loading required for physiological growth may vary, dependent on age and location of a skeletal element.

Finally, further results from Chapter 6 indicated that *in vitro* dynamic culture of the Pax3$^{Sp\text{-}d/Sp\text{-}d}$ muscleless knee and elbow rudiments led to shape profiles and mineralisation ratios comparable with the dynamically-stimulated control rudiments. The hypothesis that *in vitro* mechanical stimulation from dynamic loading promotes more normal morphogenesis and mineralisation in muscleless mutant murine prenatal limbs, compared to unloaded muscleless limbs, was corroborated. These results indicated that external movements are able to partially overcome aberrant morphological and mineralisation changes as a consequence of reduced or absent muscle activity.

7.2 Clinical applications

Using immobilised chick embryos, I identified a critical time period for movement for normal embryonic development of joints. The significance of this research is that it could lead to identification of a comparable stage in human development where movement is most critical for normal development, thus identifying a window for targeted *in utero* screening and possible intervention. The uniform, undifferentiated mesenchymal cells within the chick hind limb at the beginning of e3 (Goel 1970, Searls, Hilfer et al. 1972) correspond with the third week of human embryonic life, where limb buds are filled with mesenchyme (Bardeen 1905). At the start of e4, the increase in mesenchymal density and packing corresponds with the fifth week of human development, where the mesenchymal tissue at the centre of the base of the hind limb becomes condensed (Bardeen 1905). Between e4–7, the basic hip joint shape and rudiments of the pelvis become visible, with the first limb movements of the femur at e6.5 (Nowlan, Chandaria et al. 2014), which correspond from the seventh to the ninth week of human development (Bardeen 1905). As reviewed in section 2.5, a reduction of fetal movement is a known risk factor for developing DDH, AMC, FADS, and other debilitating skeletal conditions (Nowlan 2015). Enhanced monitoring of fetal movements during these early, critical periods of development may act to rapidly identify babies at risk of developing these conditions. Despite the introduction of the NHS screening programme for DDH in 1986, the incidence of late diagnosis of DDH has been reported at 1.28 per 1000 live births, and has not decreased in the last 35 years (Broadhurst, Rhodes et al.

2019). The later a diagnosis of DDH, the more expensive, invasive, and less favourable the outcome than those treated early in infancy (Studer, Williams et al. 2016). AMC is also very poorly diagnosed prenatally, with only 22% of cases detected before birth (Lowry, Sibbald et al. 2010). This research may lead to novel *in utero* monitoring and post-natal interventions, necessary to fully understand a lack of movement as a risk factor.

Further work in the chick embryo used external mechanical stimulation to ameliorate the regressive effects of immobility on cavitation and morphogenesis. This time period is at e8, around the time point where the hip joint should normally cavitate (Nowlan and Sharpe 2014). In the human fetus, the joint cavity appears around 10–11 weeks of development (Strayer 1943). The strength of this work is that it suggests this may be an appropriate developmental stage to consider external mechanical stimulation in a fetus at high risk of AMC or DDH, for example, upon detection of infrequent or absent movement. As DDH and arthrogryposis are associated with repeated surgeries and rehabilitation, with long-term consequences on mobility and independent living (Kowalczyk and Feluś 2016), an intervention to reduce severity may make a substantial improvement in patients' adult lives. It is important to state that I am not proposing *in utero* manipulation of the developing human limb. Rather, vibroacoustic stimulation may be a potential avenue for treatment in the future.

7.3 Limitations and future work

There are some overall limitations within this thesis. Sample numbers were low in the time immobilisation chick cavitational study due to high mortality, and the mutant mouse bioreactor study due to a limited number of mutants. Further to this, joint morphology and cavitation could not both be investigated in a single rudiment, as the joint cavity is not present using OPT. A single end timepoint of e9 was used throughout for both chick studies as this allowed a balance between investigation immediately after hip joint cavitation and high enough survival.

This thesis presented work with a clinical outlook, and focused on the phenotypical changes in joint development, not the cellular or molecular changes in joint development (discussed in sections 4.4 and 6.4). The developing limb surrounding the joint was also not investigated.

Drachman and Coulombre reported that some chick embryos immobilised for a single day developed joint ankyloses and altered ranges of movement upon hatching (Drachman and Coulombre 1962). The study presented in Chapter 4 only considered the effects of immobilisation immediately after hip joint cavitation in the e9 chick embryo, of which a single day of immobility did not lead to notable shape or cavitational changes. An obvious continuation of this work would be to harvest immobilised chicks at different development periods, as a very short period of early immobilisation may lead to joint shape and cavitational changes of increasing severity as

development progresses. Further knowledge of how joint morphology and cavitation are affected by the timing of movement will enable more sophisticated screening protocols for at-risk fetuses.

The recovery study in Chapter 5 explored the effects of a single, pre-cavitational intervention on immobilised chicks. Although preliminary recovery was promising, there is no knowledge on whether joint recovery persists after a single period of applied movement, whether continual applied movements are needed, or indeed, whether the timing of local applied movements is important to promote more normal skeletal development. Therefore, harvesting of chicks at different developmental periods with (if necessary) several timed manipulation interventions, including assessment of joint structure and mobility of the hatched chick may inform us of the potential benefits and outcomes of treatment to stimulate *in utero* infants, and the timing that such treatment should occur.

The scope of the study in Chapter 6 was limited by a small number of mutant embryos. Future work aims to analyse the difference between statically- and dynamically-cultured mutants, in order to see whether shape and mineralisation changes due to immobility persist under *in vitro* static culture. Future avenues of interest lay in the direction of increasing or changing the dose of mechanical stimulation between a) different joints and b) at different developmental stages. The mutant culture was performed at e14.5, when the contribution of muscle forces was absent for two days. If later stimulation cannot overcome the effects of immobility, I propose enhanced early screening for at-risk prenatal infants, as early intervention to increase movements may be more critical for skeletal development. Additionally, an experimental system is currently being developed in our group, attempting *in utero* massage of muscleless embryos to alleviate skeletal abnormalities.

The mammalian bioreactor culture system described in this thesis provides a controlled environment in which mechanosensitive pathways may be elucidated. Current work in our group is looking at blocking mechanosensitive channels to observe the effects on mammalian joint morphogenesis. This work could be extended to mechanosensitive gene studies in a highly regulated whole tissue system. However, the bioreactor is not simply limited to observing limb joint development, and may also be used to study loaded tendons, ligaments, and even other developing structures, such as the embryonic jaw, giving insights into not simply limb defects, but craniofacial development.

7.4 Conclusions

The research presented in this thesis has advanced our basic understanding of fetal skeletal development, and has provided a novel insight into how the timing of movement, be it the absence, the application of, or *in vitro* flexion, can alter the progression of joint shape, cavitation,

or mineralisation. Advancing our knowledge on the role of fetal movements on physiological skeletal development is critical to developing strategies for early screening, diagnosis, prevention, and treatment of musculoskeletal abnormalities.

References

Ahrens, J. G., Berk & Law, Charles (2005). ParaView: An End-User Tool for Large Data Visualization, Elsevier.

Aly, H., M. F. Moustafa, S. M. Hassanein, A. N. Massaro, H. A. Amer and K. Patel (2004). "Physical activity combined with massage improves bone mineralization in premature infants: a randomized trial." J Perinatol **24**(5): 305-309.

Andersson, J. E. and A. Oden (2001). "The breech presentation and the vertex presentation following an external version represent risk factors for neonatal hip instability." Acta Paediatr **90**(8): 895-898.

Archer, C. W., H. Morrison and A. A. Pitsillides (1994). "Cellular aspects of the development of diarthrodial joints and articular cartilage." J Anat **184 (Pt 3)**: 447-456.

Aronsson, D. D., M. J. Goldberg, T. F. Kling, Jr. and D. R. Roy (1994). "Developmental dysplasia of the hip." Pediatrics **94**(2 Pt 1): 201-208.

Auerbach, R. (1954). "Analysis of the developmental effects of a lethal mutation in the house mouse." Journal of Experimental Zoology **127**(2): 305-329.

Bamshad, M., A. E. Van Heest and D. Pleasure (2009). "Arthrogryposis: a review and update." The Journal of bone and joint surgery. American volume **91 Suppl 4**: 40-46.

Bardeen, C. R. (1905). "Studies of the development of the human skeleton. (A). The development of the lumbab, sacbal and coccygeal vertebwe. (B). The cubves and the pbopobtionate regional lengths of the spinal column during the first thbee months of embbyonic developnent. (C). The development of the skeleton of the posterior limb." American Journal of Anatomy **4**(3): 265-302.

Bayat, A., A. Petersen, M. Moller, G. Andersen and F. Ebbesen (2009). "Incidence of fetal akinesia-hypokinesia deformation sequence: a population-based study." Acta Paediatr **98**(1): 3-4.

Betts, J. G., K. A. Young, J. A. Wise, E. Johnson, B. Poe, D. H. Kruse, O. Korol, J. E. Johnson, M. Womble and P. DeSaix (2013). Anatomy of Selected Synovial Joints - Anatomy and Physiology - OpenStax. Anatomy and Physiology. Houston, Texas, OpenStax.

Betts, J. G., K. A. Young, J. A. Wise, E. Johnson, B. Poe, D. H. Kruse, O. Korol, J. E. Johnson, M. Womble and P. DeSaix (2013). Bone Formation and Development - Anatomy and Physiology - OpenStax. Anatomy and Physiology. Houston, Texas, OpenStax.

Betts, J. G., K. A. Young, J. A. Wise, E. Johnson, B. Poe, D. H. Kruse, O. Korol, J. E. Johnson, M. Womble and P. DeSaix (2013). Bones of the Lower Limb - Anatomy and Physiology - OpenStax. Anatomy and Physiology. Houston, Texas, OpenStax.

Betts, J. G., K. A. Young, J. A. Wise, E. Johnson, B. Poe, D. H. Kruse, O. Korol, J. E. Johnson, M. Womble and P. DeSaix (2013). Bones of the Upper Limb - Anatomy and Physiology - OpenStax. Anatomy and Physiology. Houston, Texas, OpenStax.

Betts, J. G., K. A. Young, J. A. Wise, E. Johnson, B. Poe, D. H. Kruse, O. Korol, J. E. Johnson, M. Womble and P. DeSaix (2013). Muscle Fiber Contraction and Relaxation - Anatomy and Physiology - OpenStax. Anatomy and Physiology. Houston, Texas, OpenStax.

Betts, J. G., K. A. Young, J. A. Wise, E. Johnson, B. Poe, D. H. Kruse, O. Korol, J. E. Johnson, M. Womble and P. DeSaix (2013). The Pelvic Girdle and Pelvis - Anatomy and Physiology - OpenStax. Anatomy and Physiology. Houston, Texas, OpenStax.

Betts, J. G., K. A. Young, J. A. Wise, E. Johnson, B. Poe, D. H. Kruse, O. Korol, J. E. Johnson, M. Womble and P. DeSaix (2013). Synovial Joints - Anatomy and Physiology - OpenStax. Anatomy and Physiology. Houston, Texas, OpenStax.

Blitz, E., A. Sharir, H. Akiyama and E. Zelzer (2013). "Tendon-bone attachment unit is formed modularly by a distinct pool of Scx- and Sox9-positive progenitors." Development **140**(13): 2680-2690.

Broadhurst, C., A. M. L. Rhodes, P. Harper, D. C. Perry, N. M. P. Clarke and A. Aarvold (2019). "What is the incidence of late detection of developmental dysplasia of the hip in England?" Bone Joint J **101-b**(3): 281-287.

Brunt, L. H., J. L. Norton, J. A. Bright, E. J. Rayfield and C. L. Hammond (2015). "Finite element modelling predicts changes in joint shape and cell behaviour due to loss of muscle strain in jaw development." J Biomech **48**(12): 3112-3122.

Brunt, L. H., R. E. Skinner, K. A. Roddy, N. M. Araujo, E. J. Rayfield and C. L. Hammond (2016). "Differential effects of altered patterns of movement and strain on joint cell behaviour and skeletal morphogenesis." Osteoarthritis Cartilage **24**(11): 1940-1950.

Buckwalter, J. A. and H. J. Mankin (1998). "Articular cartilage: tissue design and chondrocyte-matrix interactions." Instr Course Lect **47**: 477-486.

Caplan, A. I. and D. G. Pechak (1987). The Cellular and Molecular Embryology of Bone Formation. New York, NY, Elsevier Science Publishers.

Carlevaro, M. F., S. Cermelli, R. Cancedda and F. Descalzi Cancedda (2000). "Vascular Endothelial Growth Factor (VEGF) in Cartilage Neovascularization and Chondrocyte Differentiation: Auto-paracrine Role During Endochondral Bone Formation." J Cell Sci **113 (Pt 1)**: 59-69.

Chambers, S. H., N. S. Bradley and M. D. Orosz (1995). "Kinematic analysis of wing and leg movements for type I motility in E9 chick embryos." Exp Brain Res **103**(2): 218-226.

Chan, A., K. A. McCaul, P. J. Cundy, E. A. Haan and R. Byron-Scott (1997). "Perinatal risk factors for developmental dysplasia of the hip." Arch Dis Child Fetal Neonatal Ed **76**(2): F94-100.

Chandaria, V. V. (2017). Mechanical Stimulation and Morphogenesis of the Embryonic Chick Knee Joint, Imperial College London.

Chandaria, V. V., J. McGinty and N. C. Nowlan (2016). "Characterising the effects of in vitro mechanical stimulation on morphogenesis of developing limb explants." J Biomech **49**(15): 3635-3642.

Chen, C., D. T. Tambe, L. Deng and L. Yang (2013). "Biomechanical properties and mechanobiology of the articular chondrocyte." Am J Physiol Cell Physiol **305**(12): C1202-1208.

Chen, X., J. Guo, Y. Yuan, Z. Sun, B. Chen, X. Tong, L. Zhang, C. Shen and J. Zou (2017). "Cyclic compression stimulates osteoblast differentiation via activation of the Wnt/beta-catenin signaling pathway." Mol Med Rep **15**(5): 2890-2896.

Chinoy, A., M. Z. Mughal and R. Padidela (2019). "Metabolic bone disease of prematurity: causes, recognition, prevention, treatment and long-term consequences." Arch Dis Child Fetal Neonatal Ed **104**(5): F560-f566.

Clarke, B. (2008). Normal Bone Anatomy and Physiology. Clin J Am Soc Nephrol. **3:** S131-139.

Davey, M. G., M. Towers, N. Vargesson and C. Tickle (2018). "The chick limb: embryology, genetics and teratology." Int J Dev Biol **62**(1-2-3): 85-95.

de Frutos, C. A., S. Vega, M. Manzanares, J. M. Flores, H. Huertas, M. L. Martinez-Frias and M. A. Nieto (2007). "Snail1 is a Transcriptional Effector of FGFR3 Signaling During Chondrogenesis and Achondroplasias." Dev Cell **13**(6): 872-883.

De Pellegrin, M. and D. Moharamzadeh (2010). "Developmental dysplasia of the hip in twins: the importance of mechanical factors in the etiology of DDH." J Pediatr Orthop **30**(8): 774-778.

Dowthwaite, G. P., J. C. Edwards and A. A. Pitsillides (1998). "An essential role for the interaction between hyaluronan and hyaluronan binding proteins during joint development." J Histochem Cytochem **46**(5): 641-651.

Dowthwaite, G. P., C. R. Flannery, J. Flannelly, J. C. Lewthwaite, C. W. Archer and A. A. Pitsillides (2003). "A Mechanism Underlying the Movement Requirement for Synovial Joint Cavitation." Matrix Biol **22**(4): 311-322.

Drachman, D. B. and A. J. Coulombre (1962). "Experimental clubfoot and arthrogryposis multiplex congenita." Lancet **2**(7255): 523-526.

Drachman, D. B. and L. Sokoloff (1966). "The role of movement in embryonic joint development." Developmental Biology **14**: 401-420.

Dumont, E. R. (2010). "Bone Density and the Lightweight Skeletons of Birds." Proceedings. Biological Sciences **277**(1691): 2193-2198.

Dy, P., P. Smits, A. Silvester, A. Penzo-Mendez, B. Dumitriu, Y. Han, C. A. de la Motte, D. M. Kingsley and V. Lefebvre (2010). "Synovial joint morphogenesis requires the chondrogenic action of Sox5 and Sox6 in growth plate and articular cartilage." Dev Biol **341**(2): 346-359.

Eliakim, A., D. Nemet, O. Friedland, T. Dolfin and R. H. Regev (2002). "Spontaneous activity in premature infants affects bone strength." J Perinatol **22**(8): 650-652.

Fell, H. B. (1925). "The Histogenesis of Cartilage and Bone in the Long Bones of the Embryonic Fowl." Journal of Morphology and Physiology **40**: 417–459.

Fell, H. B. and R. G. Canti (1934). "Experiments on the Development in vitro of the Avian Knee-Joint." Proceedings of the Royal Society B: Biological Sciences **116**: 316-351.

Flaherty, K. and J. T. Richtsmeier (2018). "It's about Time: Ossification Center Formation in C57BL/6 Mice from E12–E16." J Dev Biol **6**(4).

Fox, S., J. A. Bedi, A. Rodeo and A. Scott (2009). "The Basic Science of Articular Cartilage: Structure, Composition, and Function." Sports health **1**: 461-468.

Franz, T. (1993). "The Splotch (Sp1H) and Splotch-delayed (Spd) alleles: differential phenotypic effects on neural crest and limb musculature." Anat Embryol (Berl) **187**(4): 371-377.

Gardner, E., D. J. Gray and R. O'Rahilly (1959). "The Prenatal Development of the Skeleton and Joints of the Human Foot." J Bone Joint Surg Am **41-A**(5): 847-876.

Gardner, E. and R. O'Rahilly (1968). "The Early Development of the Knee Joint in Staged Human Embryos." J Anat **102**(Pt 2): 289-299.

Gerber, H. P., T. H. Vu, A. M. Ryan, J. Kowalski, Z. Werb and N. Ferrara (1999). "VEGF Couples Hypertrophic Cartilage Remodeling, Ossification and Angiogenesis During Endochondral Bone Formation." Nat Med **5**(6): 623-628.

Germiller, J. A. and S. A. Goldstein (1997). "Structure and function of embryonic growth plate in the absence of functioning skeletal muscle." J Orthop Res **15**(3): 362-370.

Gilbert, S. F. (2000). Osteogenesis: The Development of Bones. Sunderland, MA, Sinauer Associates.

Giorgi, M., A. Carriero, S. J. Shefelbine and N. C. Nowlan (2014). "Mechanobiological simulations of prenatal joint morphogenesis." J Biomech **47**(5): 989-995.

Giorgi, M., A. Carriero, S. J. Shefelbine and N. C. Nowlan (2015). "Effects of normal and abnormal loading conditions on morphogenesis of the prenatal hip joint: application to hip dysplasia." J Biomech **48**(12): 3390-3397.

Goel, S. C. (1970). "Electron microscopic studies on developing cartilage. I. The membrane system related to the synthesis and secretion of extracellular materials." J Embryol Exp Morphol **23**(1): 169-184.

Gray, H. (2004). Musculoskeletal system. Gray's Anatomy. S. S. New York, Elsevier**:** 83-135.

Haines, R. W. (1947). "The Development of Joints." J Anat **81**(Pt 1): 33-55.

Hall, B. K. (1987). "Earliest Evidence of Cartilage and Bone Development in Embryonic Life." Clin Orthop Relat Res(225): 255-272.

Hall, B. K. and T. Miyake (1992). "The Membranous Skeleton: The Role of Cell Condensations in Vertebrate Skeletogenesis." Anat Embryol (Berl) **186**(2): 107-124.

Hall, J. G. (2009). "Pena-Shokeir phenotype (fetal akinesia deformation sequence) revisited." Birth Defects Res A Clin Mol Teratol **85**(8): 677-694.

Hall, J. G., S. D. Reed and E. P. Driscoll (1983). "Part I. Amyoplasia: a common, sporadic condition with congenital contractures." Am J Med Genet **15**(4): 571-590.

Hamburger, V. and M. Balaban (1963). "Observations and experiments on spontaneous rhythmical behavior in the chick embryo." Dev Biol **6**: 533-545.

Hamburger, V. and H. L. Hamilton (1951). "A series of normal stages in the development of the chick embryo." Journal of Morphology **88**: 49-92.

Hamburger, V. and M. Waugh (1940). "The Primary Development of the Skeleton in Nerveless and Poorly Innervated Limb Transplants of Chick Embryos." Physiol Zoo **13**: 367-380.

Hartmann, C. and C. J. Tabin (2001). "Wnt-14 Plays a Pivotal Role in Inducing Synovial Joint Formation in the Developing Appendicular Skeleton." Cell **104**(3): 341-351.

Hasty, P., A. Bradley, J. H. Morris, D. G. Edmondson, J. M. Venuti, E. N. Olson and W. H. Klein (1993). "Muscle deficiency and neonatal death in mice with a targeted mutation in the myogenin gene." Nature **364**(6437): 501-506.

Hata, K., Y. Takahata, T. Murakami and R. Nishimura (2017). "Transcriptional Network Controlling Endochondral Ossification." J Bone Metab **24**(2): 75-82.

Heilman, J. (2010). "File:Congenitaldislocation10.JPG - Wikimedia Commons." from https://commons.wikimedia.org/wiki/File:Congenitaldislocation10.JPG.

Henstock, J. R., M. Rotherham, J. B. Rose and A. J. El Haj (2013). "Cyclic hydrostatic pressure stimulates enhanced bone development in the foetal chick femur in vitro." Bone **53**(2): 468-477.

Hogan, B., R. Beddington, E. Constantini and E. Lacy (1994). Manipulating the Mouse Embryo: A Laboratory Manual. C. S. H. Laboratory. NY, Cold Spring Harbor.

Holder, N. (1977). "An Experimental Investigation Into the Early Development of the Chick Elbow Joint." Journal of embryology and experimental morphology.

Inada, M., T. Yasui, S. Nomura, S. Miyake, K. Deguchi, M. Himeno, M. Sato, H. Yamagiwa, T. Kimura, N. Yasui, T. Ochi, N. Endo, Y. Kitamura, T. Kishimoto and T. Komori (1999). "Maturational Disturbance of Chondrocytes in Cbfa1-Deficient Mice." Dev Dyn **214**(4): 279-290.

Ito, M. M. and M. Y. Kida (2000). "Morphological and biochemical re-evaluation of the process of cavitation in the rat knee joint: cellular and cell strata alterations in the interzone." J Anat **197 Pt 4**: 659-679.

Ito, M. M. and M. Y. Kida (2000). "Morphological and biochemical re-evaluation of the process of cavitation in the rat knee joint: cellular and cell strata alterations in the interzone." Journal of anatomy.

Jahan, E., A. Matsumoto, A. M. Rafiq, R. Hashimoto, T. Inoue, J. Udagawa, J. Sekine and H. Otani (2014). "Fetal jaw movement affects Ihh signaling in mandibular condylar cartilage development: the possible role of Ihh as mechanotransduction mediator." Arch Oral Biol **59**(10): 1108-1118.

Jukic, A., D. Baird, C. Weinberg, D. McConnaughey and A. Wilcox (2013). Length of human pregnancy and contributors to its natural variation. Hum Reprod. **28:** 2848-2855.

Kahn, J., Y. Shwartz, E. Blitz, S. Krief, A. Sharir, D. A. Breitel, R. Rattenbach, F. Relaix, P. Maire, R. B. Rountree, D. M. Kingsley and E. Zelzer (2009). "Muscle Contraction is Necessary to Maintain Joint Progenitor Cell Fate." Dev Cell **16**(5): 734-743.

Kanczler, J. M., E. L. Smith, C. A. Roberts and R. O. Oreffo (2012). "A novel approach for studying the temporal modulation of embryonic skeletal development using organotypic bone cultures and microcomputed tomography." Tissue Eng Part C Methods **18**(10): 747-760.

Kaufman, M. H. and J. B. L. Bard (1999). The anatomical basis of mouse development. San Diego ; London, Academic.

Keller-Peck, C. R. and R. J. Mullen (1996). "Patterns of neuronal differentiation in neural tube mutant mice: curly tail and Pax3 splotch-delayed." J Comp Neurol **368**(4): 516-526.

Kelly, D. J. and C. R. Jacobs (2010). "The role of mechanical signals in regulating chondrogenesis and osteogenesis of mesenchymal stem cells." Birth Defects Res C Embryo Today **90**(1): 75-85.

Khan, I. M., S. N. Redman, R. Williams, G. P. Dowthwaite, S. F. Oldfield and C. W. Archer (2007). "The Development of Synovial Joints." Curr Top Dev Biol **79**: 1-36.

Kirkinen, P., R. Herva and J. Leisti (1987). "Early prenatal diagnosis of a lethal syndrome of multiple congenital contractures." Prenat Diagn **7**(3): 189-196.

Kowalczyk, B. and J. Feluś (2016). Arthrogryposis: an update on clinical aspects, etiology, and treatment strategies. Arch Med Sci. **12:** 10-24.

Koyama, E., T. Ochiai, R. B. Rountree, D. M. Kingsley, M. Enomoto-Iwamoto, M. Iwamoto and M. Pacifici (2007). "Synovial Joint Formation During Mouse Limb Skeletogenesis: Roles of Indian Hedgehog Signaling." Ann N Y Acad Sci **1116**: 100-112.

Koyama, E., Y. Shibukawa, M. Nagayama, H. Sugito, B. Young, T. Yuasa, T. Okabe, T. Ochiai, N. Kamiya, R. B. Rountree, D. M. Kingsley, M. Iwamoto, M. Enomoto-Iwamoto and M. Pacifici (2008). "A Distinct Cohort of Progenitor Cells Participates in Synovial Joint and Articular Cartilage Formation During Mouse Limb Skeletogenesis." Dev Biol **316**(1): 62-73.

Lakens, D. (2017). "Equivalence Tests: A Practical Primer for t Tests, Correlations, and Meta-Analyses." Soc Psychol Personal Sci **8**(4): 355-362.

Langenbach, F. and J. Handschel (2013). "Effects of dexamethasone, ascorbic acid and beta-glycerophosphate on the osteogenic differentiation of stem cells in vitro." Stem Cell Res Ther **4**(5): 117.

Leck, I. (2000). Congenital dislocation of the hip.

Lefebvre, V. and P. Bhattaram (2010). "Vertebrate Skeletogenesis." Curr Top Dev Biol **90**: 291-317.

Lefebvre, V., P. Li and B. de Crombrugghe (1998). "A New Long Form of Sox5 (L-Sox5), Sox6 and Sox9 are Coexpressed in Chondrogenesis and Cooperatively Activate the Type II Collagen Gene." EMBO J **17**(19): 5718-5733.

Lelkes, G. (1958). "Experiments in vitro on the role of movement in the development of joints." Journal of embryology and experimental morphology.

Limentani, G. B., M. C. Ringo, F. Ye, M. L. Berquist and E. O. McSorley (2005). "Beyond the t-test: statistical equivalence testing." Anal Chem **77**(11): 221a-226a.

Lowry, R. B., B. Sibbald, T. Bedard and J. G. Hall (2010). "Prevalence of multiple congenital contractures including arthrogryposis multiplex congenita in Alberta, Canada, and a strategy for classification and coding." Birth Defects Res A Clin Mol Teratol **88**(12): 1057-1061.

Macharia, R., K. Patel, W. R. Otto, I. W. McKinnell and B. Christ (2004). "Decamethonium bromide-mediated inhibition of embryonic muscle development." Anat Embryol (Berl) **208**(1): 75-85.

Manoukian, D. and A. Rehm (2019). "Oligohydramnios: Should it be considered a risk factor for developmental dysplasia of the hip?" J Pediatr Orthop B.

Martin, P. (1990). "Tissue patterning in the developing mouse limb." Int J Dev Biol **34**(3): 323-336.

Martin, R. B., D. B. Burr and N. A. Sharkey (1998). Forces in Joints. Skeletal Tissue Mechanics. New York, NY, Springer New York**:** 1-28.

Matsumoto, K., Y. Li, C. Jakuba, Y. Sugiyama, T. Sayo, M. Okuno, C. N. Dealy, B. P. Toole, J. Takeda, Y. Yamaguchi and R. A. Kosher (2009). "Conditional inactivation of Has2 reveals a crucial role for hyaluronan in skeletal growth, patterning, chondrocyte maturation and joint formation in the developing limb." Development **136**(16): 2825-2835.

Mitrovic, D. (1978). "Development of the Diarthrodial Joints in the Rat Embryo." The American journal of anatomy **151**: 475-485.

Mitrovic, D. (1982). "Development of the Articular Cavity in Paralyzed Chick Embryos and in Chick Embryo Limb Buds Cultured on Chorioallantoic Membranes." Cells Tissues Organs **113**: 313-324.

Mitrovic, D. R. (1977). "Development of the Metatarsophalangeal Joint of the Chick Embryo: Morphological, Ultrastructural and Histochemical Studies." The American journal of anatomy **150**: 333-347.

Moase, C. E. and D. G. Trasler (1992). "Splotch locus mouse mutants: models for neural tube defects and Waardenburg syndrome type I in humans." J Med Genet **29**(3): 145-151.

Muller, G. M. and H. J. Seddon (1953). "Late results of treatment of congenital dislocation of the hip." J Bone Joint Surg Br **35-b**(3): 342-362.

Murray, P. D. and D. B. Drachman (1969). "The role of movement in the development of joints and related structures: the head and neck in the chick embryo." Journal of embryology and experimental morphology.

Nemec, U., S. F. Nemec, D. Krakow, P. C. Brugger, G. Malinger, J. M. Graham, Jr., D. L. Rimoin and D. Prayer (2011). "The skeleton and musculature on foetal MRI." Insights Imaging **2**(3): 309-318.

Nowlan, N. C. (2015). "Biomechanics of foetal movement." Eur Cell Mater **29**: 1-21; discussion 21.

Nowlan, N. C., C. Bourdon, G. Dumas, S. Tajbakhsh, P. J. Prendergast and P. Murphy (2010). "Developing Bones are Differentially Affected by Compromised Skeletal Muscle Formation." Bone.

Nowlan, N. C., V. Chandaria and J. Sharpe (2014). "Immobilized chicks as a model system for early-onset developmental dysplasia of the hip." Journal of Orthopaedic Research.

Nowlan, N. C., P. Murphy and P. J. Prendergast (2007). Mechanobiology of embryonic limb development. Annals of the New York Academy of Sciences.

Nowlan, N. C., P. J. Prendergast and P. Murphy (2008). "Identification of mechanosensitive genes during embryonic bone formation." PLoS Comput Biol **4**(12): e1000250.

Nowlan, N. C. and J. Sharpe (2014). "Joint shape morphogenesis precedes cavitation of the developing hip joint." Journal of Anatomy.

Nowlan, N. C., J. Sharpe, K. A. Roddy, P. J. Prendergast and P. Murphy (2010). Mechanobiology of embryonic skeletal development: Insights from animal models. Birth Defects Research Part C - Embryo Today: Reviews.

O'Rahilly, R. and E. Gardner (1972). "The Initial Appearance of Ossification in Staged Human Embryos." Am J Anat **134**(3): 291-301.

O'Conor, C. J., N. Case and F. Guilak (2013). Mechanical regulation of chondrogenesis. Stem Cell Res Ther. **4:** 61.

Ortiz-Neira, C. L., E. O. Paolucci and T. Donnon (2012). "A meta-analysis of common risk factors associated with the diagnosis of developmental dysplasia of the hip in newborns." Eur J Radiol **81**(3): e344-351.

Osborne, A. C., K. J. Lamb, J. C. Lewthwaite, G. P. Dowthwaite and A. A. Pitsillides (2002). "Short-term rigid and flaccid paralyses diminish growth of embryonic chick limbs and abrogate joint cavity formation but differentially preserve pre-cavitated joints." Journal of Musculoskeletal Neuronal Interactions.

Ouyang, X., Y. Xie and G. Wang (2019). "Mechanical stimulation promotes the proliferation and the cartilage phenotype of mesenchymal stem cells and chondrocytes co-cultured in vitro." Biomed Pharmacother **117**: 109146.

Pacifici, M., E. Koyama and M. Iwamoto (2005). Mechanisms of synovial joint and articular cartilage formation: Recent advances, but many lingering mysteries. Birth Defects Research Part C - Embryo Today: Reviews.

Pacifici, M., E. Koyama, Y. Shibukawa, C. Wu, Y. Tamamura, M. Enomoto-Iwamoto and M. Iwamoto (2006). "Cellular and molecular mechanisms of synovial joint and articular cartilage formation." Annals of the New York Academy of Sciences **1068**: 74-86.

Palacios, J., J. I. Rodriguez, A. Ruiz, M. Sanchez, I. Alvarez and E. DeMiguel (1992). "Long bone development in extrinsic fetal akinesia: an experimental study in rat fetuses subjected to oligohydramnios." Teratology **46**(1): 79-84.

Parisi, C., V. V. Chandaria and N. C. Nowlan (2018). "Blocking mechanosensitive ion channels eliminates the effects of applied mechanical loading on chick joint morphogenesis." Philos Trans R Soc Lond B Biol Sci **373**(1759).

Pitsillides, A. A., C. W. Archer, P. Prehm, M. T. Bayliss and J. C. Edwards (1995). "Alterations in hyaluronan synthesis during developing joint cavitation." J Histochem Cytochem **43**(3): 263-273.

Pollard, A. S., B. G. Charlton, J. R. Hutchinson, T. Gustafsson, I. M. McGonnell, J. A. Timmons and A. A. Pitsillides (2017). "Limb proportions show developmental plasticity in response to embryo movement." Sci Rep **7**: 41926.

Quintana, L. and J. Sharpe (2011). "Preparation of mouse embryos for optical projection tomography imaging." Cold Spring Harb Protoc **2011**(6): 664-669.

Rafipay, A., A. L. R. Berg, L. Erskine and N. Vargesson (2018). "Expression analysis of limb element markers during mouse embryonic development." Dev Dyn **247**(11): 1217-1226.

Robling, A. G. and C. H. Turner (2009). "Mechanical Signaling for Bone Modeling and Remodeling." Crit Rev Eukaryot Gene Expr **19**(4): 319-338.

Roddy, K. A., G. M. Kelly, M. H. van Es, P. Murphy and P. J. Prendergast (2011). "Dynamic patterns of mechanical stimulation co-localise with growth and cell proliferation during morphogenesis in the avian embryonic knee joint." J Biomech **44**(1): 143-149.

Roddy, K. A., P. J. Prendergast and P. Murphy (2011). "Mechanical influences on morphogenesis of the knee joint revealed through morphological, molecular and computational analysis of immobilised embryos." PLoS ONE.

Rodriguez, J. I., J. Palacios, A. Garcia-Alix, I. Pastor and R. Paniagua (1988). "Effects of immobilization on fetal bone development. A morphometric study in newborns with congenital neuromuscular diseases with intrauterine onset." Calcif Tissue Int **43**(6): 335-339.

Rodriguez, J. I., J. Palacios, A. Ruiz, M. Sanchez, I. Alvarez and E. Demiguel (1992). "Morphological changes in long bone development in fetal akinesia deformation sequence: an experimental study in curarized rat fetuses." Teratology **45**(2): 213-221.

Rolfe, R. A., N. C. Nowlan, E. M. Kenny, P. Cormican, D. W. Morris, P. J. Prendergast, D. Kelly and P. Murphy (2014). "Identification of mechanosensitive genes during skeletal development: alteration of genes associated with cytoskeletal rearrangement and cell signalling pathways." BMC Genomics **15**: 48.

Rooney, P. and C. W. Archer (1992). "The Development of the Perichondrium in the Avian Ulna." J Anat **181**(Pt 3): 393-401.

Rot-Nikcevic, I., K. J. Downing, B. K. Hall and B. Kablar (2007). "Development of the mouse mandibles and clavicles in the absence of skeletal myogenesis." Histol Histopathol **22**(1): 51-60.

Rot-Nikcevic, I., T. Reddy, K. J. Downing, A. C. Belliveau, B. Hallgrimsson, B. K. Hall and B. Kablar (2006). "Myf5-/- :MyoD-/- amyogenic fetuses reveal the importance of early contraction and static loading by striated muscle in mouse skeletogenesis." Dev Genes Evol **216**(1): 1-9.

Rux, D., R. S. Decker, E. Koyama and M. Pacifici (2019). "Joints in the Appendicular Skeleton: Developmental Mechanisms and Evolutionary Influences." Curr Top Dev Biol **133**: 119-151.

Sandell, L. J. (2012). "Etiology of osteoarthritis: genetics and synovial joint development." Nat Rev Rheumatol **8**(2): 77-89.

Schneider, C. A., W. S. Rasband and K. W. Eliceiri (2012). "NIH Image to ImageJ: 25 years of image analysis." Nat Methods **9**(7): 671-675.

Searls, R. L., S. R. Hilfer and S. M. Mirow (1972). "An ultrastructural study of early chondrogenesis in the chick wing bud." Dev Biol **28**(1): 123-137.

Senior, H. D. (1919). "An Interpretation of the Recorded Arterial Anomalies of the Human Leg and Foot." J Anat **53**(Pt 2-3): 130-171.

Sharp, M. (2007). "Bone disease of prematurity." Early Hum Dev **83**(10): 653-658.

Sharpe, J., U. Ahlgren, P. Perry, B. Hill, A. Ross, J. Hecksher-Sørensen, R. Baldock and D. Davidson (2002). "Optical projection tomography as a tool for 3D microscopy and gene expression studies." Science (New York, N.Y.) **296**: 541-545.

Shwartz, Y., S. Viukov, S. Krief and E. Zelzer (2016). "Joint Development Involves a Continuous Influx of Gdf5-Positive Cells." Cell Rep **15**(12): 2577-2587.

Singh, P. N. P., C. A. Shea, S. K. Sonker, R. A. Rolfe, A. Ray, S. Kumar, P. Gupta, P. Murphy and A. Bandyopadhyay (2018). "Precise spatial restriction of BMP signaling in developing joints is perturbed upon loss of embryo movement." Development **145**(5).

Smith, E. L., M. Locke, R. J. Waddington and A. J. Sloan (2010). "An ex vivo rodent mandible culture model for bone repair." Tissue Eng Part C Methods **16**(6): 1287-1296.

Sotiriou, V., R. A. Rolfe, P. Murphy and N. C. Nowlan (2019). "Effects of Abnormal Muscle Forces on Prenatal Joint Morphogenesis in Mice." J Orthop Res **37**(11): 2287-2296.

Speight, T. M. and G. S. Avery (1972). "Pancuronium bromide: a review of its pharmacological properties and clinical application." Drugs **4**(3): 163-226.

Spurlin, J. and P. Lwigale (2013). "A Technique to Increase Accessibility to Late-Stage Chick Embryos for In Ovo Manipulations." Developmental Dynamics **242**: 148-154.

Sridharan, G. and A. A. Shankar (2012). "Toluidine blue: A review of its chemistry and clinical utility." J Oral Maxillofac Pathol **16**(2): 251-255.

St-Jacques, B., M. Hammerschmidt and A. P. McMahon (1999). "Indian Hedgehog Signaling Regulates Proliferation and Differentiation of Chondrocytes and is Essential for Bone Formation." Genes Dev **13**(16): 2072-2086.

Stein, M. J., M. R. Buckley, D. Manuele, A. Gutierrez, J. S. Loor, P. K. Nguyen and C. K. Kuo (2019). "Design of a Bioreactor to Assess the Effect of Passive Joint Loading in a Live Chick Embryo In Ovo." Tissue Eng Part C Methods.

Steward, A. J. and D. J. Kelly (2015). "Mechanical regulation of mesenchymal stem cell differentiation." J Anat **227**(6): 717-731.

Storm, E. E. and D. M. Kingsley (1996). "Joint Patterning Defects Caused by Single and Double Mutations in Members of the Bone Morphogenetic Protein (BMP) Family." Development **122**(12): 3969-3979.

Storm, E. E. and D. M. Kingsley (1999). "GDF5 Coordinates Bone and Joint Formation During Digit Development." Developmental biology **209**: 11-27.

Strayer, L. M. (1943). "The Embryology of the Human Hip Joint." Yale J Biol Med **16**(1): 13-26.16.

Studer, K., N. Williams, G. Antoniou, C. Gibson, H. Scott, W. K. Scheil, B. K. Foster and P. J. Cundy (2016). "Increase in late diagnosed developmental dysplasia of the hip in South Australia: risk factors, proposed solutions." Med J Aust **204**(6): 240.

Tan, K. H. and R. Smyth (2001). "Fetal vibroacoustic stimulation for facilitation of tests of fetal wellbeing." Cochrane Database Syst Rev(1): Cd002963.

Tremblay, P., S. Dietrich, M. Mericskay, F. R. Schubert, Z. Li and D. Paulin (1998). "A crucial role for Pax3 in the development of the hypaxial musculature and the long-range migration of muscle precursors." Developmental biology.

Verbruggen, S. W., B. Kainz, S. C. Shelmerdine, J. V. Hajnal, M. A. Rutherford, O. J. Arthurs, A. T. M. Phillips and N. C. Nowlan (2018). "Stresses and strains on the human fetal skeleton during development." J R Soc Interface **15**(138).

Vortkamp, A., K. Lee, B. Lanske, G. V. Segre, H. M. Kronenberg and C. J. Tabin (1996). "Regulation of Rate of Cartilage Differentiation by Indian Hedgehog and PTH-Related Protein." Science **273**(5275): 613-622.

Watson, S. J. and A. Bekoff (1990). "A kinematic analysis of hindlimb motility in 9- and 10-day-old chick embryos." J Neurobiol **21**(4): 651-660.

Wedge, J. H. and M. J. Wasylenko (1979). "The natural history of congenital disease of the hip." J Bone Joint Surg Br **61-b**(3): 334-338.

Woodacre, T., T. Ball and P. Cox (2016). "Epidemiology of developmental dysplasia of the hip within the UK: refining the risk factors." J Child Orthop **10**(6): 633-642.

Wu, Q. Q. and Q. Chen (2000). "Mechanoregulation of chondrocyte proliferation, maturation, and hypertrophy: ion-channel dependent transduction of matrix deformation signals." Exp Cell Res **256**(2): 383-391.

Yang, Y. (2013). Skeletal Morphogenesis and Embryonic Development. Primer on the Metabolic Bone Diseases and Disorders of Mineral Metabolism. C. J. Rosen, John Wiley & Sons, Ltd**:** 1-14.

Zelzer, E., R. Mamluk, N. Ferrara, R. S. Johnson, E. Schipani and B. R. Olsen (2004). "VEGFA is Necessary for Chondrocyte Survival During Bone Development." Development **131**(9): 2161-2171.

Zelzer, E., W. McLean, Y. S. Ng, N. Fukai, A. M. Reginato, S. Lovejoy, P. A. D'Amore and B. R. Olsen (2002). "Skeletal Defects in VEGF(120/120) Mice Reveal Multiple Roles for VEGF in Skeletogenesis." Development **129**(8): 1893-1904.

APPENDIX I – COPYRIGHT PERMISSIONS

Figure Number	Source Work	Copyright Holder	Permission Requested	Permission Note
2.1	(Betts, Young *et al*. 2013)	© Rice University, 1999	Oct 10th, 2019	Licensed with a Creative Commons Attribution License (CC BY)
2.2	(Betts, Young *et al*. 2013)	© Rice University, 1999	Oct 10th, 2019	Licensed with a Creative Commons Attribution License (CC BY)
2.3	(Betts, Young *et al*. 2013)	© Rice University, 1999	Oct 10th, 2019	Licensed with a Creative Commons Attribution License (CC BY)
2.4	(Betts, Young *et al*. 2013)	© Rice University, 1999	Oct 10th, 2019	Licensed with a Creative Commons Attribution License (CC BY)
2.6	(Betts, Young *et al*. 2013)	© Rice University, 1999	Oct 10th, 2019	Licensed with a Creative Commons Attribution License (CC BY)
2.7	(Kozhemyakina *et al*. 2015)	© The Company of Biologists Ltd	Nov 16th, 2020	Licensed with a Creative Commons Attribution License (CC BY)
2.9	(Rux, Decker *et al*. 2019)	© Elsevier Inc., 2019	Nov 5th, 2019	Licensed with a Creative Commons Attribution License (CC BY)
2.11	(Heilman 2010)	© James Heilman, 2010	Oct 10th, 2019	Licensed with a Creative Commons Attribution ShareAlike License (CC BY-SA)
2.12	(Nowlan, Chandaria *et al*. 2014)	© Orthopaedic Research Society, 2014	Oct 10th, 2019	Licensed with a Creative Commons Attribution License (CC BY)
2.13	(Roddy, Prendergast *et al*. 2011)	© Roddy *et al*, 2011	Oct 10th, 2019	Licensed with a Creative Commons Attribution License (CC BY)
2.14	(Chandaria, McGinty *et al*. 2016)	© The Authors. Published by Elsevier Ltd., 2016	Oct 10th, 2019	Licensed with a Creative Commons Attribution License (CC BY)
2.15	(Sotiriou, Rolfe *et al*. 2019)	© Orthopaedic Research Society, 2019	Oct 10th, 2019	Licensed with a Creative Commons Attribution License (CC BY)
2.16	(Brunt, Norton *et al*. 2015)	© The Authors. Published by Elsevier Ltd., 2015	Oct 10th, 2019	Licensed with a Creative Commons Attribution License (CC BY)

Permission order for Figure 2.7:

1. Development

Billing Status: Open

Print License

Order license ID	1077687-1	**Type of use**	Republish in a thesis/dissert...
Order detail status	Completed	**Publisher**	COMPANY OF BIOLOGISTS,
ISSN	1477-9129	**Portion**	Image/photo/illustration

0.00 GBP

Republication Permission

Hide Details

Publisher Terms and Conditions

LICENSED CONTENT

Publication Title	Development	**Country**	United Kingdom of Great Bri...
Author/Editor	Company of Biologists.	**Rightsholder**	The Company of Biologists L...
Date	01/01/1987	**Publication Type**	e-Journal
Language	English	**URL**	http://dev.biologists.org/

REQUEST DETAILS

Portion Type	Image/photo/illustration	**Distribution**	Worldwide
Number of images / photos / illustrations	1	**Translation**	Original language of publica...
		Copies for the disabled?	No
Format (select all that apply)	Electronic	**Minor editing privileges?**	No
Who will republish the content?	Academic institution	**Incidental promotional use?**	No
		Currency	GBP
Duration of Use	Life of current and all future...		
Lifetime Unit Quantity	Up to 499		
Rights Requested	Main product		

NEW WORK DETAILS

Title	The Role of Movement in Ea...	**Institution name**	Imperial College London
Instructor name	Devi Bridglal	**Expected presentation date**	2020-11-19

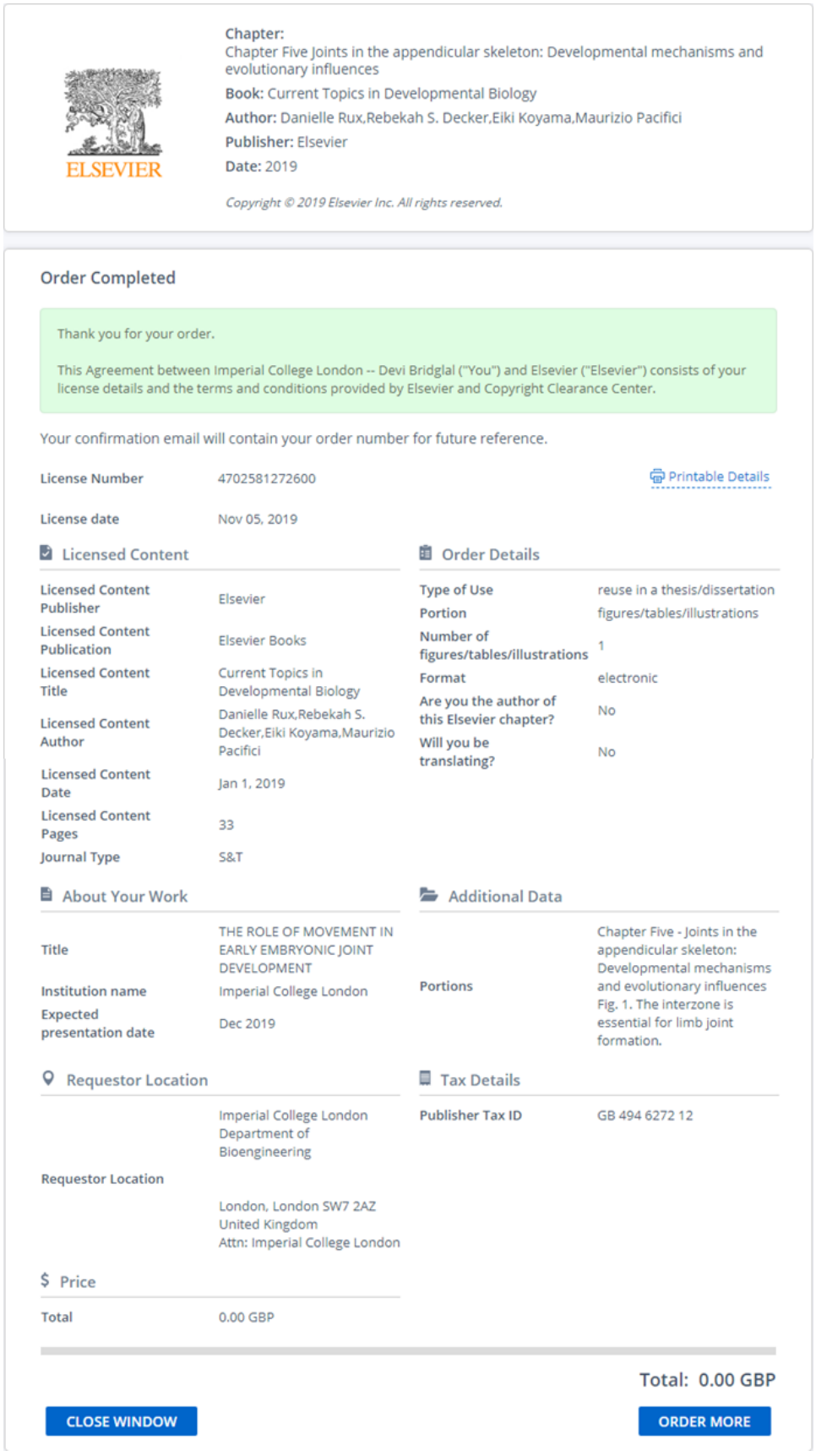
ADDITIONAL DETAILS

The requesting person / organization to appear on the license	Devi Bridglal/Imperial Colleg...

REUSE CONTENT DETAILS

Title, description or numeric reference of the portion(s)	Fig. 2. Summary of regionali...	**Title of the article/chapter the portion is from**	A pathway to bone: signalin...
Editor of portion(s)	James Briscoe	**Author of portion(s)**	Elena Kozhemyakina, Andre...
Volume of serial or monograph	vol. 142	**Issue, if republishing an article from a serial**	5
Page or page range of portion	Pg 819	**Publication date of portion**	2015-02-24

Permission order for Figure 2.9:



Chapter:
Chapter Five Joints in the appendicular skeleton: Developmental mechanisms and evolutionary influences
Book: Current Topics in Developmental Biology
Author: Danielle Rux,Rebekah S. Decker,Eiki Koyama,Maurizio Pacifici
Publisher: Elsevier
Date: 2019

Copyright © 2019 Elsevier Inc. All rights reserved.

Order Completed

Thank you for your order.

This Agreement between Imperial College London -- Devi Bridglal ("You") and Elsevier ("Elsevier") consists of your license details and the terms and conditions provided by Elsevier and Copyright Clearance Center.

Your confirmation email will contain your order number for future reference.

License Number	4702581272600
License date	Nov 05, 2019

Printable Details

Licensed Content

Licensed Content Publisher	Elsevier
Licensed Content Publication	Elsevier Books
Licensed Content Title	Current Topics in Developmental Biology
Licensed Content Author	Danielle Rux,Rebekah S. Decker,Eiki Koyama,Maurizio Pacifici
Licensed Content Date	Jan 1, 2019
Licensed Content Pages	33
Journal Type	S&T

Order Details

Type of Use	reuse in a thesis/dissertation
Portion	figures/tables/illustrations
Number of figures/tables/illustrations	1
Format	electronic
Are you the author of this Elsevier chapter?	No
Will you be translating?	No

About Your Work

Title	THE ROLE OF MOVEMENT IN EARLY EMBRYONIC JOINT DEVELOPMENT
Institution name	Imperial College London
Expected presentation date	Dec 2019

Additional Data

Portions	Chapter Five - Joints in the appendicular skeleton: Developmental mechanisms and evolutionary influences Fig. 1. The interzone is essential for limb joint formation.

Requestor Location

Requestor Location	Imperial College London Department of Bioengineering London, London SW7 2AZ United Kingdom Attn: Imperial College London

Tax Details

Publisher Tax ID	GB 494 6272 12

$ Price

Total	0.00 GBP

Total: 0.00 GBP

CLOSE WINDOW ORDER MORE

APPENDIX II – TIMED IMMOBILISATION CONTROL GROUPS

Tables below list all the *p*-values for all measurements between groups.

Table S1. List of *p*-values obtained with Tukey's test for significant differences in the measurements of femoral head to piriformis.

	Mean ± SD (µm)	**Physiological**	**Alb removal**	**Sham e3-8**	**Sham e4-8**	**Sham e5-8**	**Sham e6-8**	**Sham e7-8**	**Sham e8**	**DMB e5-8**	**DMB e5-8/MD**
Mean ± SD (µm)		745.7 ± 68.2	739.3 ± 51.9	750.2 ± 57.5	726.0 ± 50.1	736.9 ± 51.1	791.0 ± 8.96	723.7 ± 40.5	736.6 ± 49.1	614.9 ± 49.7	523.5 ± 43.0
Physiological	745.7 ± 68.2	-	1.000	1.000	0.999	1.000	0.758	0.997	1.000	0.000	0.000
Alb removal	739.3 ± 51.9		-	1.000	1.000	1.000	0.528	1.000	1.000	0.000	0.000
Sham e3-8	750.2 ± 57.5			-	0.992	1.000	0.811	0.985	1.000	0.000	0.000
Sham e4-8	726.0 ± 50.1				-	1.000	0.316	1.000	1.000	0.001	0.000
Sham e5-8	736.9 ± 51.1					-	0.532	1.000	1.000	0.000	0.000
Sham e6-8	791.0 ± 8.96						-	0.270	0.571	0.000	0.000
Sham e7-8	723.7 ± 40.5							-	1.000	0.001	0.000
Sham e8	736.6 ± 49.1								-	0.000	0.000
DMB e5-8	614.9 ± 49.7									-	0.992
DMB e5-8/MD	523.5 ± 43.0										-

Table S2. List of *p*-values obtained with Tukey's test for significant differences in the measurements of femoral neck length.

	Mean ± SD (µm)	**Physiological**	**Alb removal**	**Sham e3-8**	**Sham e4-8**	**Sham e5-8**	**Sham e6-8**	**Sham e7-8**	**Sham e8**	**DMB e5-8**	**DMB e5-8/MD**
Mean ± SD (µm)		225.3 ± 37.6	207.2 ± 19.8	213.5 ± 21.8	222.8 ± 21.3	211.5 ± 29.5	211.8 ± 25.8	219.0 ± 26.3	226.5 ± 27.3	232.0 ± 21.9	224.4 ± 21.6
Physiological	225.3 ± 37.6	-	0.901	0.994	1.000	0.987	0.991	1.000	1.000	1.000	1.000
Alb removal	207.2 ± 19.8		-	1.000	0.959	1.000	1.000	0.994	0.863	0.428	0.858
Sham e3-8	213.5 ± 21.8			-	0.999	1.000	1.000	1.000	0.988	0.803	0.992
Sham e4-8	222.8 ± 21.3				-	0.997	0.998	1.000	1.000	0.999	1.000
Sham e5-8	211.5 ± 29.5					-	1.000	1.000	0.977	0.760	0.982
Sham e6-8	211.8 ± 25.8						-	1.000	0.984	0.813	0.989
Sham e7-8	219.0 ± 26.3							-	1.000	0.986	1.000
Sham e8	226.5 ± 27.3								-	1.000	1.000
DMB e5-8	232.0 ± 21.9									-	0.999
DMB e5-8/MD	224.4 ± 21.6										-

Table S3. List of *p*-values obtained with Tukey's test for significant differences in the measurements of femoral head to greater trochanter.

	Mean ± SD (µm)	**Physiological**	**Alb removal**	**Sham e3-8**	**Sham e4-8**	**Sham e5-8**	**Sham e6-8**	**Sham e7-8**	**Sham e8**	**DMB e5-8**	**DMB e5-8/MD**
Mean ± SD (µm)		449.1 ± 26.7	442.6 ± 26.4	437.4 ± 24.7	445.4 ± 20.6	435.3 ± 16.9	449.0 ± 22.5	439.2 ± 23.2	450.2 ± 27.0	416.2 ± 23.4	397.2 ± 12.8
Physiological	449.1 ± 26.7	-	1.000	0.988	1.000	0.973	1.000	0.998	1.000	0.097	0.000
Alb removal	442.6 ± 26.4		-	1.000	1.000	1.000	1.000	1.000	1.000	0.208	0.001
Sham e3-8	437.4 ± 24.7			-	0.999	1.000	0.989	1.000	0.978	0.504	0.004
Sham e4-8	445.4 ± 20.6				-	0.997	1.000	1.000	1.000	0.208	0.001
Sham e5-8	435.3 ± 16.9					-	0.975	1.000	0.957	0.728	0.018
Sham e6-8	449.0 ± 22.5						-	0.998	1.000	0.100	0.000
Sham e7-8	439.2 ± 23.2							-	0.996	0.532	0.009
Sham e8	450.2 ± 27.0								-	0.076	0.000
DMB e5-8	416.2 ± 23.4									-	0.621
DMB e5-8/MD	397.2 ± 12.8										-

Table S4. List of *p*-values obtained with Tukey's test for significant differences in the measurements of epiphyseal width.

	Mean ± SD (µm)	**Physiological**	**Alb removal**	**Sham e3-8**	**Sham e4-8**	**Sham e5-8**	**Sham e6-8**	**Sham e7-8**	**Sham e8**	**DMB e5-8**	**DMB e5-8/MD**
Mean ± SD (µm)		631.0 ± 68.8	608.2 ± 35.3	614.8 ± 39.7	611.7 ± 19.5	618.3 ± 41.7	618.2 ± 33.6	609.7 ± 25.6	619.2 ± 38.9	496.9 ± 40.3	488.6 ± 58.0
Physiological	631.0 ± 68.8	-	0.985	0.999	0.998	1.000	1.000	0.995	1.000	0.000	0.000
Alb removal	608.2 ± 35.3		-	1.000	1.000	1.000	1.000	1.000	1.000	0.000	0.000
Sham e3-8	614.8 ± 39.7			-	1.000	1.000	1.000	1.000	1.000	0.000	0.000
Sham e4-8	611.7 ± 19.5				-	1.000	1.000	1.000	1.000	0.000	0.000
Sham e5-8	618.3 ± 41.7					-	1.000	1.000	1.000	0.000	0.000
Sham e6-8	618.2 ± 33.6						-	1.000	1.000	0.000	0.000
Sham e7-8	609.7 ± 25.6							-	1.000	0.000	0.000
Sham e8	619.2 ± 38.9								-	0.000	0.000
DMB e5-8	496.9 ± 40.3									-	1.000
DMB e5-8/MD	488.6 ± 58.0										-

Table S5. List of *p*-values obtained with Tukey's test for significant differences in the measurements of acetabular height.

	Mean ± SD (µm)	**Physiological**	**Alb removal**	**Sham e3-8**	**Sham e4-8**	**Sham e5-8**	**Sham e6-8**	**Sham e7-8**	**Sham e8**	**DMB e5-8**	**DMB e5-8/MD**
Mean ± SD (µm)		676.8 ± 61.1	712.4 ± 32.5	705.0 ± 30.3	687.8 ± 24.2	694.3 ± 24.0	695.1 ± 36.8	695.3 ± 29.3	704.6 ± 42.5	537.1 ± 32.7	522.1 ± 31.3
Physiological	676.8 ± 61.1	-	0.563	0.830	1.000	0.993	0.993	0.992	0.895	0.000	0.000
Alb removal	712.4 ± 32.5		-	1.000	0.916	0.985	0.992	0.992	1.000	0.000	0.000
Sham e3-8	705.0 ± 30.3			-	0.992	1.000	1.000	1.000	1.000	0.000	0.000
Sham e4-8	687.8 ± 24.2				-	1.000	1.000	1.000	0.996	0.000	0.000
Sham e5-8	694.3 ± 24.0					-	1.000	1.000	1.000	0.000	0.000
Sham e6-8	695.1 ± 36.8						-	1.000	1.000	0.000	0.000
Sham e7-8	695.3 ± 29.3							-	1.000	0.000	0.000
Sham e8	704.6 ± 42.5								-	0.000	0.000
DMB e5-8	537.1 ± 32.7									-	0.992
DMB e5-8/MD	522.1 ± 31.3										-

Table S6. List of *p*-values obtained with Tukey's test for significant differences in the measurements of acetabular width.

	Mean ± SD (µm)	**Physiological**	**Alb removal**	**Sham e3-8**	**Sham e4-8**	**Sham e5-8**	**Sham e6-8**	**Sham e7-8**	**Sham e8**	**DMB e5-8**	**DMB e5-8/MD**
Mean ± SD (µm)		545.7 ± 43.7	517.8 ± 19.8	526.3 ± 24.3	521.4 ± 20.1	530.8 ± 25.0	519.0 ± 21.7	510.9 ± 25.9	523.4 ± 23.7	410.1 ± 19.2	385.4 ± 24.8
Physiological	545.7 ± 43.7	-	0.432	0.860	0.725	0.978	0.612	0.241	0.814	0.000	0.432
Alb removal	517.8 ± 19.8		-	0.999	1.000	0.984	1.000	1.000	1.000	0.000	0.000
Sham e3-8	526.3 ± 24.3			-	1.000	1.000	1.000	0.963	1.000	0.000	0.000
Sham e4-8	521.4 ± 20.1				-	0.999	1.000	0.999	1.000	0.000	0.000
Sham e5-8	530.8 ± 25.0					-	0.996	0.877	1.000	0.000	0.000
Sham e6-8	519.0 ± 21.7						-	1.000	1.000	0.000	0.000
Sham e7-8	510.9 ± 25.9							-	0.995	0.000	0.000
Sham e8	523.4 ± 23.7								-	0.000	0.000
DMB e5-8	410.1 ± 19.2									-	0.394
DMB e5-8/MD	385.4 ± 24.8										-

Table S7. List of *p*-values obtained with Tukey's test for significant differences in the measurements of acetabular depth.

	Mean ± SD (µm)	**Physiological**	**Alb removal**	**Sham e3-8**	**Sham e4-8**	**Sham e5-8**	**Sham e6-8**	**Sham e7-8**	**Sham e8**	**DMB e5-8**	**DMB e5-8/MD**
Mean ± SD (µm)		317.7 ± 43.8	293.5 ± 38.6	288.2 ± 35.0	300.4 ± 32.7	300.7 ± 39.8	318.2 ± 19.7	305.4 ± 35.6	296.2 ± 30.9	180.0 ± 38.3	150.5 ± 35.8
Physiological	317.7 ± 43.8	-	0.935	0.812	0.996	0.996	1.000	1.000	0.981	0.000	0.000
Alb removal	293.5 ± 38.6		-	1.000	1.000	1.000	0.926	1.000	1.000	0.000	0.000
Sham e3-8	288.2 ± 35.0			-	1.000	0.999	0.797	0.993	1.000	0.000	0.000
Sham e4-8	300.4 ± 32.7				-	1.000	0.995	1.000	1.000	0.000	0.000
Sham e5-8	300.7 ± 39.8					-	0.994	1.000	1.000	0.000	0.000
Sham e6-8	318.2 ± 19.7						-	1.000	0.978	0.000	0.000
Sham e7-8	305.4 ± 35.6							-	1.000	0.000	0.000
Sham e8	296.2 ± 30.9								-	0.000	0.000
DMB e5-8	180.0 ± 38.3									-	0.655
DMB e5-8/MD	150.5 ± 35.8										-